Supporting Information

Visible Light Activated Energy Storage in Solid-State Azo-BF_2 Switches

Qianfeng Qiu[†a], Qingkai Qi[†b], Junichi Usuba[a], Karina Lee[a], Ivan Aprahamian[b*], Grace G. D. Han[a*]

[a] Department of Chemistry, Brandeis University, 415 South Street, Waltham, MA 02453 USA

[b] Department of Chemistry, Dartmouth College, Hanover, NH 03755 USA

[†] These authors contributed equally.

Emails: gracehan@brandeis.edu, ivan.aprahamian@dartmouth.edu

1. General Methods

All reagents and starting materials were purchased from commercial suppliers and used as received unless otherwise indicated. All experiments were conducted under air unless otherwise noted. Thin-layer chromatography (TLC) was conducted using a glass plate coated with a silica gel 60 matrix (F254 Fluorescent Indicator) purchased from MilliporeSigma. The product was visualized under UV light on the TLC plate. Column chromatography was performed on a CombiFlash automatic flash chromatography system (NextGen 300+) using RediSep Gold® normal-phase silica columns as stationary phase and solvents mixtures used during chromatography were reported as volume ratios unless otherwise noted. Deuterated solvents were purchased from Cambridge Isotope Laboratories, Inc. and used as received. ^{1}H NMR, ^{13}C NMR, and ^{19}F NMR spectra were recorded on a 500 or 600 MHz NMR spectrometer, with working frequencies of 500.13 or 600.13 MHz for ^{1}H nuclei, 125.8 or 150.9 MHz for ^{13}C nuclei, and 565 MHz for ^{19}F nuclei, respectively. Chemical shifts are quoted in ppm relative to tetramethylsilane (TMS), using the residual solvent peak as the reference standard. Hi-Res mass spectra were obtained on a Micromass Q-Tof Ultima ESI mass spectrometer. Common resolution ESI mass spectra were obtained on a Waters Quattro II ESI mass spectrometer. Melting points were measured on an Electrothermal Thermo Scientific IA9100X1 digital melting point instrument. UV-vis absorption spectra and quantum yield characterization were recorded on a Shimadzu UV-1800 UV-vis spectrophotometer. Solution kinetic spectra and thin film UV-vis spectra were obtained with a Cary 50 Bio UV-vis spectrophotometer.

2. Synthesis and characterization

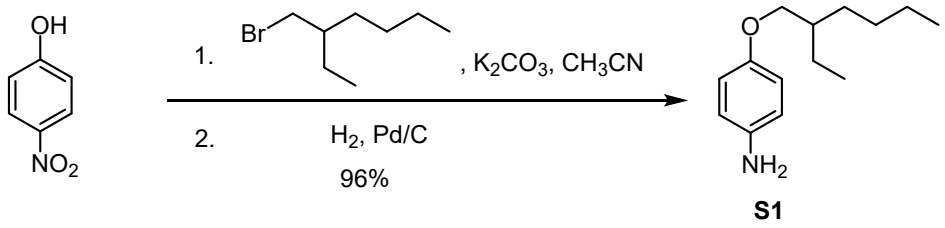

Scheme S1. Synthetic routes for 4-((2-ethylhexyl)oxy)aniline (**S1**).

S1: A stirred mixture of 4-nitrophenol (1.97 g, 14.2 mmol), 3-(bromomethyl)heptane (2.74 mL, 15.6 mmol), and K_2CO_3 (2.94 g, 21.3 mmol) in dry dimethylformamide (25 mL) was heated to 80 °C for 4 h. The reaction mixture was cooled, filtered over celite, concentrated, and the residue was dissolved in DCM (120 mL). The organic phase was washed with H_2O (3 x 100 mL) and brine (1 x 50 mL) and then dried over $MgSO_4$. After removing solvent under reduced pressure, the crude 1-((2-ethylhexyl)oxy)-4-nitrobenzene was obtained and directly used in the next step without any purification and characterization. The 1-((2-ethylhexyl)oxy)-4-nitrobenzene was further dissolved in 40 mL methanol/CH_2Cl_2 (3:1 v/v) mixture solvent and reduced with 178 mg 10% Pd/C under hydrogen atmosphere at room temperature (RT) for 12 h. The reaction mixture was filtered over celite, and then the filtrate was concentrated *in vacuo*. The residue was purified by flash column chromatography (SiO_2) eluting with a mixed solvent of ethyl acetate and hexanes (1:3, v/v) to afford **S1** (3.02 g, 96%) as a light-yellow liquid. ^{1}H NMR (500 MHz, $CDCl_3$) δ 6.75 (d, J = 8.8 Hz, 2H), 6.65 (d, J = 8.7 Hz, 2H), 3.80 – 3.72 (m, 2H), 3.45 (s, 2H), 1.69 (hept, J = 6.1 Hz, 1H), 1.54 – 1.24 (m, 8H), 0.95 – 0.87 (m, 6H). ^{13}C NMR (151 MHz, $CDCl_3$) δ 152.78, 139.76, 139.74, 116.53, 115.76, 71.37, 39.57, 30.63, 29.19, 23.95, 23.17, 14.19, 11.20. ESI-MS: m/z found [M+H$^+$] for $C_{14}H_{24}NO^+$ 222.15 (calcd. 222.18).

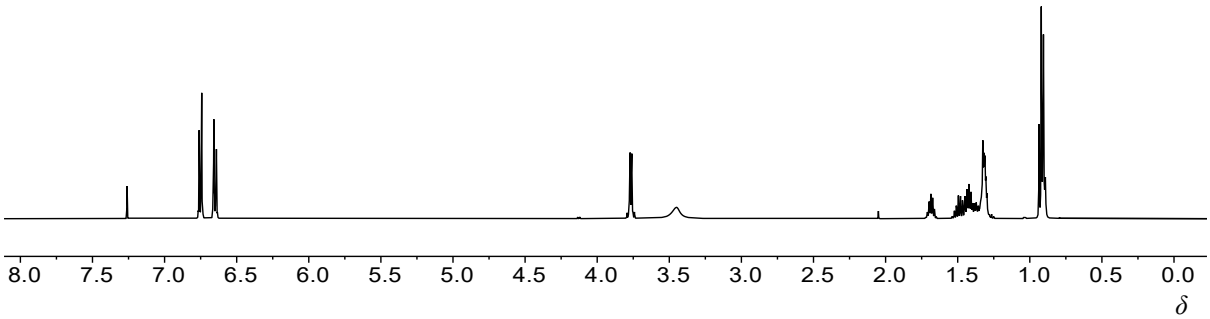

^{1}H NMR spectrum of **S1** in $CDCl_3$

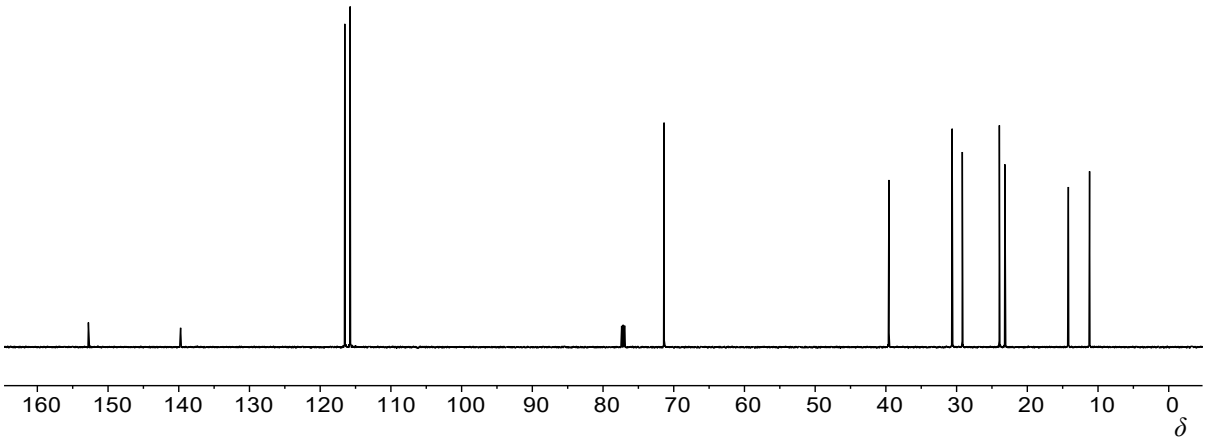

^{13}C NMR spectrum of **S1** in $CDCl_3$

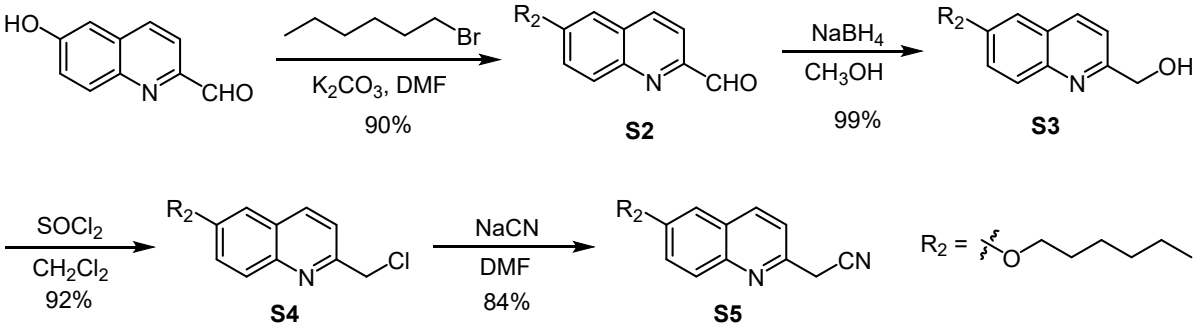

Scheme S2. Synthetic routes for 2-(6-(hexyloxy)quinolin-2-yl)acetonitrile (**S5**).

S2: A stirred mixture of 6-hydroxyquinoline-2-carboxaldehyde (1.73 g, 10 mmol), 1-bromohexane (1.82 g, 11 mmol) and K_2CO_3 (2.07 g, 15 mmol) in dry dimethylformamide (20 mL) was heated to 80 °C for 4 h. The reaction mixture was cooled, filtered over celite, concentrated and residue dissolved in DCM (120 mL). The organic phase was washed with H_2O (3 x 50 mL) and brine (1 x 25 mL), and then dried over anhydrous $MgSO_4$. Removal of the solvent followed by flash column chromatography (SiO_2) eluting with a mixed solvent of ethyl acetate and hexanes (1:3, v/v) gave **S2** (2.32 g, 90%) as a white solid. m.p. 60 °C; ^{1}H NMR (600 MHz, $CDCl_3$) δ 10.25 (d, J = 26.9 Hz, 1H), 8.27 – 8.14 (m, 2H), 8.01 (m, 1H), 7.53 – 7.45 (m, 1H), 7.19 – 7.09 (m, 1H), 4.13 (t, J = 6.8 Hz, 2H), 1.94 – 1.84 (m, 2H), 1.56 – 1.48 (m, 2H), 1.42 – 1.33 (m, 4H), 0.95 – 0.90 (m, 3H). ^{13}C NMR (151 MHz, $CDCl_3$) δ 193.38, 193.36, 159.42, 150.39, 143.78, 135.42, 131.72, 131.58, 123.82, 117.67, 105.51, 68.48, 31.51,

28.98, 25.67, 22.55, 13.99. ESI-MS: m/z found [M+H$^+$] for $C_{16}H_{20}NO_2^+$ 258.15 (calcd. 258.14).

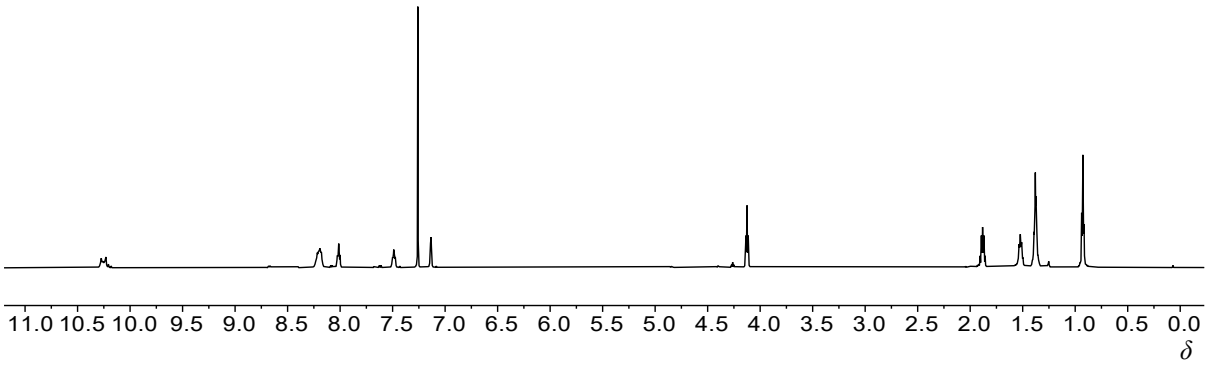

^{1}H NMR spectrum of **S2** in $CDCl_3$

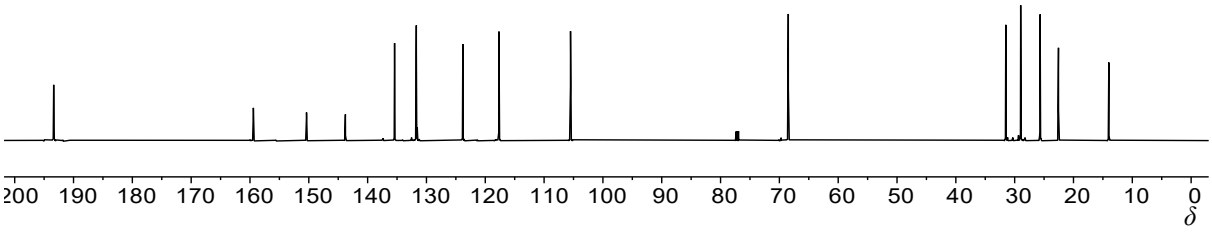

^{13}C NMR spectrum of **S2** in $CDCl_3$

S3: To a cooled solution (-20 °C) of **S2** (2.06 g, 8 mmol) in dry methanol (30 mL), sodium borohydride (0.45 g, 12 mmol) was added in small portions. The reaction solution was stirred to slowly warm to RT in 2 h. Then, the mixture was acidified with dilute HCl acid at 0 °C. The evaporation of the solvent under reduced pressure afforded **S3** (2.05 g, 99%) as a white solid. The product was used for the next step without any purification or characterization.

S4: Compound **S3** (1.04 g, 4 mmol) was dissolved in dry DCM (10 mL). $SOCl_2$ (0.44 mL, 6 mmol) was added dropwise at 0 °C. The reaction solution was stirred for 1 h and then quenched by the slow addition of water in an ice bath. The mixture was washed with H_2O (3 x 5 mL), dried over $MgSO_4$, and concentrated *in vacuo.* The residue was purified by flash column chromatography (SiO_2) eluting with a mixed solvent of ethyl acetate and hexanes (1:3, v/v) to afford **S4** (1.02 g, 92%) as a light-yellow solid. m.p. 63 °C; ^{1}H NMR (600 MHz, $CDCl_3$) δ 7.97 (d, J = 8.4 Hz, 1H), 7.91 (d, J = 9.2 Hz, 1H), 7.45 (d, J = 8.5 Hz, 1H), 7.33 (d, J = 9.2 Hz, 1H),

6.98 (s, 1H), 4.76 (s, 2H), 4.00 (t, J = 6.6 Hz, 2H), 1.80 (p, J = 7.0 Hz, 2H), 1.50 – 1.41 (m, 4H), 1.21 (t, J = 7.6 Hz, 2H), 0.89 (t, J = 6.7Hz, 3H). ^{13}C NMR (151 MHz, $CDCl_3$) δ 157.68, 153.91, 143.31, 135.94, 130.48, 128.57, 123.00, 120.73, 105.69, 68.33, 47.41, 31.58, 29.12, 25.75, 22.61, 14.04. ESI-MS: m/z found [M+H$^+$] for $C_{16}H_{21}ClNO^+$ 278.15 (calcd. 278.12).

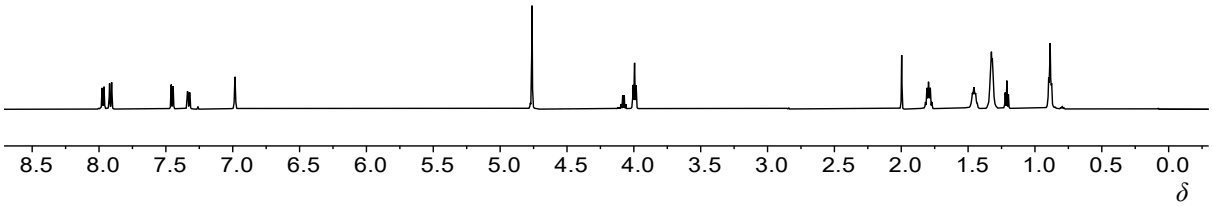

^{1}H NMR spectrum of **S4** in $CDCl_3$

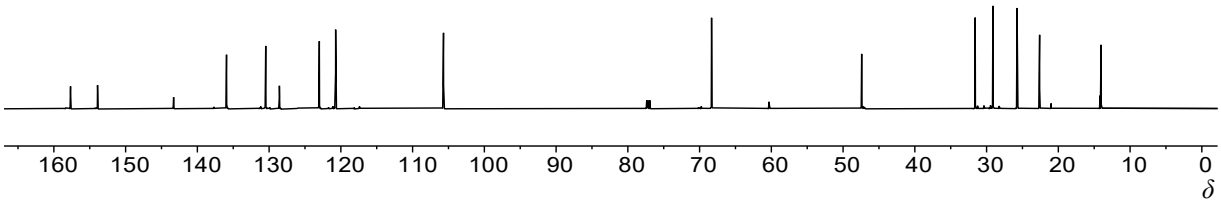

^{13}C NMR spectrum of **S4** in $CDCl_3$

S5: A stirred solution of **S4** (0.56 g, 2 mmol) in dimethylformamide (10 mL) was heated to 80 °C for 30 min. Sodium cyanide (0.15 g, 3 mmol) in H_2O (2 mL) was added dropwise into the above solution. The reaction kept stirring for 1 h at 80 °C. Then, H_2O (2.5 mL) was added to the mixture to quench the reaction and followed by adding DCM (20 mL). The mixture was washed with H_2O (3 x 10 mL) and brine (1 x 10 mL), dried over $MgSO_4$ and concentrated *in vacuo.* The residue was purified by flash column chromatography (SiO_2) eluting with a mixed solvent of ethyl acetate and hexanes (1:3, v/v) to give **S5** (0.45 g, 84%) as a dark yellow solid. m.p. 56 °C; ^{1}H NMR (600 MHz, $CDCl_3$) δ 8.05 (d, J = 8.5 Hz, 1H), 7.92 (d, J = 9.2 Hz, 1H), 7.44 (d, J = 8.6 Hz, 1H), 7.38 (d, J = 9.2 Hz, 1H), 7.05 (d, J = 2.8 Hz, 1H), 4.10 – 4.01 (m, 4H), 1.84 (p, J = 6.6 Hz, 2H), 1.49 (p, J = 7.2 Hz, 2H), 1.40 – 1.30 (m, 4H), 0.91 (t, J = 6.9 Hz,

3H). ^{13}C NMR (151 MHz, $CDCl_3$) δ 157.77, 147.67, 143.86, 136.46, 130.33, 128.44, 123.54, 119.97, 117.25, 105.74, 68.48, 31.65, 29.18, 27.15, 25.82, 22.68, 14.12. ESI-MS: m/z found [M+H$^+$] for $C_{17}H_{21}N_2O^+$ 269.15 (calcd. 269.16).

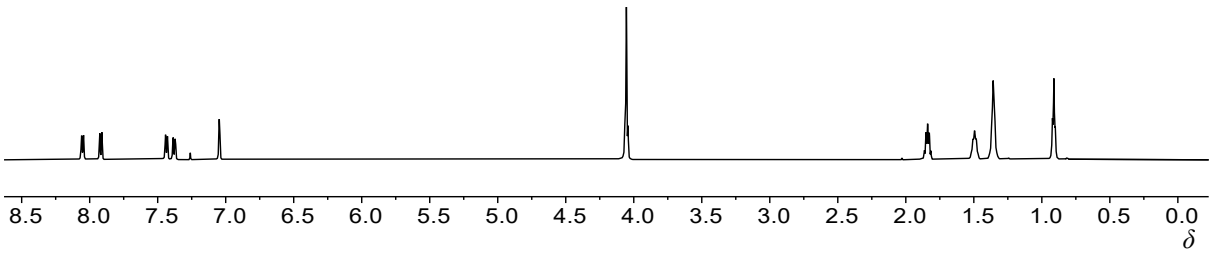

^{1}H NMR spectrum of **S5** in $CDCl_3$

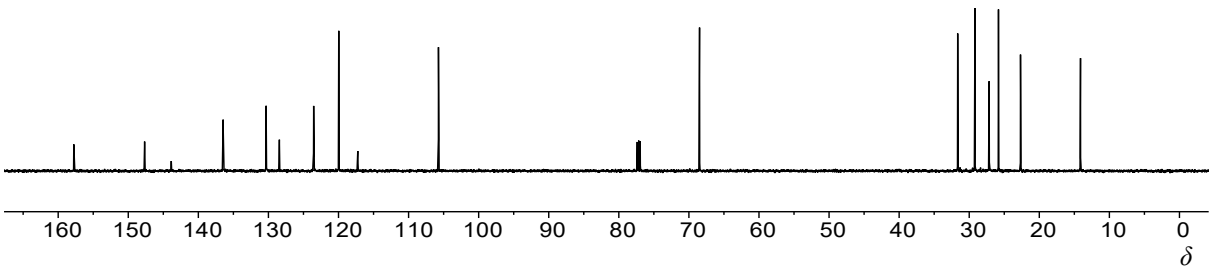

^{13}C NMR spectrum of **S5** in $CDCl_3$

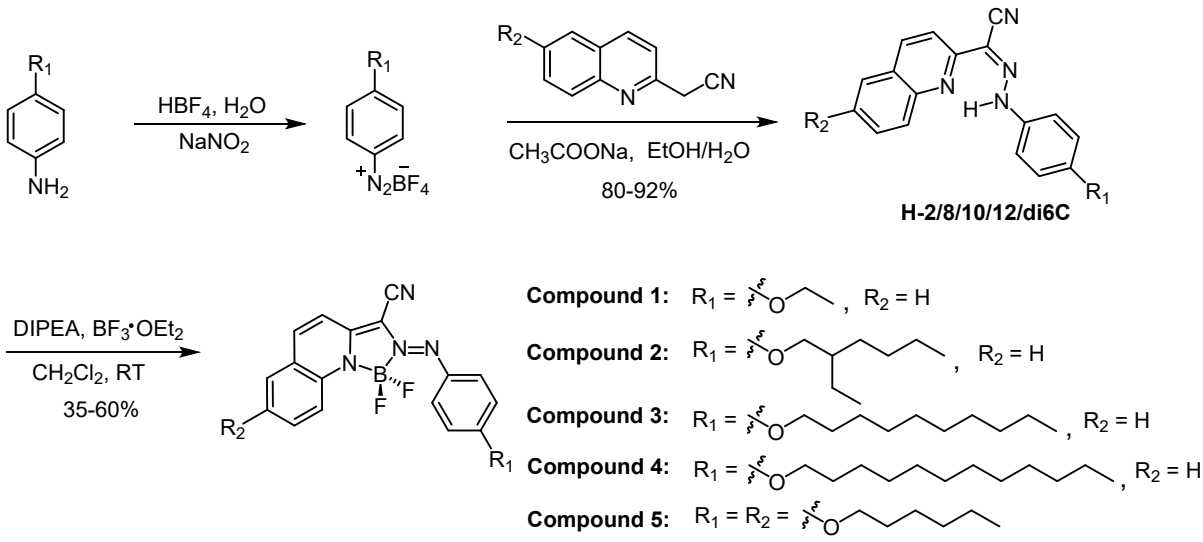

Scheme S2. General synthetic procedure for obtaining the hydrazone precursors (**H-nC**) and azo-BF_2s (**1-5**) with different length of alkyl chains.

General Synthetic Procedure for the Hydrazone Precursors: Hydrazones **H-nC** substituted with different length of alkyl chains were synthesized following the procedure described in our previous publication.[1] 1.7 mL of HBF_4 (48%) was added dropwise to a mixture of 4-(alkoxy)aniline (1 equiv., 3.4 mmol) in 1 mL water. After stirring in an ice-bath for 30 min, a precooled aqueous solution of $NaNO_2$ (1 equiv., 0.235 g, 3.4 mmol) was added dropwise over a period of 15 min. The pinkish diazonium salt was collected by filtration after 60 min and added to a mixture solution of 2-(quinolin-2-yl)acetonitrile or 2-(6-(hexyloxy)quinolin-2-yl)acetonitrile (0.8 equiv., 2.7 mmol) and sodium acetate (3.2 equiv., 0.890 g, 10.8 mmol) in a cooled and well stirred 30 mL ethanol/water (2:1) mixture. The resulting reaction mixture was left to stir overnight at RT. The precipitated compound was then collected by filtration and dried over air. The crude product was purified by silica gel column chromatography (hexane/ethyl acetate 9:1) to give hydrazones **H-nC**.

H-2C: Compound **H-2C** (0.79 g, 92%) was obtained as a dark yellow solid. m.p. 181 °C; ^{1}H NMR (600 MHz, CD_2Cl_2) δ 16.06 (s, 1H), 8.23 (d, *J* = 8.8 Hz, 1H), 7.97 (d, *J* = 8.3 Hz, 1H), 7.79 (d, *J* = 8.0 Hz, 1H), 7.75 – 7.69 (m, 2H), 7.54 (ddd, *J* = 8.2, 6.9, 1.2 Hz, 1H), 7.32 (d, *J* = 9.0 Hz, 2H), 6.88 (d, *J* = 9.0 Hz, 2H), 3.97 (q, *J* = 7.0 Hz, 2H), 1.33 (t, *J* = 7.0 Hz, 3H). ^{13}C NMR (151 MHz, CD_2Cl_2) δ 156.83, 152.62, 145.90, 137.97, 136.24, 131.09, 128.25, 128.20, 127.79, 127.07, 119.69, 118.44, 116.81, 116.38, 115.86, 110.55, 64.28, 15.07. ESI-MS: m/z found [M+H$^+$] for $C_{19}H_{17}N_4O^+$ 317.15 (calcd. 317.13).

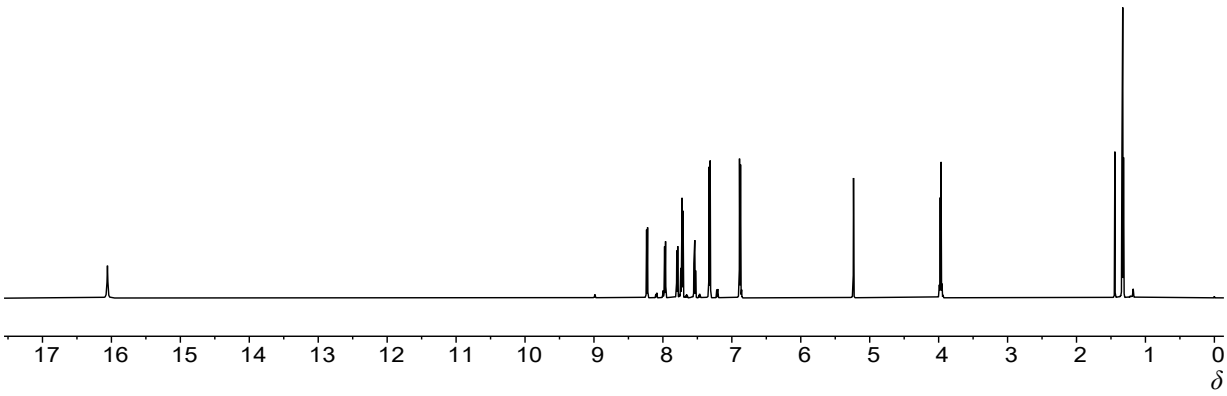

^{1}H NMR spectrum of **H-2C** in CD_2Cl_2

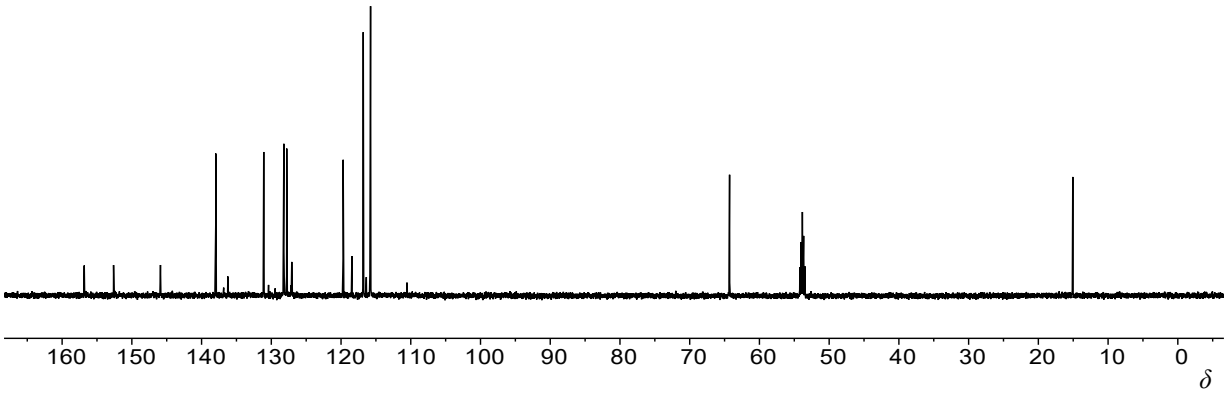

^{13}C NMR spectrum of **H-2C** in CD_2Cl_2

H-8C: Compound **H-8C** (0.87 g, 80%) was obtained as a sticky and dark yellow liquid. ^{1}H NMR (600 MHz, CD_2Cl_2) δ 16.13 (s, 1H), 8.30 (d, *J* = 9.6 Hz, 1H), 8.05 (d, *J* = 8.4 Hz, 1H), 7.87 (d, *J* = 8.2 Hz, 1H), 7.83 – 7.77 (m, 2H), 7.62 (ddd, *J* = 8.1, 6.9, 1.2 Hz, 1H), 7.40 (d, *J* = 9.0 Hz, 2H), 6.98 (d, *J* = 9.0 Hz, 2H), 3.88 (dd, *J* = 5.8, 2.5 Hz, 2H), 1.74 (p, *J* = 6.1 Hz, 1H), 1.56 – 1.39 (m, 4H), 1.38 – 1.31 (m, 4H), 0.98 – 0.90 (m, 6H). ^{13}C NMR (151 MHz, CD_2Cl_2) δ 157.19, 152.33, 145.60, 137.60, 135.97, 130.94, 128.07, 128.02, 127.64, 126.80, 119.38, 118.33, 116.63, 115.68, 110.25, 71.30, 39.86, 30.91, 29.51, 24.26, 23.50, 14.34, 11.36. ESI-MS: m/z found [M+H$^+$] for $C_{25}H_{29}N_4O^+$ 401.25 (calcd. 401.23).

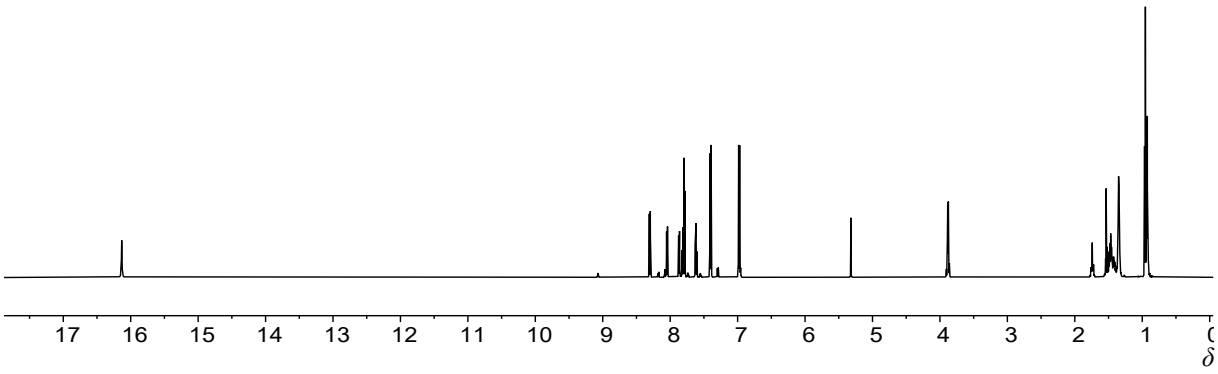

^{1}H NMR spectrum of **H-8C** in CD_2Cl_2

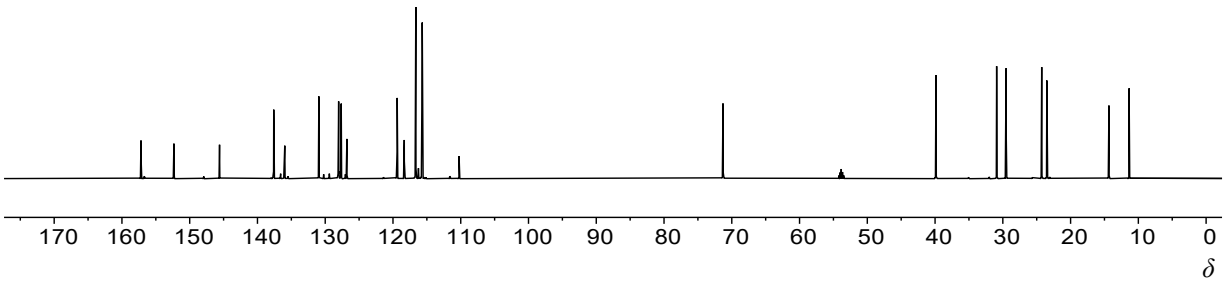

^{13}C NMR spectrum of **H-8C** in CD_2Cl_2

H-10C: Compound **H-10C** (1.02 g, 88%) was obtained as a dark yellow solid. m.p. 132 °C; ^{1}H NMR (500 MHz, CD_2Cl_2) δ 16.09 (s, 1H), 8.25 (d, *J* = 8.7 Hz, 1H), 7.99 (d, *J* = 8.3 Hz, 1H), 7.81 (d, *J* = 8.2 Hz, 1H), 7.76 – 7.71 (m, 2H), 7.59 – 7.51 (m, 1H), 7.34 (d, *J* = 8.9 Hz, 2H), 6.89 (d, *J* = 9.0 Hz, 2H), 3.90 (t, *J* = 6.6 Hz, 2H), 1.74 – 1.66 (m, 2H), 1.42 – 1.34 (m, 2H), 1.33 – 1.13 (m, 12H), 0.80 (t, *J* = 6.8 Hz, 3H). ^{13}C NMR (151 MHz, CD_2Cl_2) δ 157.06, 152.65, 145.92, 137.98, 136.20, 131.10, 128.27, 128.21, 127.79, 127.08, 119.71, 118.46, 116.81, 115.79, 110.53, 68.87, 32.33, 30.02, 29.99, 29.84, 29.75, 29.74, 26.44, 23.11, 14.30. ESI-MS: m/z found [M+H$^+$] for $C_{27}H_{32}N_4O^+$ 429.25 (calcd. 429.26).

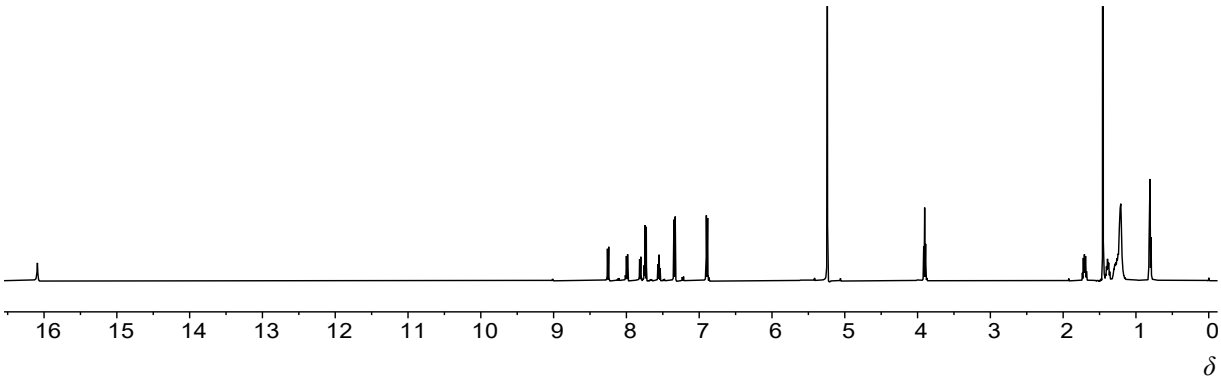

^{1}H NMR spectrum of **H-10C** in CD_2Cl_2

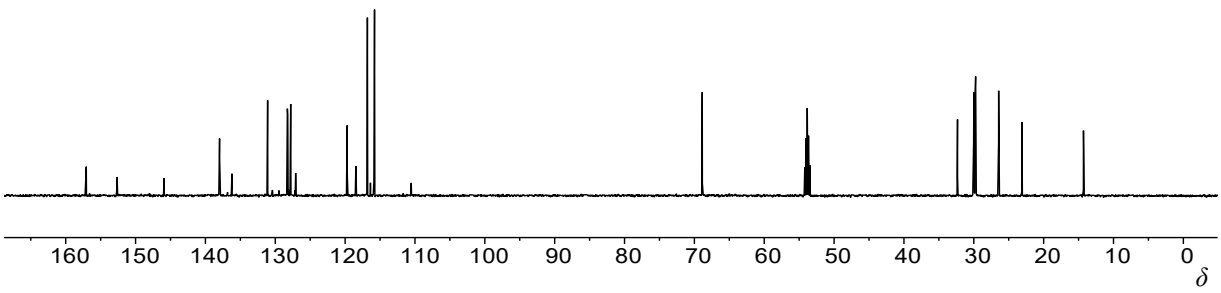

^{13}C NMR spectrum of **H-10C** in CD_2Cl_2

H-12C: Compound **H-12C** (1.11 g, 90%) was obtained as a dark yellow solid. m.p. 125 °C; ^{1}H NMR (500 MHz, CD_2Cl_2) δ 16.13 (d, *J* = 6.6 Hz, 1H), 8.30 (d, *J* = 8.7 Hz, 1H), 8.04 (d, *J* = 8.5 Hz, 1H), 7.87 (d, *J* = 8.1 Hz, 1H), 7.83 – 7.76 (m, 2H), 7.65 – 7.59 (m, 1H), 7.39 (d, *J* = 9.0 Hz, 2H), 6.96 (d, *J* = 8.9 Hz, 2H), 3.97 (t, *J* = 6.6 Hz, 2H), 1.82 – 1.74 (m, 2H), 1.51 – 1.42 (m, 2H), 1.41 – 1.22 (m, 16H), 0.89 (t, *J* = 6.8 Hz, 3H). ^{13}C NMR (151 MHz, CD_2Cl_2) δ 156.65, 152.27, 145.54, 137.60, 135.81, 130.70, 127.87, 127.82, 127.39, 126.70, 119.33, 118.06, 116.42, 115.40, 110.15, 68.47, 31.93, 29.67, 29.65, 29.62, 29.60, 29.42, 29.36, 29.32, 26.02, 22.70, 13.88. ESI-MS: m/z found [M+H$^+$] for $C_{29}H_{37}N_4O^+$ 457.25 (calcd. 457.29).

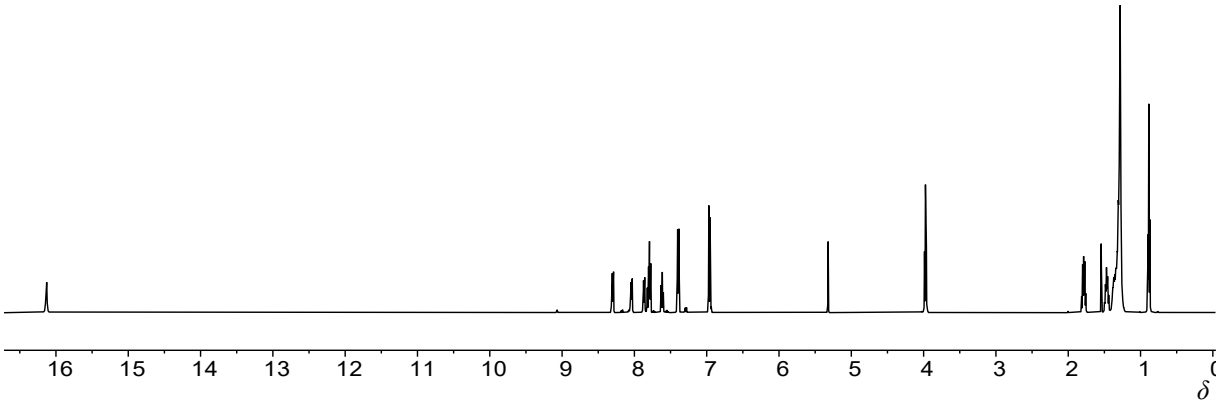

^{1}H NMR spectrum of **H-12C** in CD_2Cl_2

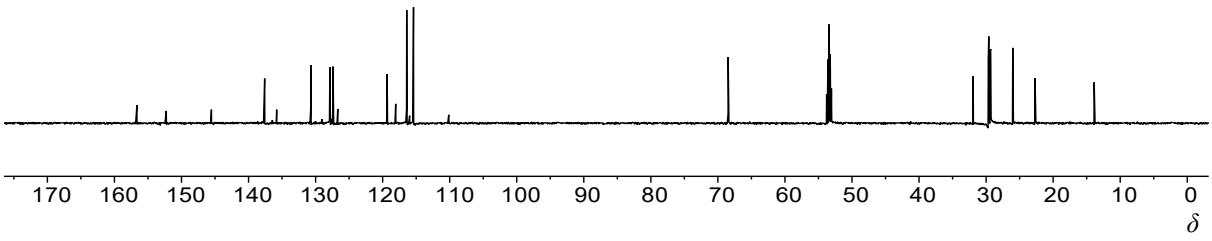

^{13}C NMR spectrum of **H-12C** in CD_2Cl_2

H-di6C: Compound **H-di6C** was synthesized following the general synthetic procedure used for the hydrazone precursors with **S5** (0.27 g, 1 mmol) as the starting material. The product was further purified by flash column chromatography (SiO_2) eluting with a mixed solvent of ethyl acetate and hexane (1:8, v/v) to give hydrazone **H-di6C** (0.43 g, 92%) as a dark yellow solid. m.p. 98 °C; ^{1}H NMR (600 MHz, CD_2Cl_2) δ 15.76 (s, 1H), 8.07 (d, J = 8.7 Hz, 1H), 7.80 (d, J = 9.1 Hz, 1H), 7.63 (d, J = 8.7 Hz, 1H), 7.37 (d, J = 6.2 Hz, 1H), 7.29 (d, J = 9.0 Hz, 2H), 7.03 (s, 1H), 6.92 (d, J = 8.8 Hz, 2H), 4.03 (t, J = 6.7 Hz, 2H), 3.95 (t, J = 6.6 Hz, 2H), 1.88 –1.73 (m, 4H), 1.55 – 1.44 (m, 4H), 1.43 – 1.32 (m, 8H), 1.00 – 0.89 (m, 6H). ^{13}C NMR (151 MHz, CD_2Cl_2) δ 158.58, 156.74, 150.14, 141.51, 136.39, 136.31, 129.74, 129.59, 128.33, 123.95, 119.87, 118.50, 116.47, 115.71, 110.72, 106.39, 68.97, 68.83, 68.28, 32.06, 32.04, 29.74, 29.68, 29.51, 26.14, 26.12, 23.06, 14.25. ESI-MS: m/z found [M+H$^+$] for $C_{29}H_{37}N_4O_2^+$ 473.25 (calcd. 473.28).

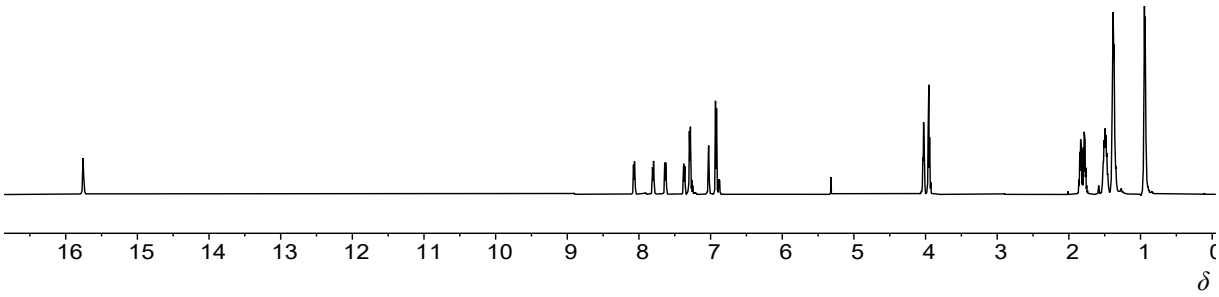

^{1}H NMR spectrum of **H-di6C** in CD_2Cl_2

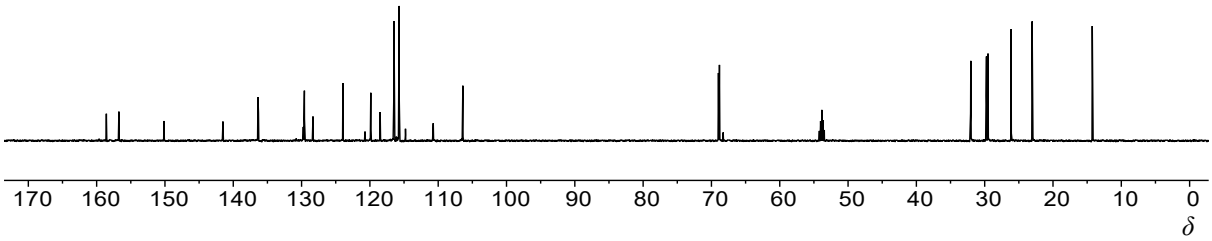

^{13}C NMR spectrum of **H-di6C** in CD_2Cl_2

General Synthetic Procedure for the Azo-BF_2s: Azo-BF_2s (**1-5**) were synthesized following the procedure described in our previous publication.[1] Hydrazone (**H-nC**, 1 equiv., 2 mmol) was dissolved in a mixture of dry DCM (10 mL) and N,N-diisopropylethylamine (DIPEA, 7 equiv., 2.44 mL, 14 mmol). A solution of boron trifluoride etherate (10 equiv., 2.47 mL, 20 mmol) in dry DCM (10 mL) was added dropwise at RT under stirring. The reaction mixture was stirred for 6 h, followed by water quenching. The organic layer was washed with H_2O (10 mL), dried over $MgSO_4$, and then concentrated *in vacuo*. The azo-BF_2s product was further purified by flash column chromatography (SiO_2) eluting with a mixed solvent of ethyl acetate and hexane (1:3, v/v) to give Azo-BF_2s (**1-5**).

Compound 1: Compound **1** (0.44 g, 60%) was obtained as a dark purple solid. ^{1}H NMR (600 MHz, CD_2Cl_2) δ 8.18 (d, *J* = 9.0 Hz, 1H), 7.82 – 7.77 (m, 2H), 7.74 (t, *J* = 7.8 Hz, 1H), 7.70 (d, *J* = 9.1 Hz, 2H), 7.47 (t, *J* = 7.8 Hz, 1H), 7.32 (d, *J* = 9.0 Hz, 1H), 7.00 (d, *J* = 9.1 Hz, 2H), 4.13 (q, *J* = 7.0 Hz, 2H), 1.45 (t, *J* = 7.0 Hz, 3H). ^{13}C NMR (151 MHz, CD_2Cl_2) δ 161.06, 143.61, 139.39, 134.45, 133.89, 129.79, 126.16, 126.13, 126.09, 125.92, 125.22, 118.53, 115.26, 114.41, 113.15, 64.49, 14.94. ^{19}F NMR (565 MHz, CD_2Cl_2) δ -145.71 (dd, *J* = 64.8, 29.2 Hz). Hi-Res ESI-MS: m/z found [M+H$^+$] for $C_{19}H_{16}BF_2N_4O^+$ 365.1374 (calcd. 365.1385).

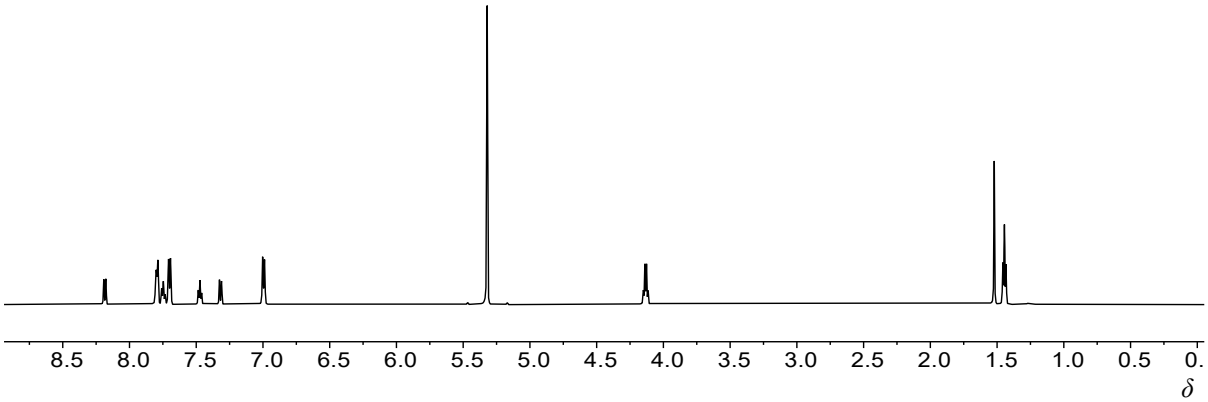

^{1}H NMR spectrum of **1** in CD_2Cl_2

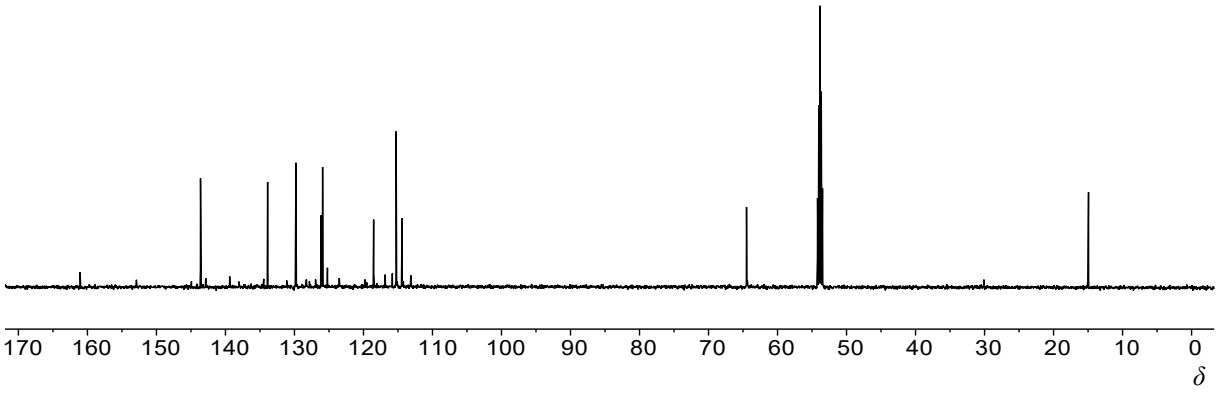

^{13}C NMR spectrum of **1** in CD_2Cl_2

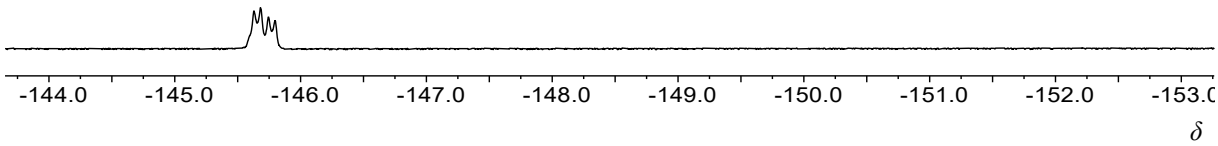

^{19}F NMR spectrum of **1** in CD_2Cl_2

Compound 2: Compound **2** (0.31 g, 35%) was obtained as a dark purple and sticky liquid. ^{1}H NMR (600 MHz, CD_2Cl_2) δ 8.18 (d, *J* = 8.9 Hz, 1H), 7.81 – 7.77 (m, 2H), 7.74 (t, *J* = 7.8 Hz, 1H), 7.70 (d, *J* = 9.1 Hz, 2H), 7.47 (t, *J* = 7.5 Hz, 1H), 7.31 (d, *J* = 9.0 Hz, 1H), 7.01 (d, *J* = 9.1 Hz, 2H), 3.96 (dd, *J* = 5.7, 2.2 Hz, 2H), 1.77 (m, 1H), 1.57 – 1.40 (m, 4H), 1.38 – 1.31 (m, 4H), 0.95 (t, *J* = 7.5 Hz, 3H), 0.92 (t, *J* = 7.2 Hz, 3H). ^{13}C NMR (151 MHz, CD_2Cl_2) δ 161.54, 143.55, 142.78, 139.37, 133.86, 129.78, 126.18, 126.14, 126.10, 125.88, 125.18, 118.50, 115.30, 114.39, 113.17, 71.37, 39.78, 30.87, 30.86, 29.46, 24.23, 23.46, 14.26, 11.29. ^{19}F NMR (565 MHz, CD_2Cl_2) δ -145.76 (dd, *J* = 64.4, 27.7 Hz). Hi-Res ESI-MS: m/z found [M+H$^+$] for $C_{25}H_{28}BF_2N_4O^+$ 449.2314 (calcd. 449.2324).

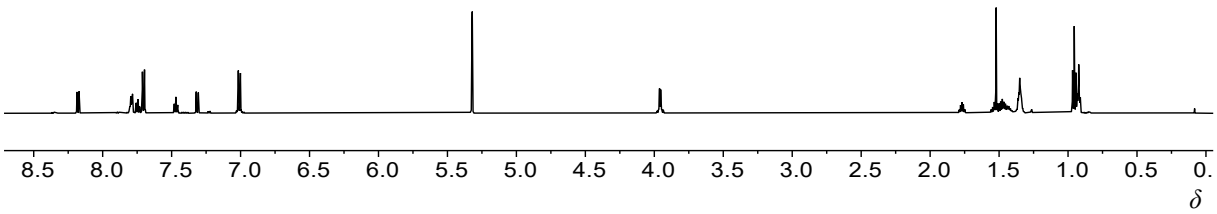

^{1}H NMR spectrum of **2** (contains a small percentage of the *cis* isomer as well) in CD_2Cl_2

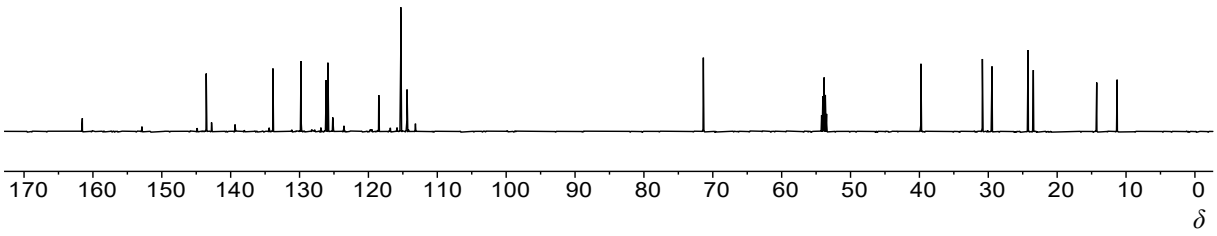

^{13}C NMR spectrum of **2** (contains a small percentage of the *cis* isomer as well) in CD_2Cl_2

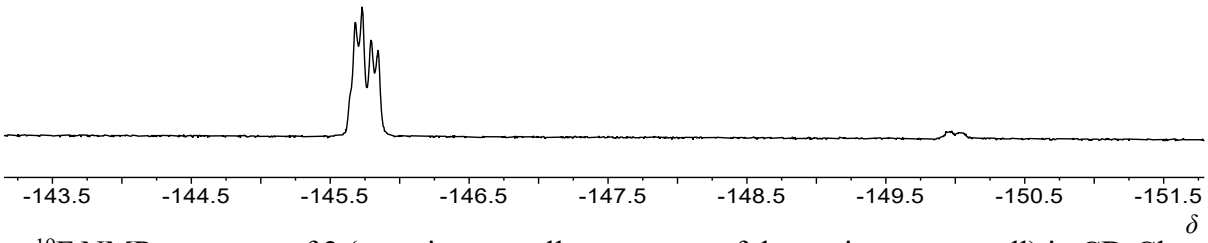

^{19}F NMR spectrum of **2** (contains a small percentage of the *cis* isomer as well) in CD_2Cl_2

Compound 3: Compound **3** (0.51 g, 54%) was obtained as a dark purple solid. ^{1}H NMR (500 MHz, CD_2Cl_2) δ 8.18 (d, *J* = 8.0 Hz, 1H), 7.82 – 7.77 (d, *J* = 9.0 Hz, 2H), 7.75 (t, *J* = 7.7 Hz, 1H), 7.70 (d, *J* = 9.1 Hz, 2H), 7.47 (d, *J* = 7.6 Hz, 1H), 7.32 (d, *J* = 9.0 Hz, 1H), 7.00 (d, *J* = 9.2 Hz, 2H), 4.06 (t, *J* = 6.6 Hz, 2H), 1.85 – 1.78 (m, 2H), 1.51 – 1.44 (m, 2H), 1.41 – 1.25 (m, 13H), 0.89 (t, *J* = 6.9 Hz, 3H). ^{13}C NMR (151 MHz, CD_2Cl_2) δ 161.31, 143.59, 142.82, 133.89, 129.79, 126.18, 126.14, 126.10, 125.91, 125.22, 118.53, 115.28, 114.43, 113.19, 68.98, 32.32, 29.99, 29.97, 29.77, 29.73, 29.56, 26.38, 23.10, 14.29. ^{19}F NMR (565 MHz, CD_2Cl_2) δ -145.75 (dd, *J* = 64.4, 27.5 Hz). Hi-Res ESI-MS: m/z found [M+H$^+$] for $C_{27}H_{32}BF_2N_4O^+$ 477.2637 (calcd. 477.2637).

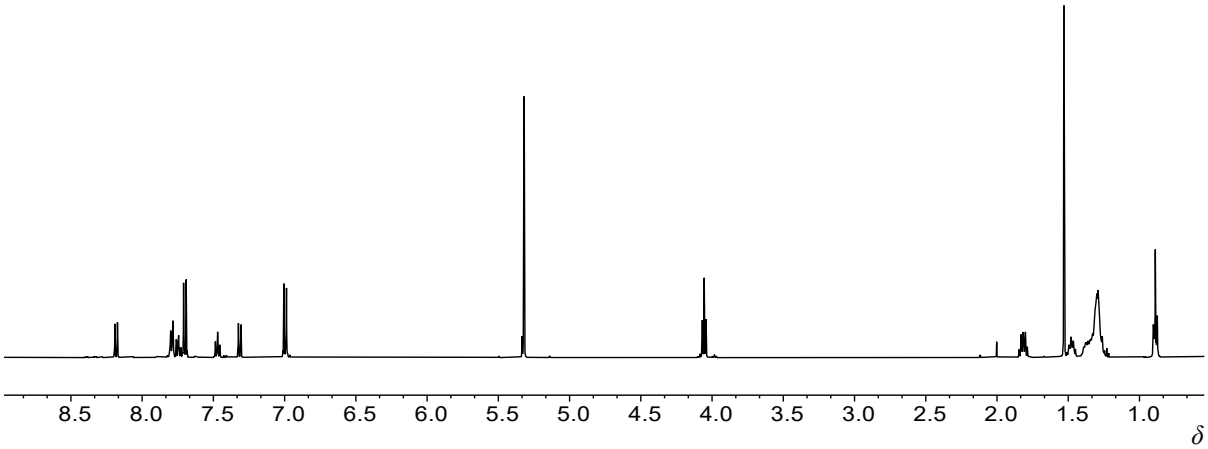

^{1}H NMR spectrum of **3** in CD_2Cl_2

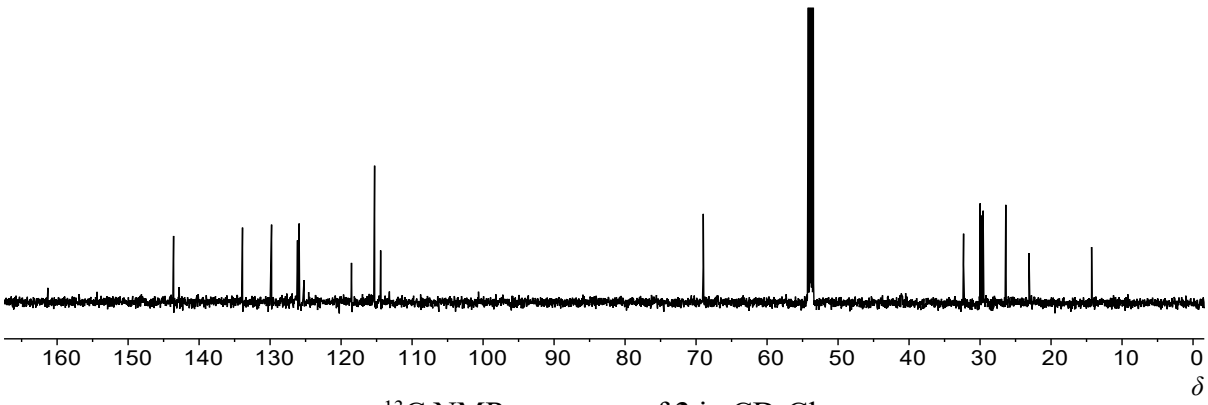

^{13}C NMR spectrum of **3** in CD_2Cl_2

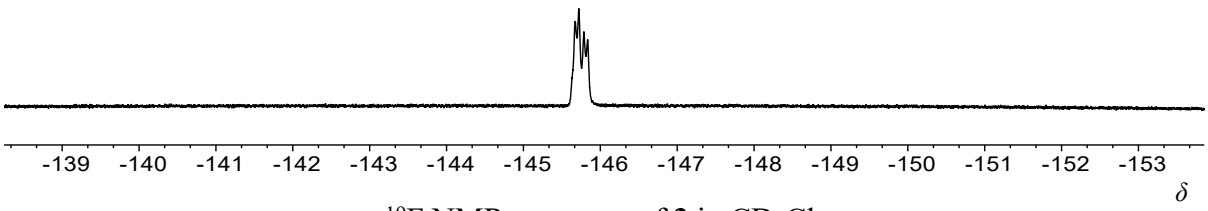

^{19}F NMR spectrum of **3** in CD_2Cl_2

Compound 4: Compound **4** (0.56 g, 56%) was obtained as a dark purple solid. ^{1}H NMR (500 MHz, CD_2Cl_2) δ 8.18 (d, *J* = 9.0 Hz, 1H), 7.79 (d, *J* = 7.4 Hz, 2H), 7.74 (t, *J* = 7.9 Hz, 1H), 7.70 (d, *J* = 9.1 Hz, 2H), 7.47 (t, *J* = 7.6 Hz, 1H), 7.31 (d, *J* = 9.0 Hz, 1H), 7.00 (d, *J* = 9.1 Hz, 2H), 4.05 (t, *J* = 6.5 Hz, 2H), 1.86 – 1.77 (m, 2H), 1.51 – 1.44 (m, 2H), 1.40 – 1.22 (m, 16H), 0.88 (t, *J* = 6.7 Hz, 3H). ^{13}C NMR (151 MHz, CD_2Cl_2) δ 161.30, 143.58, 142.81, 139.39, 138.06, 133.88, 129.79, 126.18, 126.14, 126.10, 125.90, 125.21, 118.52, 115.28, 114.42, 68.98, 32.34, 30.08, 30.05, 30.02, 29.99, 29.78, 29.77, 29.56, 26.38, 23.11, 14.29. ^{19}F NMR (565 MHz, CD_2Cl_2) δ -145.75 (dd, *J* = 64.6, 27.1 Hz). Hi-Res ESI-MS: m/z found [M+H$^+$] for $C_{29}H_{36}BF_2N_4O^+$ 505.2943 (calcd. 505.2950).

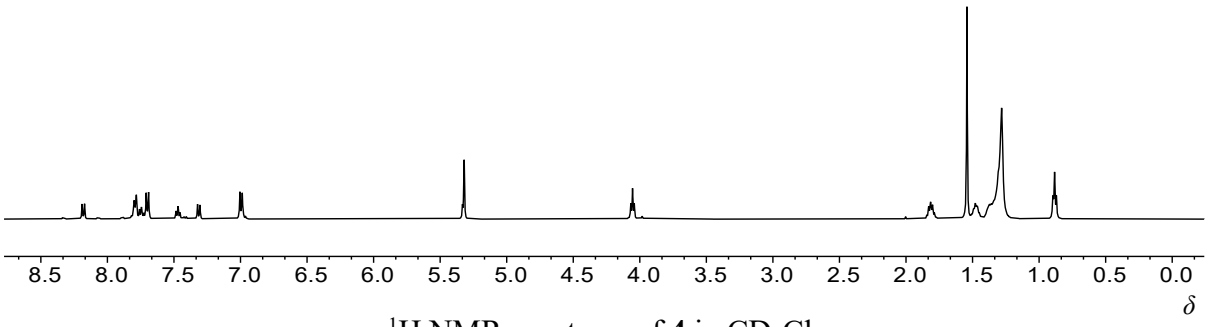

^{1}H NMR spectrum of **4** in CD_2Cl_2

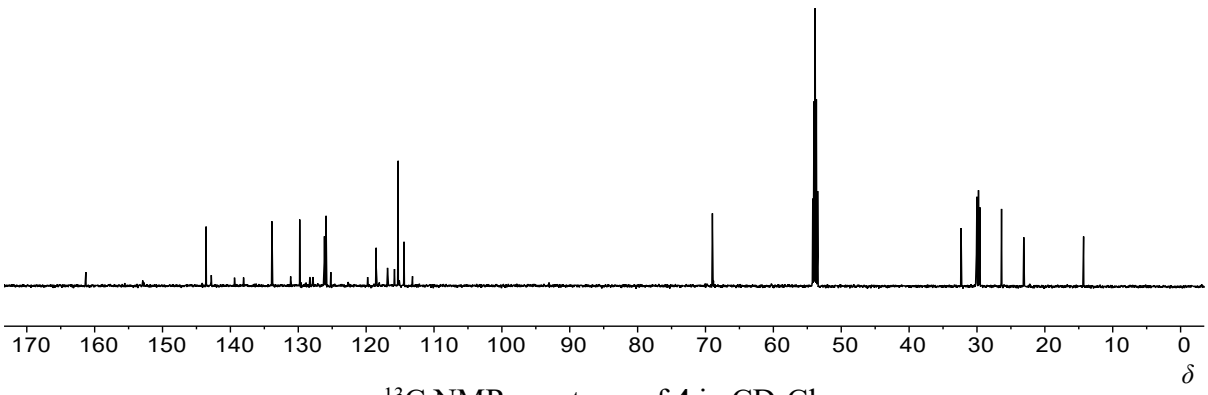

^{13}C NMR spectrum of **4** in CD_2Cl_2

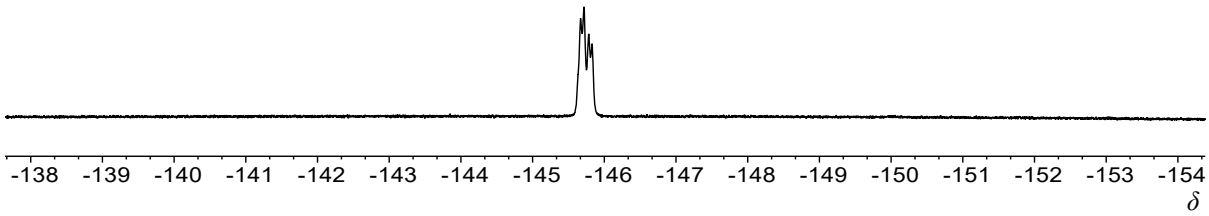

^{19}F NMR spectrum of **4** in CD_2Cl_2

Compound 5: Compound **5** was synthesized following the general procedure used for the Azo-BF_2s with hydrazone **H-di6C** (0.384 g, 0.5 mmol) as the starting material. The product was further purified by flash column chromatography (SiO_2) eluting with a mixed solvent of ethyl acetate and hexane (1:4, v/v) to give compound **5** (0.15 g, 58%) as a dark purple solid. ^{1}H NMR (600 MHz, CD_2Cl_2) δ 8.13 (d, *J* = 9.0 Hz, 1H), 7.74 (d, *J* = 9.3 Hz, 1H), 7.63 (d, *J* = 8.7 Hz, 2H), 7.39 (dd, *J* = 9.3, 2.7 Hz, 1H), 7.30 (d, *J* = 9.0 Hz, 1H), 7.13 (d, *J* = 2.7 Hz, 1H), 6.98 (d, *J* = 8.8 Hz, 2H), 4.13 – 3.99 (m, 4H), 1.88 – 1.77 (m, 4H), 1.52 – 1.44 (m, 4H), 1.42 – 1.30 (m, 8H), 0.96 – 0.86 (m, 6H). ^{13}C NMR (151 MHz, CD_2Cl_2) δ 160.72, 157.22, 150.88, 143.04, 142.74, 134.62, 126.66, 125.65, 125.61, 125.57, 125.33, 119.99, 115.16, 114.56, 109.54, 69.18, 68.90, 31.98, 31.95, 29.56, 29.43, 26.07, 26.04, 23.03, 23.01, 14.22, 14.20. ^{19}F NMR (565 MHz, CD_2Cl_2) δ -144.93 (d, *J* = 55.2 Hz). Hi-Res ESI-MS: m/z found [M+H$^+$] for $C_{29}H_{36}BF_2N_4O_2^+$ 521.2896 (calcd. 521.2899).

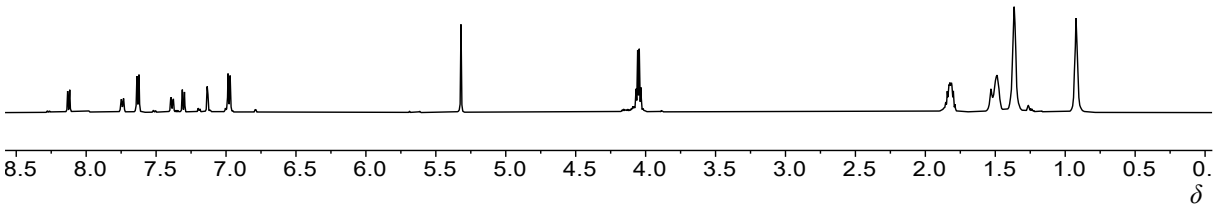

^{1}H NMR spectrum of **5** (contains a small percentage of the *cis* isomer as well) in CD_2Cl_2

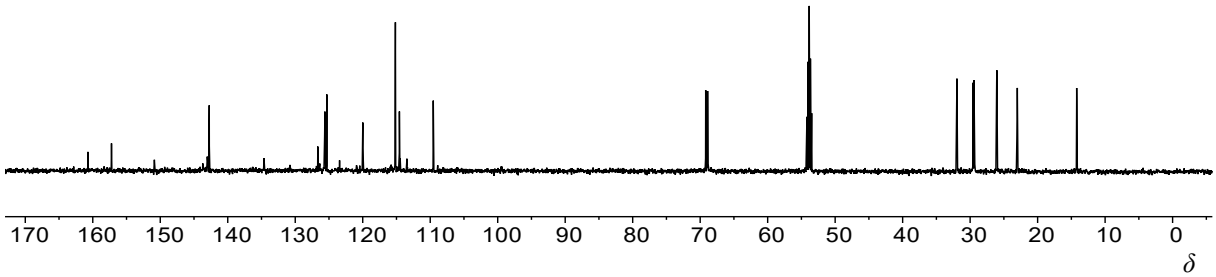

^{13}C NMR spectrum of **5** (contains a small percentage of the *cis* isomer as well) in CD_2Cl_2

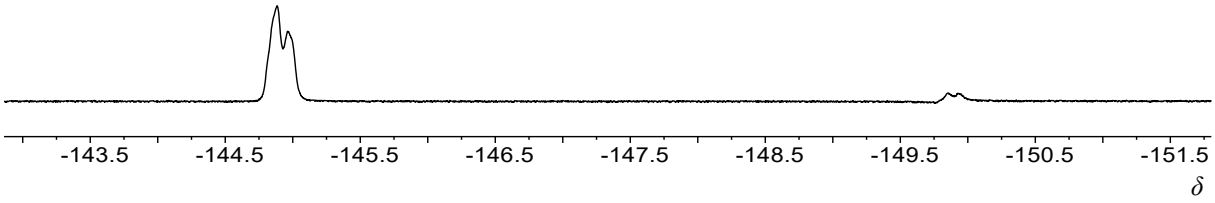

^{19}F NMR spectrum of **5** (contains a small percentage of the *cis* isomer as well) in CD_2Cl_2

3. Photoswitching properties in solution state

UV-Vis spectroscopy was employed to study the photoisomerization of all the azo-BF_2s (**1-5**) in DCM solution. **1**-*E* (3.0 mL, 2.0×10^{-5} M) and **2-5**-*E* solution (3.0 mL, 3.0×10^{-5} M) in DCM was prepared and transferred into a d=1.0 cm quartz cuvette. The solutions were then irradiated with 625 nm and 470 nm under stirring at 20 °C. The changes of UV-Vis absorption spectra were recorded and the photostationary states (PSS) were determined upon continuous irradiation of the sample until no further isomerization was observed using the UV-Vis spectroscopy.

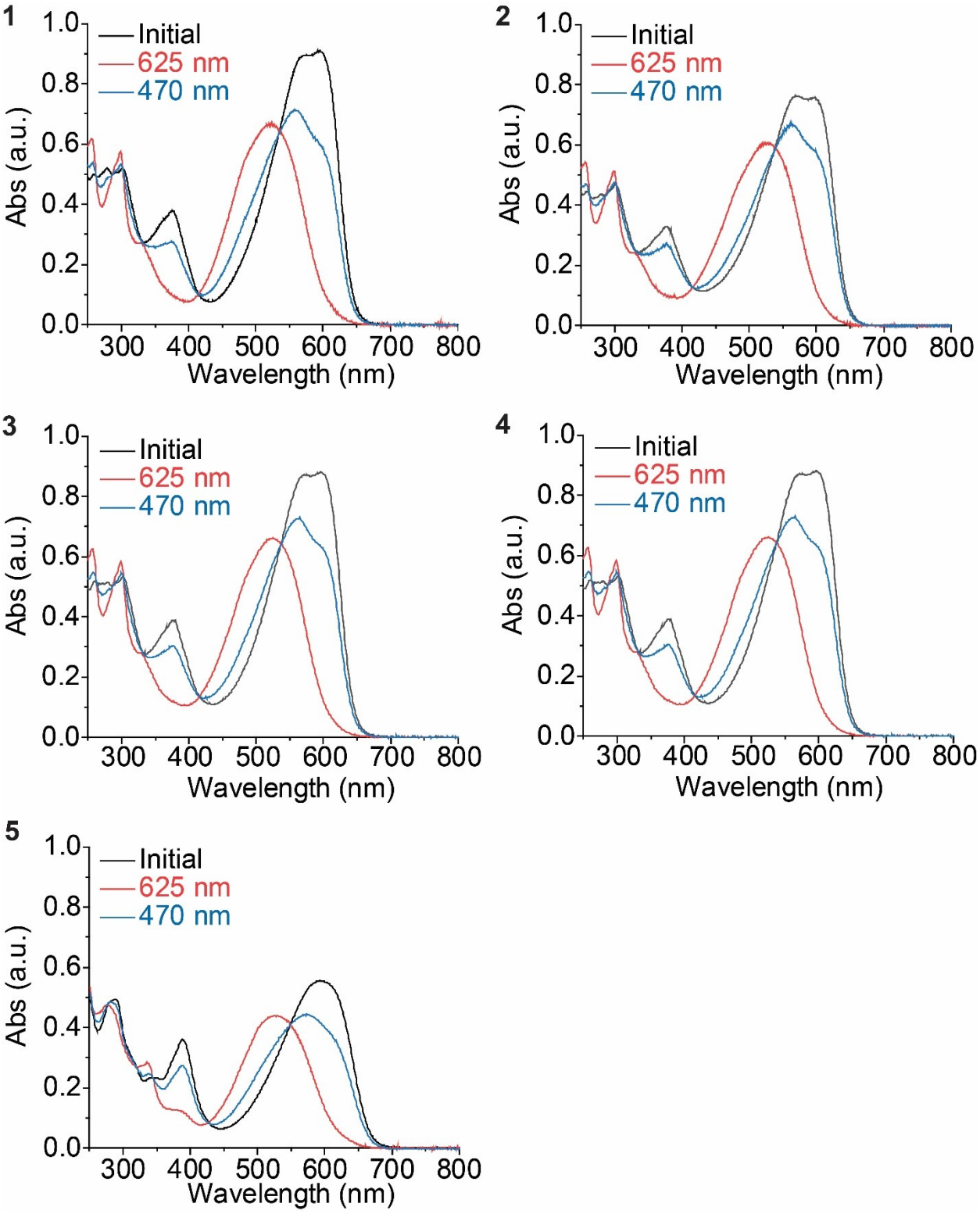

Fig. S1. UV-Vis spectral changes upon the photoisomerization of compounds **1-5** in DCM. (Black trace: Initial; Red trace: PSS_{625}, Blue trace: PSS_{470}

4. Evaluation of photostationary states

^{1}H NMR spectroscopy was employed to study the photostationary states (PSSs) of **1-5** in solutions. The PSS was determined upon continuous irradiation of the sample until no further isomerization was observed using ^{1}H NMR spectroscopy.

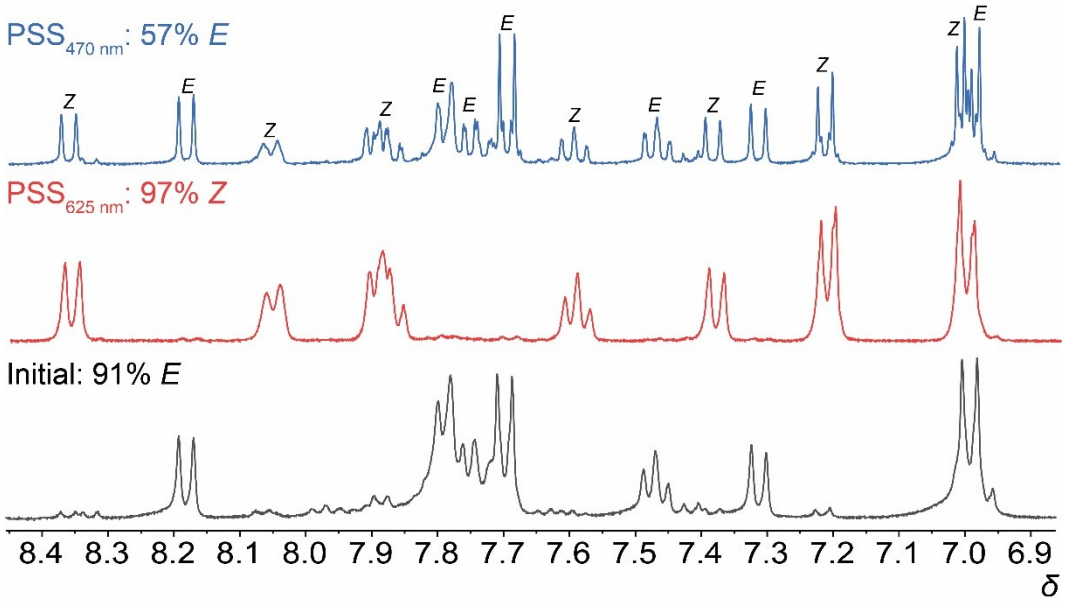

Fig. S2. ^{1}H NMR spectra of initial **1**, PSS at 625 nm, and PSS at 470 nm in CD_2Cl_2 at 294 K. The peaks corresponding to *E* and *Z* isomer are labeled for the mixture at PSS_{470}.

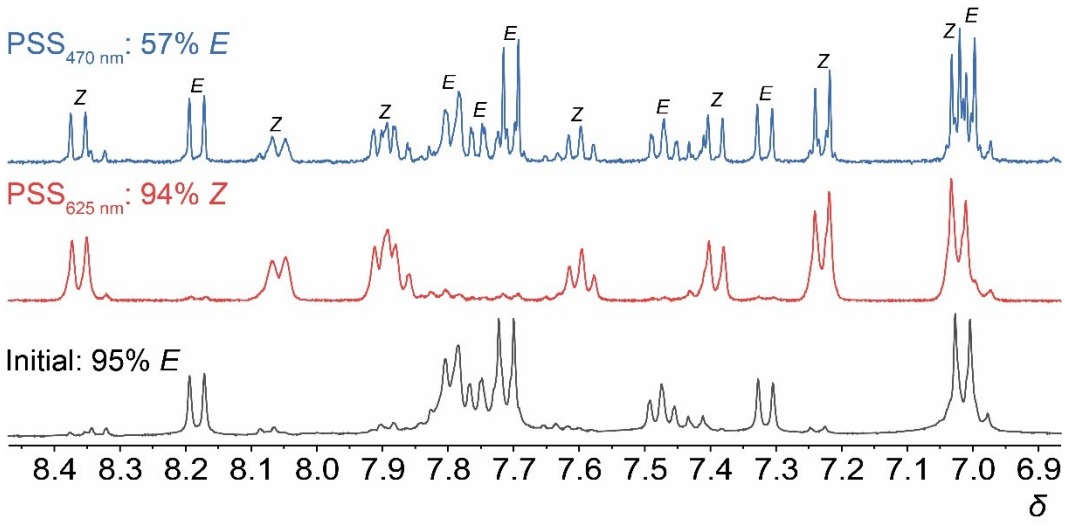

Fig. S3. ^{1}H NMR spectra of initial **2**, PSS at 625nm, and PSS at 470 nm in CD_2Cl_2 at 294 K. The peaks corresponding to *E* and *Z* isomer are labeled for the mixture at PSS_{470}.

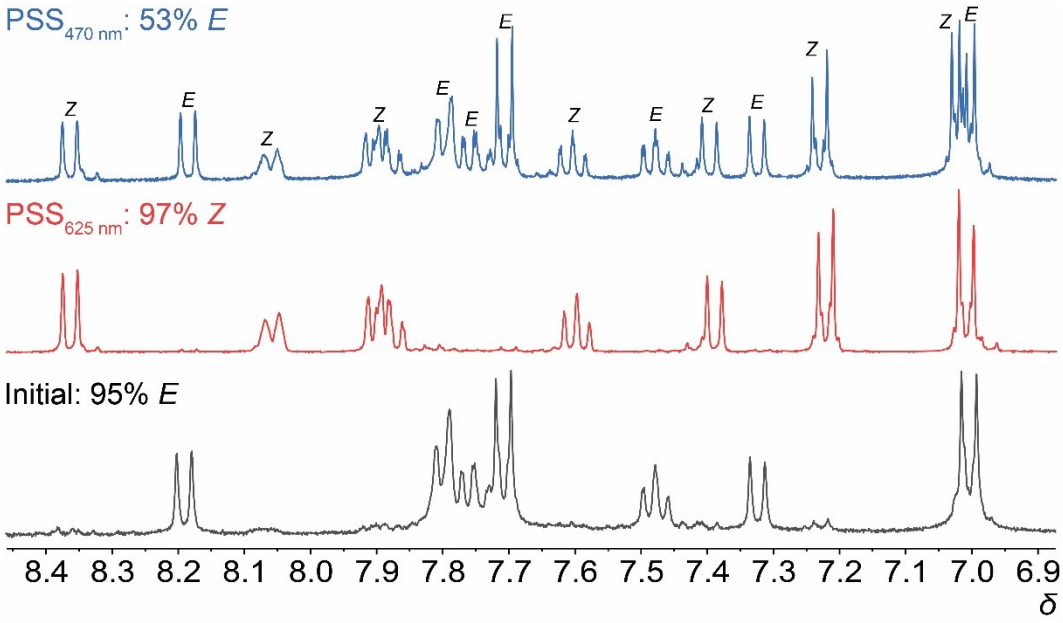

Fig. S4. ^{1}H NMR spectra of initial **3**, PSS at 625 nm, and PSS at 470 nm in CD_2Cl_2 at 294 K. The peaks corresponding to *E* and *Z* isomer are labeled for the mixture at PSS_{470}.

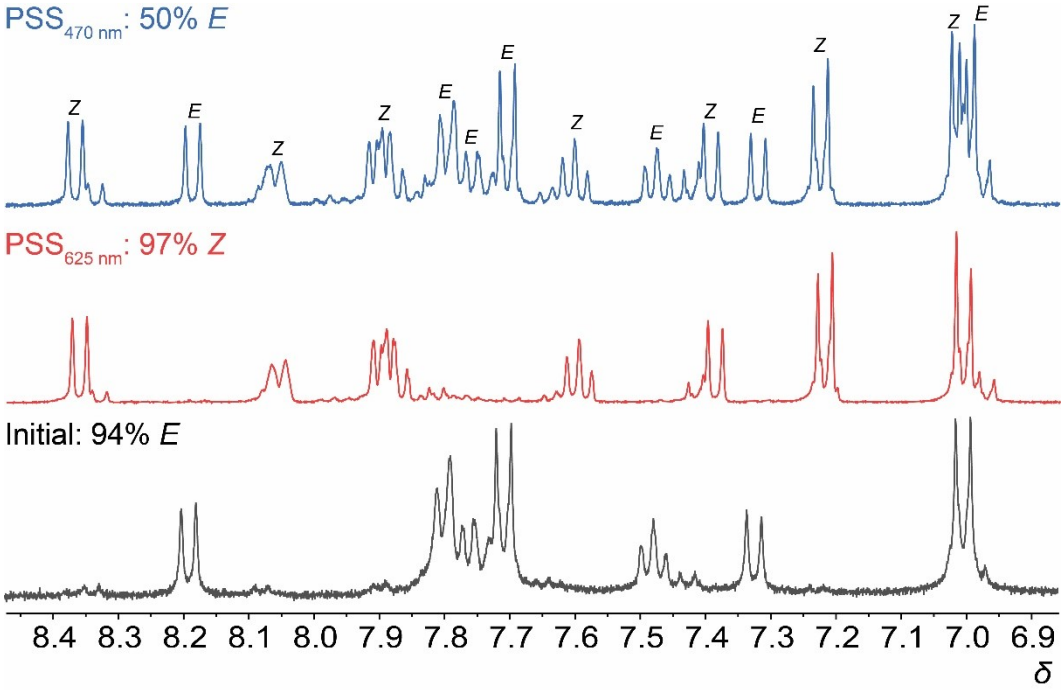

Fig. S5. ^{1}H NMR spectra of initial **4**, PSS at 625 nm, and PSS at 470 nm in CD_2Cl_2 at 294 K. The peaks corresponding to *E* and *Z* isomer are labeled for the mixture at PSS_{470}.

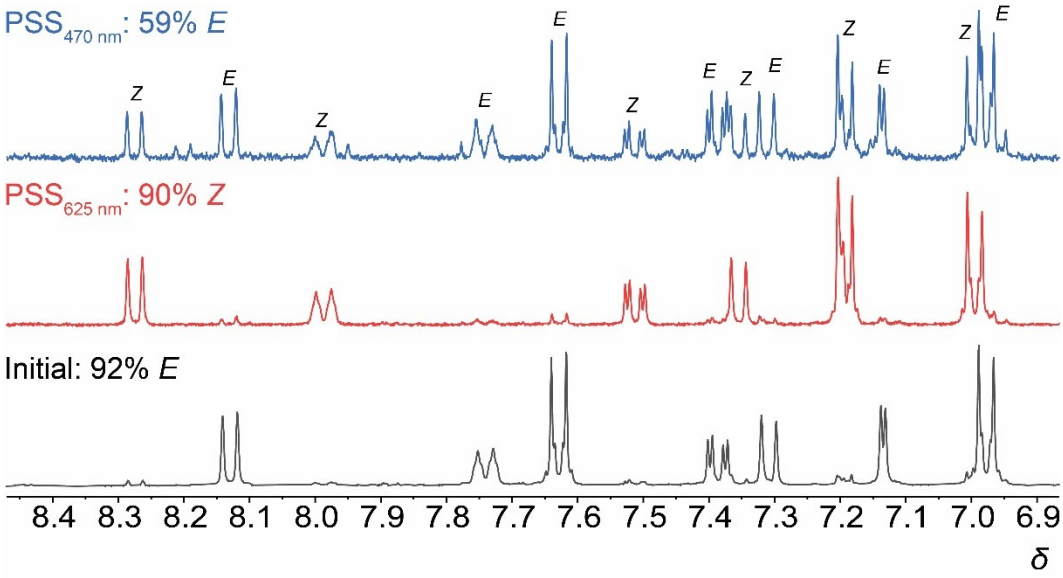

Fig. S6. ^{1}H spectra of initial **5**, PSS at 625 nm, and PSS at 470 nm in CD_2Cl_2 at 294 K. The peaks corresponding to *E* and *Z* isomer are labeled for the mixture at PSS_{470}.

5. Photoisomerization quantum yield

Quantum yield measurement: Irradiations were conducted with a stand-alone xenon arc lamp system (Model: LB-LS/30, Sutter Instrument Co.), outfitted with a SMART SHUTTER controller (Model: LB10-B/IQ, Sutter Instrument Co.) and a liquid light guide LLG/250. 340 (part number: 340HC10-25), 365 (part number: 365HC10-25), 375 (part number: 375HC10-25), 410 (part number: 410FS10-25), 442 (part number: 442F5X10-25), and 480 (part number: 480HC10-25) nm light filters, purchased from Andover Corporation, were used in the irradiation experiments.

The molar photon flux I_0 at 480 nm was determined using chemical actinometry.[3] A 2 mL (= V_0) solution of potassium ferrioxalate in 0.05 M H_2SO_4 was placed into a 1.0 cm cuvette and irradiated for 30 s (= t_0). The irradiated solution was combined with 3.5 equiv. of ferrozine and stirred under dark for an hour. The resulting solution, containing reddish-purple $[Fe(ferrozine)_3]^{2+}$ complex was diluted by a factor of n, and its absorbance was measured at 563 nm (A_{563}), where its molar absorption coefficient (ε_{563}) is 27,900 cm^{-1} M^{-1}. The molar photon flux of the light source at different wavelengths was determined using Eq. 1.

$$I_0\left(quanta \cdot s^{-1}\right) = \frac{A_{563} \cdot n \cdot N_A \cdot V_0}{\varepsilon_{563} \cdot l \cdot t_0 \cdot \phi_\lambda} \qquad \text{Eq. 1}$$

where l indicates the length of the cuvette; ϕ_λ stands for the quantum yield of the photo-reduction of Fe(III) oxalate induced by the light source (ϕ_{480} = 0.94), and N_A stands for Avogadro's number.

The photoisomerization quantum yields were measured using a previously reported method.[3]

$$A \underset{k_r}{\overset{k_f}{\rightleftharpoons}} B$$

In a photochemical reaction, species ***A*** absorbs light to generate product ***B***. The general kinetics of a basic photochemical reaction can be expressed using Eq. 2.

$$r_{A\to B} = \frac{I_0 \Phi_{A\to B}}{V}\left(1 - 10^{-\varepsilon_A C_A l}\right) \qquad \text{Eq. 2}$$

When $\varepsilon_A \cdot C_A \cdot l \cdot \ln 10 << 1$ (or $Abs_A << 0.43$), the Taylor expansion can be truncated at the first-order term, simplifying Eq. 2 to Eq. 3, which is related to the quantum yield, an observed first-order rate constant, molar photon flux, and the measurable properties of sample ***A***.

$$k_{A\to B} = \frac{I_0 \Phi_{A\to B}}{V} \varepsilon_A \cdot l \cdot \ln 10 \qquad \text{Eq. 3}$$

Rearranging Eq. 3 gives Eq. 4,

$$\Phi_{A\to B} = \frac{k_{A\to B} V}{I_0 \varepsilon_A l \ln 10} \qquad \text{Eq. 4}$$

where $\Phi_{A\to B}$ is the photoisomerization yield going from ***A*** to ***B***; $k_{A\to B}$ represents the rate constant (obtained from the exponential fit of a graph of *Abs* vs. time); V indicates sample volume; I_0 indicates molar photon flux; ε_A indicates molar absorption coefficient of sample ***A***, and l indicates light path length.

The rate law for the formation of ***B*** is,

$$C_B = \frac{k_f}{k_f + k_r} C_{total}(1 - e^{-(k_f + k_r)t}) \qquad \text{Eq. 5}$$

where $C_{total} = C_A + C_B$ is the total concentration of the photoswitches and k_f and k_r are the first-order approximate rate constants for the forward and reverse photochemical reactions under the low absorption approximation discussed above.

$$C_A = \frac{C_{total} \cdot k_r}{k_f + k_r} + \frac{C_{total} \cdot k_f}{k_f + k_r} e^{-(k_f + k_r)t} \qquad \text{Eq. 6}$$

C_A is proportional to the absorbance of species ***A***. An exponential fit of absorbance as a function of time was performed to give the observed rate constant $k_{obs} = k_f + k_r$. An exponential fit of absorbance as a function of time was performed to give the observed rate constant k_{obs} =

$k_f + k_r$. Thus, $k_{A\rightarrow B} = k_{obs} - k_r$. k_r can be measured by fitting the thermal back isomerization curve of ***B*** at 294 K.

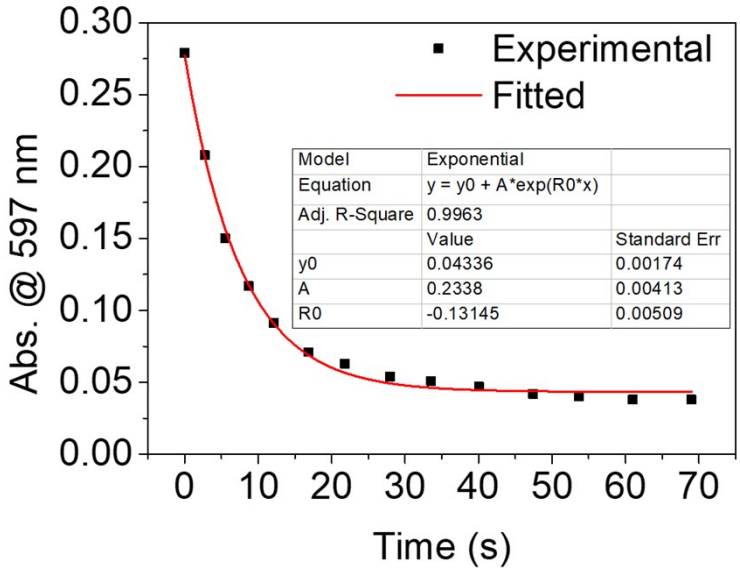

Fig. S7. Kinetics for the photoisomerization (irradiation at 650 nm) of **1**-*E* in DCM (1×10^{-5} M) at 298 K; the plot is of the absorbance (λ = 597 nm) as a function of time. $\varepsilon_{\mathbf{1}\text{-}E@650\ nm}$ = 1900 $M^{-1}\cdot cm^{-1}$ was used for quantum yield calculations. The photoisomerization quantum yield was calculated to be 95 ± 2% based on three consecutive measurements.

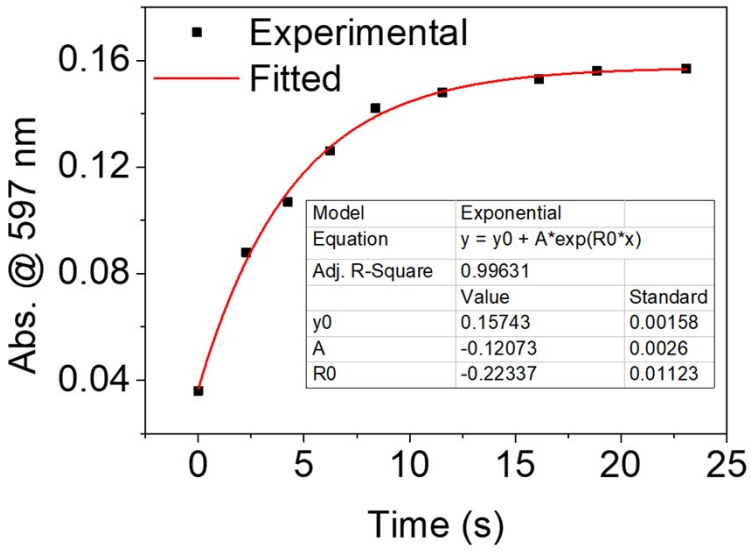

Fig. S8. Kinetics for the photoisomerization (irradiation at 480 nm) of **1**-*Z* in DCM (1×10^{-5} M) at 298 K; the plot is of the absorbance (λ = 597 nm) as a function of time. $\varepsilon_{\mathbf{1}\text{-}Z@480\ nm}$ = 13900 $M^{-1}\cdot cm^{-1}$ was used for quantum yield calculations. The photoisomerization quantum yield was calculated to be 84 ± 1.6% based on three consecutive measurements.

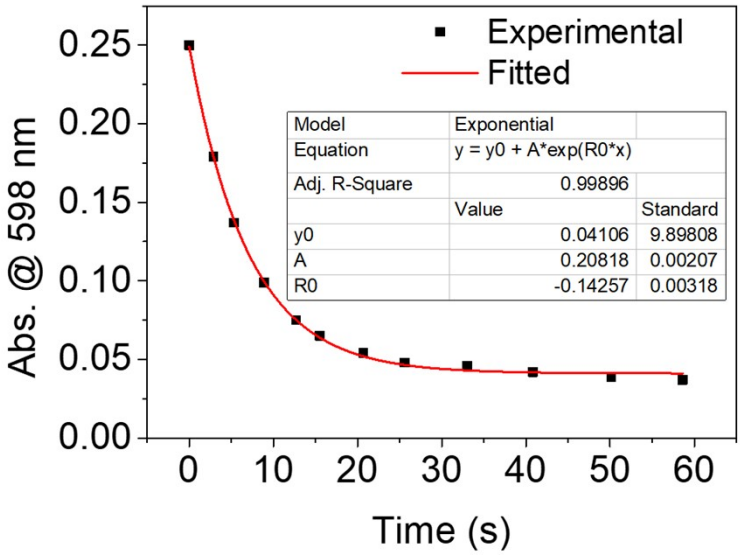

Fig. S9. Kinetics for the photoisomerization (irradiation at 650 nm) of **2**-*E* in DCM (1×10^{-5} M) at 298 K; the plot is of the absorbance ($\lambda = 598$ nm) as a function of time. $\varepsilon_{\mathbf{2}\text{-}E@650\ \text{nm}} = 2100\ \text{M}^{-1}\cdot\text{cm}^{-1}$ was used for quantum yield calculations. The photoisomerization quantum yield was calculated to be 97 ± 2% based on three consecutive measurements.

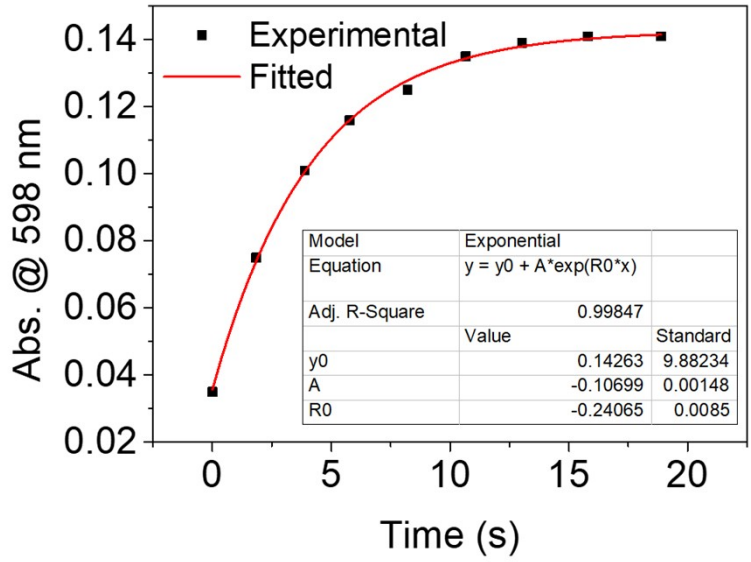

Fig. S10. Kinetics for the photoisomerization (irradiation at 480 nm) of **2**-*Z* in DCM (1×10^{-5} M) at 298 K; the plot is of the absorbance ($\lambda = 598$ nm) as a function of time. $\varepsilon_{\mathbf{2}\text{-}Z@480\ \text{nm}} = 13000\ \text{M}^{-1}\cdot\text{cm}^{-1}$ was used for quantum yield calculations. The photoisomerization quantum yield was calculated to be 96 ± 1.6% based on three consecutive measurements.

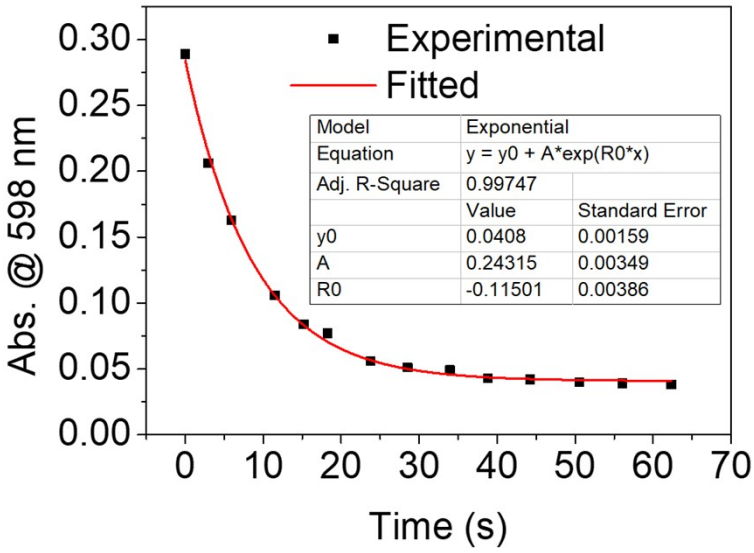

Fig. S11. Kinetics for the photoisomerization (irradiation at 650 nm) of **3**-*E* in DCM (1×10^{-5} M) at 298 K; the plot is of the absorbance ($\lambda = 598$ nm) as a function of time. $\varepsilon_{\mathbf{3}\text{-}E@650\ \text{nm}} = 2100\ \text{M}^{-1}\cdot\text{cm}^{-1}$ was used for quantum yield calculations. The photoisomerization quantum yield was calculated to be 85 ± 2% based on three consecutive measurements.

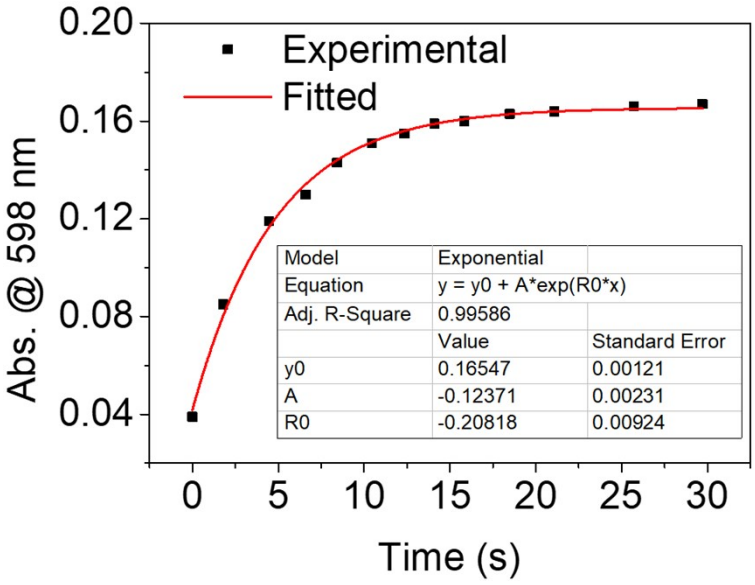

Fig. S12. Kinetics for the photoisomerization (irradiation at 480 nm) of **3**-*Z* in DCM (1×10^{-5} M) at 298 K; the plot is of the absorbance ($\lambda = 598$ nm) as a function of time. $\varepsilon_{\mathbf{3}\text{-}Z@480\ \text{nm}} = 14400\ \text{M}^{-1}\cdot\text{cm}^{-1}$ was used for quantum yield calculations. The photoisomerization quantum yield was calculated to be 76 ± 1.6% based on three consecutive measurements.

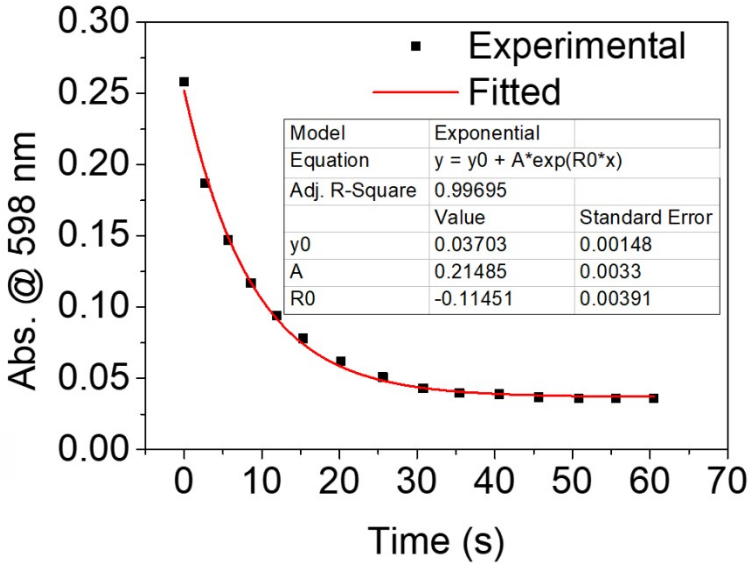

Fig. S13. Kinetics for the photoisomerization (irradiation at 650 nm) of **4**-*E* in DCM (1×10^{-5} M) at 298 K; the plot is of the absorbance (λ = 598 nm) as a function of time. $\varepsilon_{\mathbf{4}\text{-}E@650\ \text{nm}}$ = 1900 $M^{-1} \cdot cm^{-1}$ was used for quantum yield calculations. The photoisomerization quantum yield was calculated to be 94 ± 2% based on three consecutive measurements.

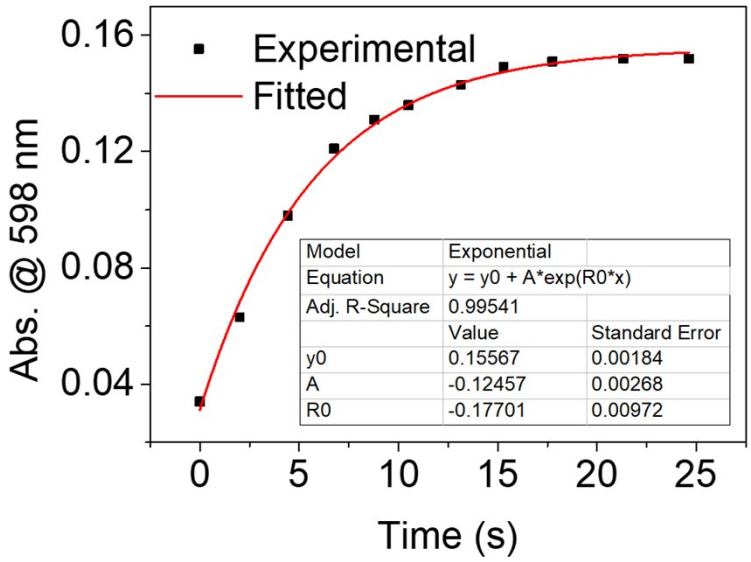

Fig. S14. Kinetics for the photoisomerization (irradiation at 480 nm) of **4**-*Z* in DCM (1×10^{-5} M) at 298 K; the plot is of the absorbance (λ = 598 nm) as a function of time. $\varepsilon_{\mathbf{4}\text{-}Z@480\ \text{nm}}$ = 14000 $M^{-1} \cdot cm^{-1}$ was used for quantum yield calculations. The photoisomerization quantum yield was calculated to be 66 ± 1.6% based on three consecutive measurements.

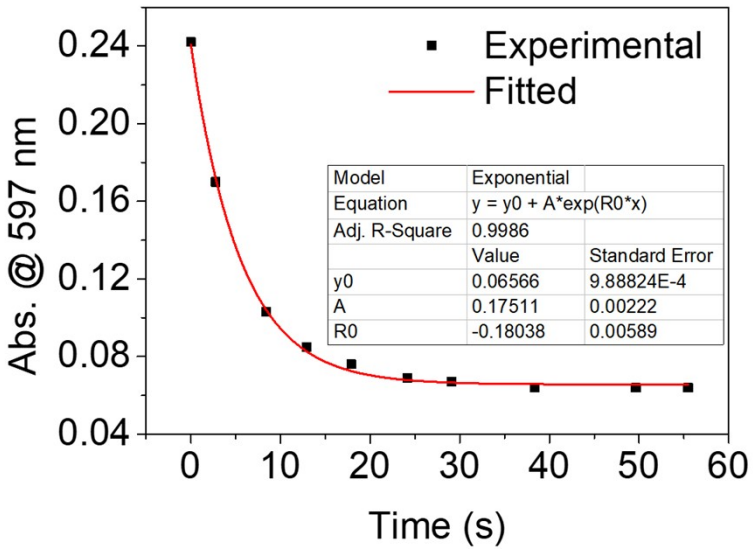

Fig. S15. Kinetics for the photoisomerization (irradiation at 650 nm) of **5**-*E* in DCM (1×10^{-5} M) at 298 K; the plot is of the absorbance ($\lambda = 597$ nm) as a function of time. $\varepsilon_{\mathbf{5}\text{-}E@650\text{ nm}} = 8500\ M^{-1}\cdot cm^{-1}$ was used for quantum yield calculations. The photoisomerization quantum yield was calculated to be 35 ± 2% based on three consecutive measurements.

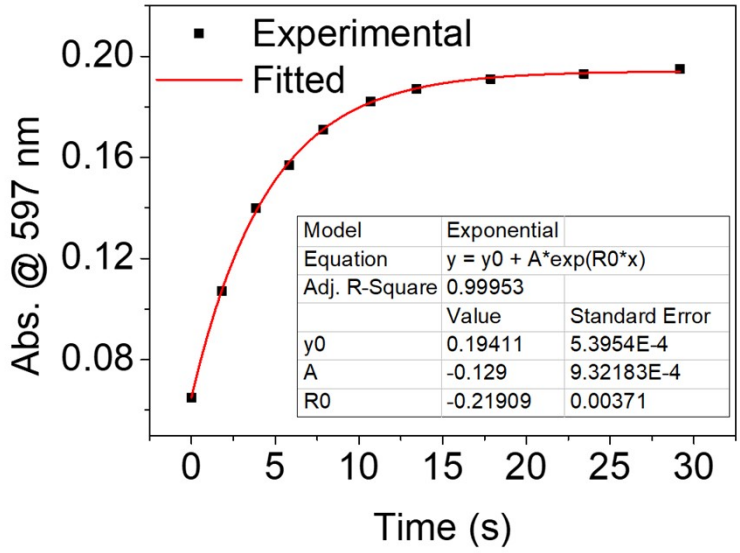

Fig. S16. Kinetics for the photoisomerization (irradiation at 480 nm) of **5**-*Z* in DCM (1×10^{-5} M) at 298 K; the plot is of the absorbance ($\lambda = 597$ nm) as a function of time. $\varepsilon_{\mathbf{5}\text{-}Z@480\text{ nm}} = 12600\ M^{-1}\cdot cm^{-1}$ was used for quantum yield calculations. The photoisomerization quantum yield was calculated to be 85 ± 5% based on three consecutive measurements.

Table S1. A summary of photoisomerization analysis data of azo-BF_2 compounds. Quantum yields were measured with lights of 650 nm and 480 nm

Comp.	λ_E (nm)	λ_Z (nm)	$\Phi_{E\rightarrow Z}$	$\Phi_{Z\rightarrow E}$	%*Z* PSS_{650}	%*E* PSS_{480}	%*Z* PSS_{625}	%*E* PSS_{470}	In dark
1	596	520	95%	84%	62%	72%	97%	57%	91%
2	598	529	97%	96%	80%	64%	94%	57%	95%
3	599	524	85%	76%	93%	50%	97%	53%	95%
4	598	524	94%	66%	92%	50%	97%	50%	94%
5	597	525	35%	85%	66%	71%	90%	59%	92%

6. Thermal reversion kinetics in solutions

The thermal half-life of compounds **1-5** in solutions, and compound **5** in the condensed phase were determined by following reported procedures.[2]

Dichloromethane solutions of compounds **1-5** (3×10^{-5} M) were prepared and stored under dark. 3 mL of solutions were transferred into 1.0 cm quartz cuvettes, respectively and irradiated at 625 nm for 1 min to obtain *Z*-rich solutions while stirring. Once the PSSs were reached, the solutions were left at 20 ℃ under dark to monitor the $Z \rightarrow E$ thermal relaxation by measuring the change in absorbance at 597 nm as a function of time.

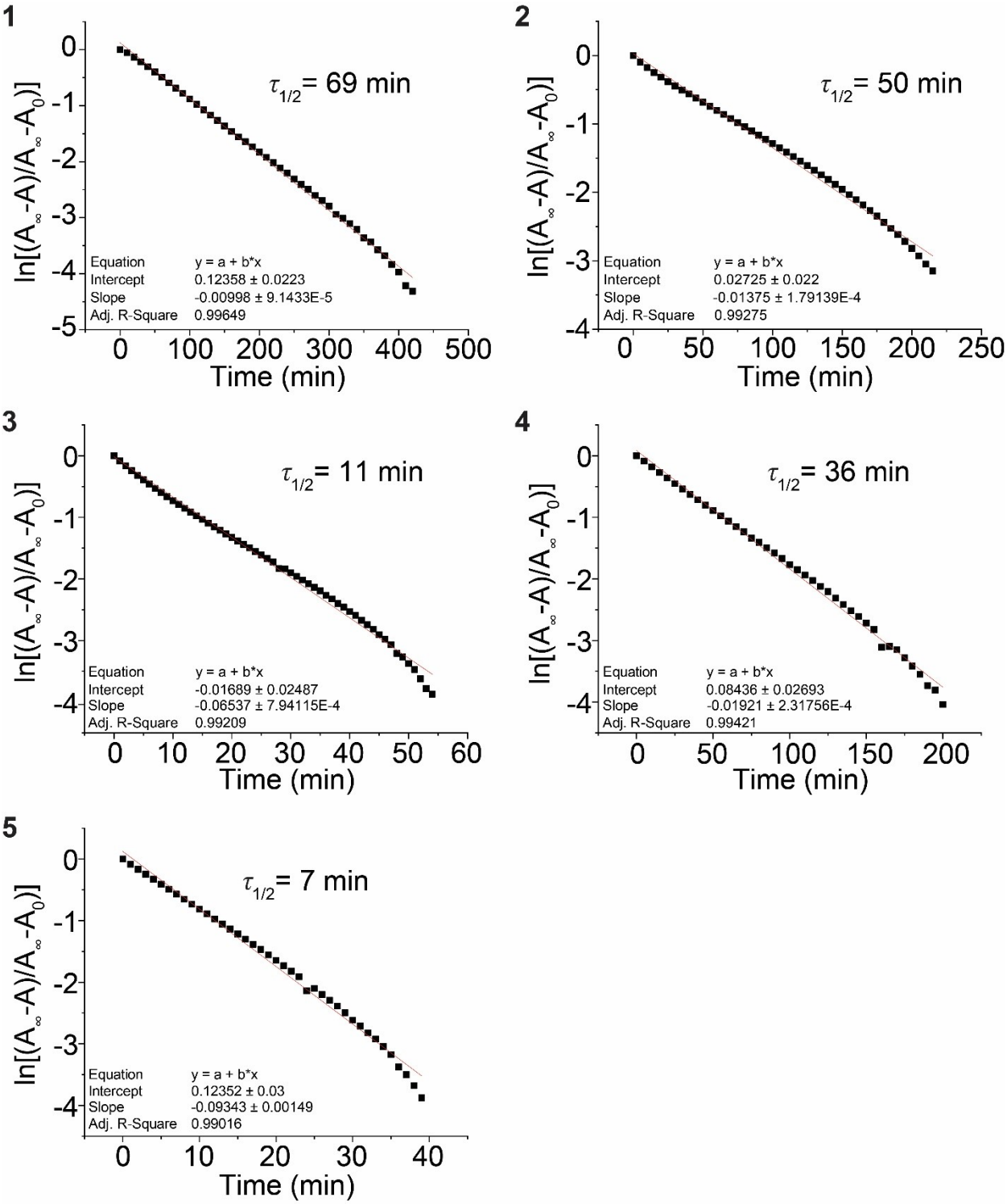

Fig. S17. Plots of $\ln[(A_\infty-A)/(A_\infty-A_0)]$ as a function of time showing the first-order decay of compounds **1**-**5** in DCM at 20 °C. A_∞ and A_0 stand for the absorbance at the beginning and end of thermal isomerization, respectively. The black dots represent experimental data, the red lines are the linear fitting curves.

Table S2. Summary of the rate of $Z \rightarrow E$ relaxation, energy barrier and half-life at 293 K in DCM solutions of Azo-BF_2 compounds.

Compound	Experimental Temperature	k (min^{-1})	$\Delta G^{\neq}$ (kJ mol^{-1})	$\tau_{1/2}$ (min)
1	293 K	1.0 E−3	92.9	69
2	293 K	1.4 E−2	92.1	50
3	293 K	6.5 E−2	88.3	11
4	293 K	1.9 E−2	91.3	36
5	293 K	9.3 E−2	87.5	7

7. Thermogravimetric analysis

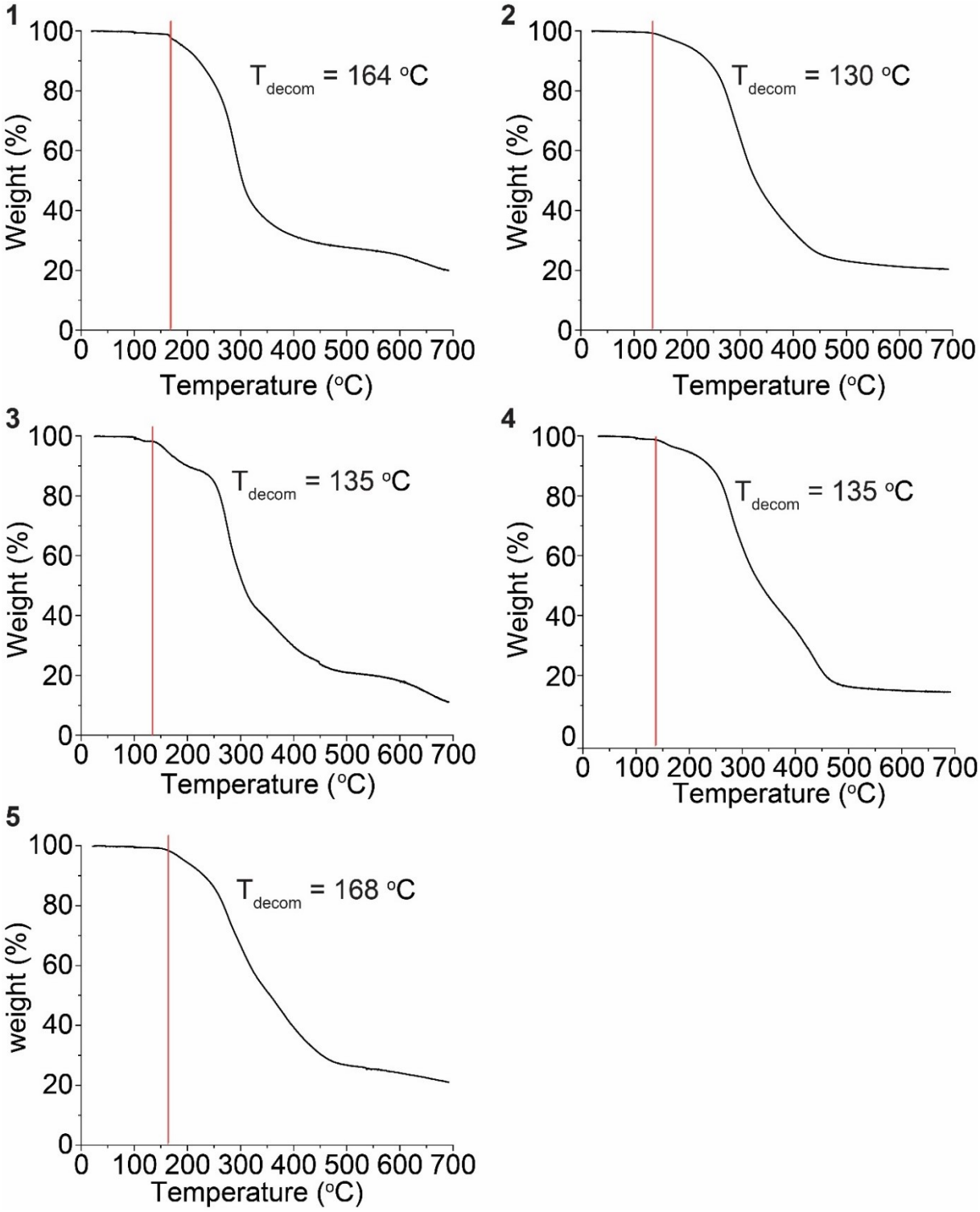

Fig. S18. TGA plots of compounds **1-5** measured at 20 °C/min showing the thermal stability of compound **1** = 164 °C, compound **2** = 130 °C, compound **3** = 135 °C, compound **4** = 135 °C, and compound **5** = 168 °C.

8. Differential scanning calorimetry (DSC) plots

DSC analysis was conducted on a DSC 250 (TA Instruments) with an RSC 90 cooling component. All DSC experiments were performed with a scan rate of 10 °C/min (unless otherwise specified). *E* isomers of compounds **1-5** were melted and cooled to −90 °C before reheating. Solid *Z* isomers of compounds **1-5** were heated before thermal reversion and cooled to −90 °C. To determine the ΔH_{iso} of *Z* isomers of compounds **1-5**, samples were heated from 20 °C until the thermal isomerization was completed. The scan rate was 10 °C/min except for **5** *Z*→*E* thermal reversion in which a scan rate of 5 °C/min was used.

Preparation of *Z*-isomer samples for DSC measurement: Z isomers were obtained by dissolving E isomers in dichloromethane and irradiating the sample with a 625 nm LED until a photostationary state (PSS) was reached. Z-rich samples were concentrated, dried under high-vacuum, and then transferred to DSC pans for analysis.

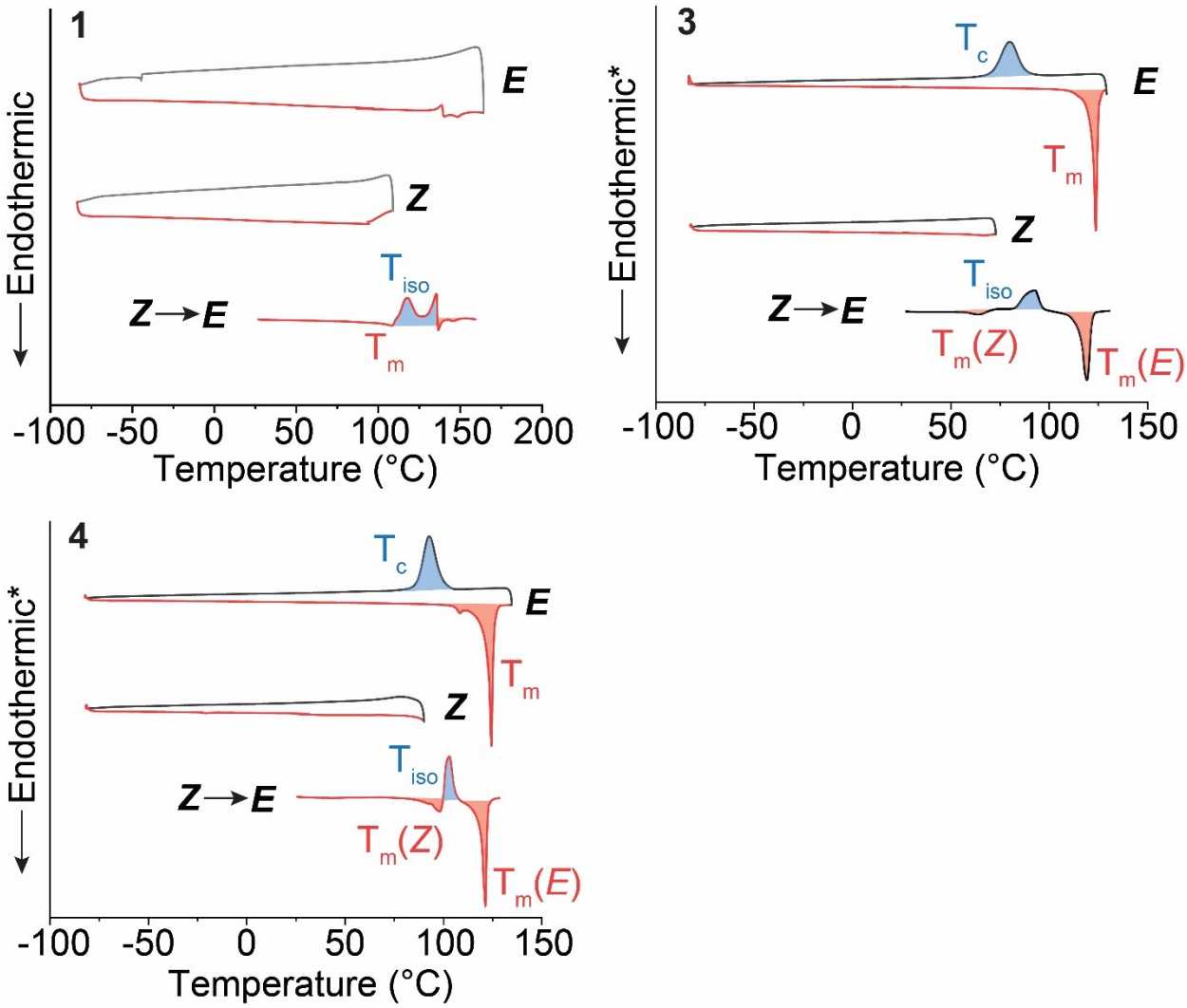

Fig. S19. DSC plots illustrating thermal properties of *E* (top curve), and *Z* (middle curve), and thermal reversion from *Z*→*E* (bottom curve) isomers for compounds **1, 3** and **4**. The following thermal parameters are labeled in plots: melting temperature (T_m), crystallization temperature (T_c), onset temperature of *Z*→*E* thermal isomerization (T_{iso}), and glass transition temperature (T_g). The heating curves are shown in red; the cooling curves are shown in grey. The integrated exothermal enthalpy of compound **1** is a combination of melting of *Z* and thermal isomerization of *Z*→*E*; compound **3** is a combination of melting of Z, thermal isomerization of *Z*→*E*, and crystallization of new-formed *E*; compound **4** is same as **3**. The scale of y axis (* marked) of **3** and **4** is 4 times larger than that of **1.**

9. Powder X-ray diffraction

X-ray powder diffraction in the 2θ range 0-50° (step size, 0.014°; time/step, 20 s; 0.04 rad Soller; 40 mA × 60 kV) was collected on a Panalytical Empyrean diffractometer equipped with a GaliPIX3D line detector and in Bragg-Brentano geometry, using Mo-Kα radiation (λ=0.7093187 ˚A) without a monochromator. Around 5 mg samples were loaded into capillary tubes (outer diameter = 0.7 mm) and the measurements were carried out on the capillary spinner.

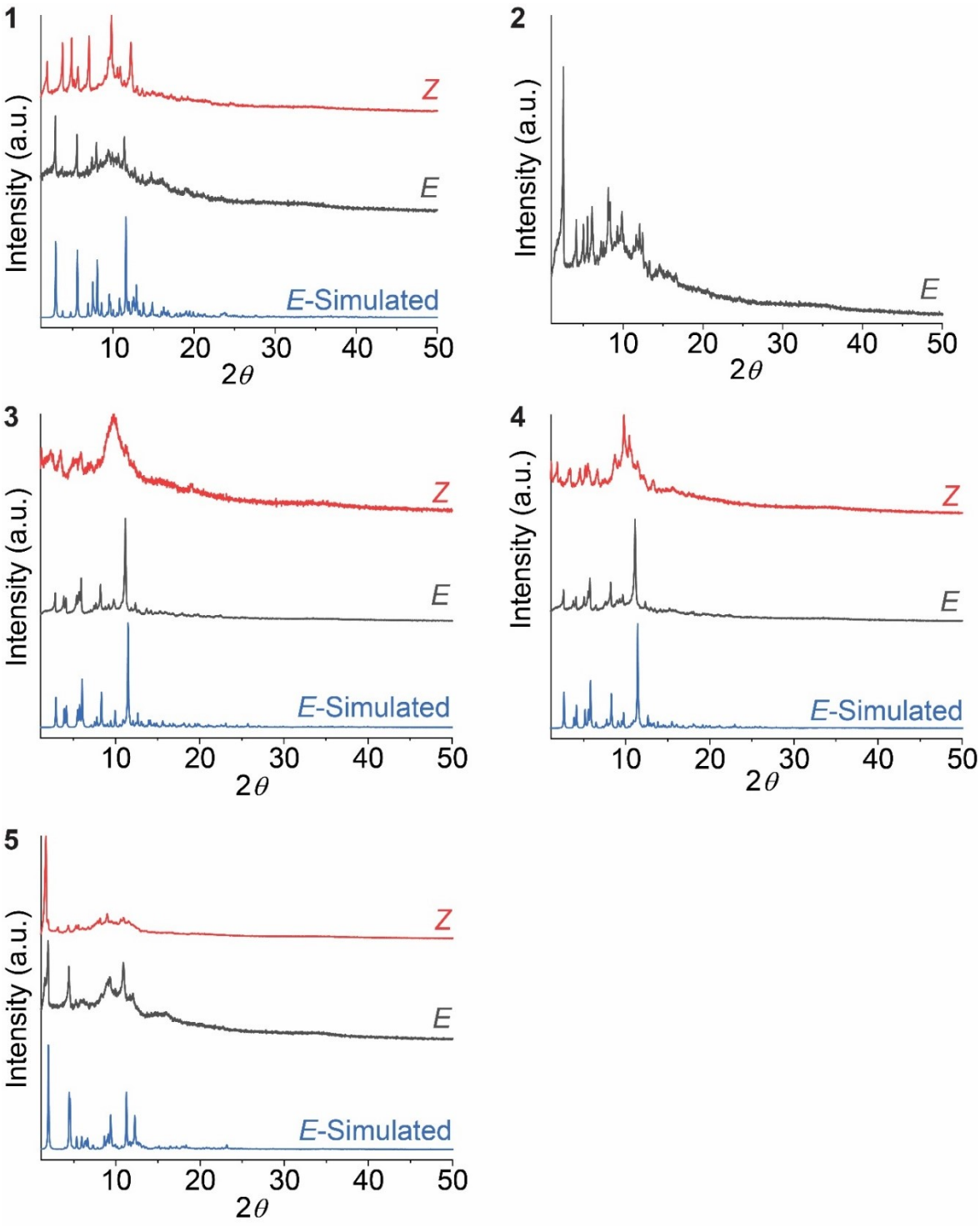

Fig. S20. Powder XRD patterns of *E*-Simulated (blue) from single crystal XRD, *E* (grey) and *Z* (red) isomers of compounds **1**-**5**. The pattern of *E*-simulated and **2**-*Z* unavailable due to its difficulty of growing single crystal and high viscosity hindering sample preparation.

10. Density Functional Theory (DFT) calculation

Geometry optimization of the series of Azo-BF_2 derivatives (**1**, **5**, and pristine Azo-BF_2 (R1 = R2 = H)) and azobenzene were carried out using DFT with B3LYP[4] and 6-31+G* basis set implemented in the Gaussian16 Revision B.01[5] with default thresholds and algorithms. The stationary points were optimized without any symmetry assumptions and characterized by frequency analysis at the same level of theory (the number of imaginary frequencies, NIMAG, was 0). The cartesian coordinates for the optimized geometry are given in Fig. S21 and Tables S4–S11. ΔH_{iso} (kJ/mol) was defined as the enthalpy difference between *E* and *Z* isomers in a vacuum state. The enthalpies were calculated by the frequency analysis of its optimized geometry without zero-point correction. The enthalpies estimated from DFT calculations and DSC are summarized in Table S3.

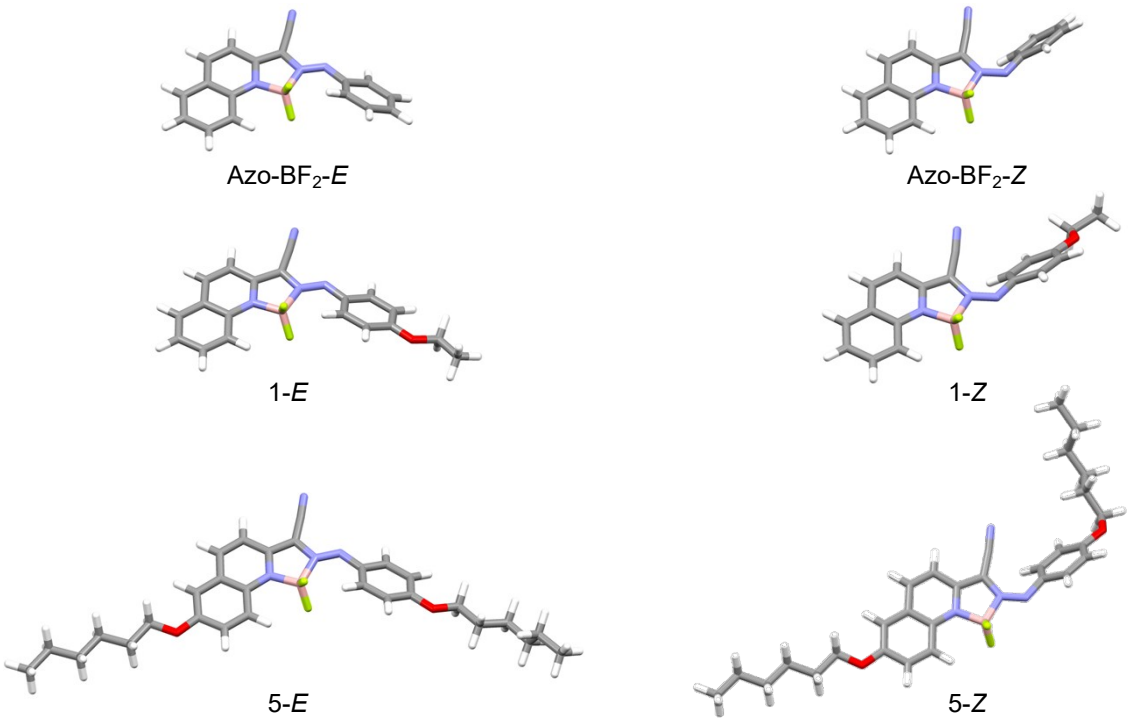

Fig. S21. Optimized structures of Azo-BF_2, compounds **1** and **5** at the B3LYP/6-31+G* level of theory.

Table S3. Cartesian coordinates (Å) of the optimized geometry for *E*-Azo-BF_2.

N	-1.34301	0.08330	-0.00872	C	4.21767	-2.03199	0.56792
B	0.08322	-0.56797	0.12283	C	3.11811	-1.18121	0.62140
N	0.96033	0.82899	0.09885	F	0.19049	-1.19481	1.34305
C	0.07492	1.88531	0.11309	F	0.41652	-1.35183	-0.94278
C	-1.26531	1.43455	0.05373	C	0.47193	3.23859	0.12322
C	-2.44380	2.22999	0.05133	N	0.73558	4.37477	0.13754
C	-3.65600	1.60291	-0.00783	H	-2.35042	3.30894	0.09959
C	-3.75396	0.17761	-0.07273	H	-4.57242	2.18755	-0.00748
C	-2.54698	-0.58071	-0.07321	H	-5.90742	0.08130	-0.13764
C	-4.99020	-0.50202	-0.13979	H	-5.98564	-2.39799	-0.25793
C	-5.03227	-1.88118	-0.20744	H	-3.86763	-3.70230	-0.27659
C	-3.83066	-2.61838	-0.21568	H	-1.68123	-2.55994	-0.17516
C	-2.60092	-1.98776	-0.15240	H	4.42625	1.46015	-1.08234
N	2.21028	1.08035	-0.02419	H	6.37725	-0.08809	-1.20682
C	3.18337	0.07987	-0.00691	H	6.23672	-2.33222	-0.13250
C	4.38391	0.47093	-0.63818	H	4.16276	-2.99833	1.06173
C	5.46687	-0.39685	-0.70089	H	2.23648	-1.47500	1.17297
C	5.38729	-1.65570	-0.09875				

Table S4. Cartesian coordinates (Å) of the optimized geometry for *Z*-Azo-BF_2.

N	-1.50844	-0.13848	0.00952	C	4.85996	0.69949	-1.16727
B	-0.51947	-1.37765	0.01545	C	5.85350	0.22349	-0.30938
N	0.86598	-0.53203	0.09020	C	5.52763	-0.70357	0.68516
C	0.59456	0.81868	0.13979	C	4.21858	-1.15300	0.82038
C	-0.82255	1.01915	0.10521	C	1.48473	1.89013	0.35792
C	-1.50439	2.26351	0.16695	N	2.12281	2.84923	0.54825
C	-2.87177	2.26392	0.12371	H	-0.92802	3.17785	0.24866
C	-3.61031	1.04724	0.01753	H	-3.41753	3.20294	0.16973
C	-2.88147	-0.17642	-0.04018	H	-5.57462	1.94184	0.01212
C	-5.02267	1.00655	-0.03276	H	-6.77044	-0.22575	-0.17420
C	-5.68575	-0.19947	-0.13650	H	-5.47923	-2.34858	-0.27952
C	-4.95106	-1.40320	-0.19533	H	-3.00969	-2.32966	-0.20119
C	-3.56962	-1.40354	-0.14989	H	2.77727	0.63824	-1.70503
N	1.93544	-1.22520	0.11836	H	5.11156	1.40353	-1.95524
F	-0.58060	-2.07117	-1.15828	H	6.87910	0.56253	-0.42378
F	-0.68029	-2.13650	1.13663	H	6.29910	-1.08826	1.34629
C	3.20738	-0.63572	-0.00778	H	3.95055	-1.89435	1.56649
C	3.53938	0.28313	-1.01942				

Table S5. Cartesian coordinates (Å) of the optimized geometry for **1**-*E*.

F	-0.64796	-1.00471	-1.35080	N	-2.37846	-0.01326	0.01307
F	-0.38048	-1.10277	0.93092	N	-1.09923	4.58353	-0.06842
O	5.76212	-1.13681	-0.13197	C	-1.31289	2.01699	-0.08396
N	-0.25036	1.13144	-0.11925	C	-2.54546	1.33376	-0.01254
N	0.93743	1.60556	-0.03114	C	-3.84928	1.90257	0.03228

H	-3.95226	2.98162	0.01275	H	1.39919	-0.99412	-1.08861
C	-4.92683	1.06708	0.09494	C	3.47562	-1.08958	-0.62575
H	-5.93325	1.47668	0.12751	H	3.60996	-2.08159	-1.04531
C	-4.76607	-0.35529	0.12012	C	4.60230	-0.43619	-0.09096
C	-5.85851	-1.24665	0.18816	C	4.46962	0.86515	0.41755
H	-6.86500	-0.83702	0.21911	H	5.32188	1.40081	0.81830
C	-5.65293	-2.61316	0.21534	C	3.22552	1.48069	0.39191
H	-6.49765	-3.29319	0.26697	H	3.10354	2.49109	0.76849
C	-4.33968	-3.12239	0.17946	C	6.95789	-0.53687	0.37737
H	-4.18036	-4.19664	0.20681	H	6.81718	-0.27625	1.43534
C	-3.24409	-2.27930	0.11347	H	7.17024	0.38823	-0.17594
H	-2.23701	-2.67843	0.09859	C	8.08114	-1.54407	0.20811
C	-3.44320	-0.88379	0.07766	H	9.01966	-1.12500	0.58626
C	-1.16135	3.41835	-0.07366	H	8.21478	-1.79949	-0.84758
C	2.07879	0.81970	-0.09656	H	7.86252	-2.46264	0.76129
C	2.23434	-0.48245	-0.63266	B	-0.86194	-0.39409	-0.13415

Table S6. Cartesian coordinates (Å) of the optimized geometry for **1**-*Z*.

F	1.94263	-2.19733	1.07140	H	4.19146	-2.16141	-0.44446
F	1.71105	-2.04755	-1.20884	C	3.93007	-0.03715	-0.13594
O	-6.18532	-0.16190	0.04365	C	-0.52678	1.68865	0.64638
N	0.23216	-0.66739	0.18117	C	-2.09977	-0.97225	0.17500
N	-0.78260	-1.44068	0.21981	C	-3.04346	-1.73987	0.89201
N	2.56289	-0.09974	-0.00702	H	-2.68313	-2.56739	1.49471
N	-1.21894	2.58171	0.94288	C	-4.38930	-1.43144	0.84528
C	0.41301	0.70002	0.29352	H	-5.11799	-1.99761	1.41629
C	1.80666	1.00028	0.19582	C	-4.84542	-0.37902	0.03010
C	2.40811	2.28415	0.29730	C	-3.92609	0.34793	-0.73949
H	1.77801	3.14970	0.46707	H	-4.25537	1.14112	-1.39972
C	3.76675	2.38310	0.18016	C	-2.56645	0.05978	-0.65763
H	4.25066	3.35370	0.25495	H	-1.87658	0.61300	-1.28424
C	4.57792	1.22882	-0.04230	C	-6.72565	0.90147	-0.74661
C	5.98389	1.29054	-0.17284	H	-6.49812	0.72579	-1.80735
H	6.47369	2.25821	-0.09985	H	-6.26126	1.85236	-0.45175
C	6.71960	0.14233	-0.38849	C	-8.22505	0.92900	-0.50955
H	7.79953	0.19502	-0.48722	H	-8.68270	1.73073	-1.09887
C	6.06474	-1.10390	-0.48323	H	-8.44507	1.10558	0.54779
H	6.64856	-2.00332	-0.65686	H	-8.68009	-0.02194	-0.80348
C	4.69115	-1.20364	-0.36218	B	1.66393	-1.40495	-0.00418

Table S7. Cartesian coordinates (Å) of the optimized geometry for **5**-*E*.

F	0.24142	0.20388	1.43184	N	2.15719	2.52617	0.00912
F	0.44664	0.01079	-0.85052	N	-1.35683	1.39639	0.07007
O	6.53284	-0.89228	0.08847	N	0.55702	5.76606	0.02008
O	-6.07295	-1.52401	-0.03130	C	-0.01062	3.25563	0.10199
N	0.91495	2.23032	0.13570	C	-1.33177	2.75156	0.06975

C	-2.54449	3.49284	0.03890
H	-2.49840	4.57603	0.03665
C	-3.73023	2.81432	0.01693
H	-4.66917	3.36177	-0.00400
C	-3.77125	1.38388	0.01970
C	-4.98722	0.66163	-0.00693
H	-5.91747	1.21791	-0.02628
C	-4.97298	-0.72453	-0.00884
C	-3.73322	-1.41050	0.00989
H	-3.75347	-2.49564	0.00043
C	-2.53684	-0.72876	0.03465
H	-1.59775	-1.26895	0.03542
C	-2.53401	0.68411	0.04623
C	0.33502	4.62077	0.05449
C	3.17364	1.58329	0.07262
C	4.38968	2.05162	-0.46772
H	4.40585	3.05613	-0.87802
C	5.52940	1.25917	-0.50142
H	6.43855	1.65020	-0.94248
C	5.48627	-0.03018	0.05073
C	4.29290	-0.49252	0.63655
H	4.29286	-1.47935	1.08871
C	3.15417	0.29086	0.65203
H	2.26713	-0.07780	1.14649
C	7.78618	-0.49258	-0.47369
H	8.15042	0.41002	0.03767
H	7.65384	-0.24921	-1.53764
C	8.76282	-1.64684	-0.29763
H	8.82382	-1.88682	0.77017
H	8.35235	-2.53341	-0.79849
C	10.15233	-1.32007	-0.86346
H	10.56682	-0.44775	-0.33671
H	10.04729	-1.01920	-1.91555
C	11.15631	-2.48217	-0.78300
H	10.74397	-3.35435	-1.31172
H	12.06395	-2.19619	-1.33290
C	11.55453	-2.89385	0.64140
H	11.93367	-2.01216	1.17821
H	10.66918	-3.23151	1.19590
C	12.61390	-4.00078	0.66518
H	13.53105	-3.68311	0.15396
H	12.25231	-4.90608	0.16210
H	12.88233	-4.27546	1.69151
C	-7.36525	-0.91451	-0.05136
H	-7.45939	-0.27515	-0.94159
H	-7.48784	-0.27715	0.83681
C	-8.40496	-2.02612	-0.06928
C	-9.84102	-1.48671	-0.09222
H	-10.00633	-0.84352	0.78473
H	-9.97800	-0.84273	-0.97345
C	-10.89905	-2.59768	-0.10972
H	-10.73432	-3.24175	-0.98602
H	-10.76266	-3.24235	0.77098
C	-12.33904	-2.06947	-0.13277
H	-12.47431	-1.42512	-1.01312
H	-12.50259	-1.42563	0.74314
C	-13.38934	-3.18469	-0.15002
H	-14.40594	-2.77596	-0.16642
H	-13.30209	-3.82532	0.73611
H	-13.27340	-3.82494	-1.03313
B	0.09484	0.80887	0.20213
H	-8.22546	-2.65952	-0.94739
H	-8.25417	-2.66092	0.81321

Table S8. Cartesian coordinates (Å) of the optimized geometry for **5**-*Z*.

F	-0.37037	-3.08251	1.00698
F	-0.49137	-3.10371	-1.28642
O	7.65603	-1.46845	0.20393
O	-6.60281	-0.65534	0.11786
N	1.23337	-1.69739	-0.23284
N	2.21581	-2.51347	-0.27115
N	-1.08004	-1.04050	-0.12762
N	2.85058	1.52609	-0.72022
C	1.11484	-0.32083	-0.27260
C	-0.27173	0.03466	-0.22657
C	-0.81964	1.34318	-0.28134
H	-0.15102	2.19217	-0.36704
C	-2.17924	1.49111	-0.22819
H	-2.61920	2.48435	-0.26995
C	-3.04554	0.36172	-0.11685
C	-4.45461	0.48577	-0.05617
H	-4.88838	1.47831	-0.09763
C	-5.24560	-0.64614	0.05316
C	-4.63571	-1.92647	0.10818
H	-5.28368	-2.79248	0.19828
C	-3.26905	-2.07227	0.05244
H	-2.81637	-3.05525	0.10322
C	-2.44728	-0.92741	-0.06554
C	2.10982	0.64582	-0.51604
C	3.54696	-2.10363	-0.14107
C	4.01516	-1.14478	0.77420
H	3.31923	-0.60483	1.40577
C	5.37868	-0.91051	0.92644
H	5.70213	-0.16752	1.64535
C	6.30634	-1.61990	0.14973
C	5.84634	-2.60220	-0.74667
H	6.57826	-3.15914	-1.32267
C	4.49350	-2.85828	-0.86663
H	4.13175	-3.63281	-1.53539
C	8.23618	-0.45000	1.02831
H	9.27656	-0.76629	1.15108

H	7.77224	-0.45689	2.02355	H	-6.98173	1.22999	0.90014
C	8.17566	0.93597	0.38643	C	-8.79273	0.29305	0.14935
H	8.63888	0.86902	-0.60486	C	-9.64769	1.56598	0.09771
H	7.12963	1.22595	0.22482	H	-9.35945	2.23628	0.92094
C	8.88046	1.99560	1.24653	H	-9.43445	2.11447	-0.83166
H	9.93782	1.71929	1.37441	C	-11.15310	1.28211	0.18182
H	8.44044	1.98752	2.25424	H	-11.44219	0.61081	-0.64013
C	8.79495	3.42521	0.68607	H	-11.36773	0.73436	1.11119
H	7.73787	3.70309	0.56339	C	-12.01679	2.54877	0.12911
H	9.20617	4.11745	1.43446	H	-11.80124	3.09545	-0.79997
C	9.53348	3.64236	-0.64214	H	-11.72669	3.21924	0.95059
H	10.58157	3.32951	-0.52716	C	-13.51854	2.25774	0.21361
H	9.10473	2.99623	-1.41920	H	-14.10730	3.18108	0.17341
C	9.48387	5.09838	-1.11716	H	-13.77064	1.74234	1.14852
H	9.94080	5.77161	-0.38122	H	-13.84570	1.61770	-0.61496
H	8.44940	5.42936	-1.27032	B	-0.23340	-2.38078	-0.15761
H	10.01839	5.22826	-2.06501	H	-9.06365	-0.37754	-0.67608
C	-7.30235	0.59019	0.06478	H	-8.98868	-0.25623	1.07904
H	-7.05864	1.11092	-0.87294				

Table S9. Cartesian coordinates (Å) of the optimized geometry for *E*-azobenzene.

H	0.33590	3.15010	0.00000	N	0.00259	-0.63037	-0.00000
C	1.29015	2.63190	0.00000	C	-1.28292	-1.23071	-0.00000
C	3.69893	1.22361	0.00000	C	-3.70403	-2.62457	-0.00000
C	1.28292	1.23071	0.00000	C	-2.49807	-0.52391	-0.00000
C	2.49807	3.32749	0.00000	C	-1.29015	-2.63190	-0.00000
C	3.70403	2.62457	0.00000	C	-2.49807	-3.32749	-0.00000
C	2.49807	0.52391	0.00000	C	-3.69893	-1.22361	-0.00000
H	2.49893	4.41398	0.00000	H	-2.47233	0.56005	0.00000
H	4.64796	3.16321	0.00000	H	-0.33590	-3.15010	-0.00000
H	2.47233	-0.56005	0.00000	H	-2.49893	-4.41398	-0.00000
H	4.64002	0.67970	0.00000	H	-4.64002	-0.67970	-0.00000
N	-0.00259	0.63037	0.00000	H	-4.64796	-3.16321	-0.00000

Table S10. Cartesian coordinates (Å) of the optimized geometry for *E*-azobenzene.

N	0.62457	1.93972	-0.01509	H	2.05513	-2.00554	1.95148
C	1.43145	0.75504	0.06658	H	3.97900	-2.15723	0.38452
C	3.26724	-1.34133	0.29511	N	-0.62452	1.93972	0.01516
C	1.26032	-0.22039	1.06019	C	-1.43143	0.75506	-0.06656
C	2.54645	0.70084	-0.78059	C	-3.26729	-1.34123	-0.29514
C	3.44355	-0.36068	-0.68449	C	-1.26043	-0.22027	-1.06033
C	2.18407	-1.25742	1.17390	C	-2.54631	0.70079	0.78072
H	0.42000	-0.15598	1.74331	C	-3.44343	-0.36072	0.68462
H	2.68935	1.49407	-1.50858	C	-2.18424	-1.25723	-1.17408
H	4.29300	-0.41092	-1.36024	H	-0.42020	-0.15577	-1.74355

H	-2.68909	1.49391	1.50884	H	-2.05544	-2.00525	-1.95179
H	-4.29279	-0.41105	1.36048	H	-3.97909	-2.15709	-0.38456

Table S11. Summary of ΔH_{iso} (kJ/mol)

Compound	R_1	R_2	DSC Measurements [a]	DFT Calculations [b]
Azo-BF_2	H	H	n.d.	19
1	OC_2H_5	H	7	21
5	OC_6H_{13}	OC_6H_{13}	3	25
azobenzene	-	-	49[6]	62

[a]: $\Delta H_{storage}$ (kJ/mol) of measured by DSC.

[b]: $\Delta H_{storage}$ (kJ/mol) calculated by DFT calculations at the B3LYP/6-31+G* level of theory.

11. Thin film preparation and characterization

Thin-film samples were prepared by adding 20 µL of 25 mg/mL dichloromethane solution of *E* isomers on a clean glass slide (2.5 × 2.5 cm^2) and spin coated until solvent was totally evaporated. Then the films were irradiated with Thorlabs LEDs M625L4 (625 nm, 21.9 µW/mm^2, 920 mW) for 10 min or M470L4 (470 nm, 19.9 µW/mm^2, 965 mW) for 2 minutes to get PSSs states films, which were further characterized by UV-vis spectroscopy. The thickness of thin films was measured using Zeta-20 Optical Profilometer.

11.1 Film thickness

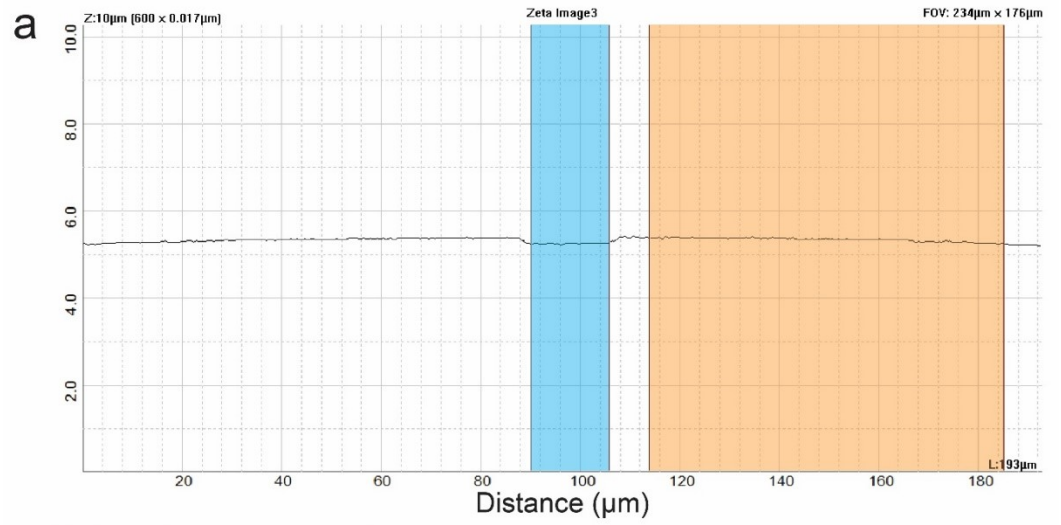

Measurement	1	2	3	4	5	6	7	8	**Average**
Thickness (µm)	0.27	0.21	0.07	0.11	0.09	0.14	0.19	0.18	**0.16**

Fig. S22. (a) Thickness measurement of compound **1** film; (b) Optical microscopic image of the measure area; (c) 3D topography of the measured area. The glass slide surface area is highlighted in blue, measured film area is in yellow, and the difference between the two areas is the thickness of film. Eight different areas were measured to get the average thickness of 0.16 µm.

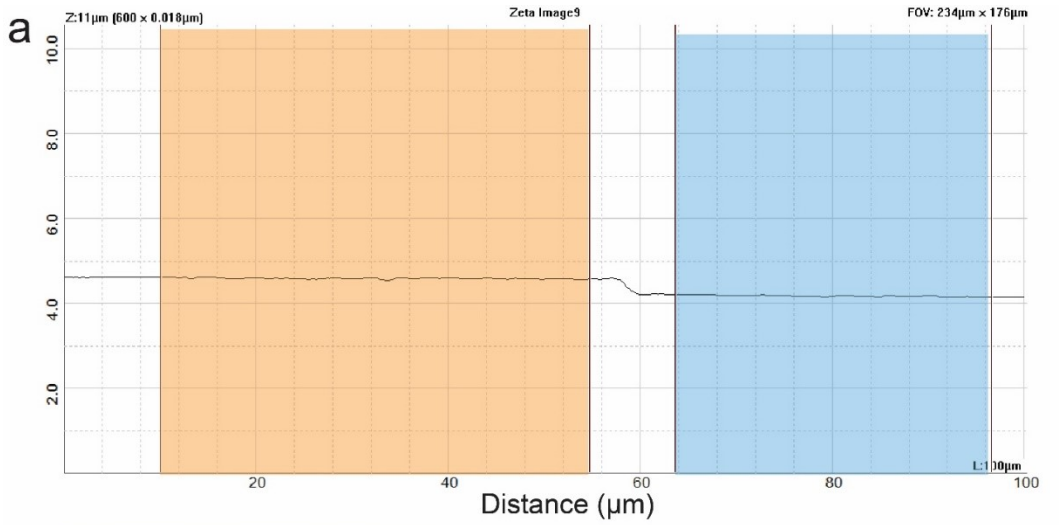

Measurement	1	2	3	4	5	6	7	8	**Average**
Thickness (µm)	0.31	0.35	0.24	0.25	0.41	0.13	0.38	0.45	**0.31**

Fig. S23. (a) Thickness measurement of compound **2** film; (b) Optical microscopic image of the measure area; (c) 3D topography of the measured area. The glass slide surface area is highlighted in blue, measured film area is in yellow, and the difference between the two areas is the thickness of film. Eight different areas were measured to get the average thickness of 0.31 µm.

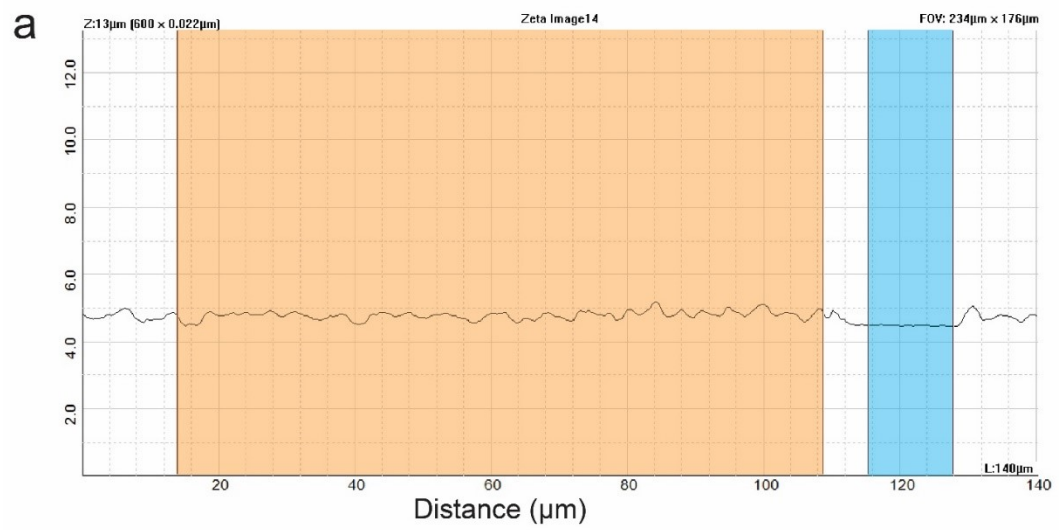

Measurement	1	2	3	4	5	6	7	8	**Average**
Thickness (µm)	0.20	0.30	0.20	0.30	0.33	0.50	0.38	0.40	**0.32**

Fig. S24. (a) Thickness measurement of compound **3** film; (b) Optical microscopic image of the measure area; (c) 3D topography of the measured area. The glass slide surface area is highlighted in blue, measured film area is in yellow, and the difference between the two areas is the thickness of film. Eight different areas were measured to get the average thickness of 0.32 µm.

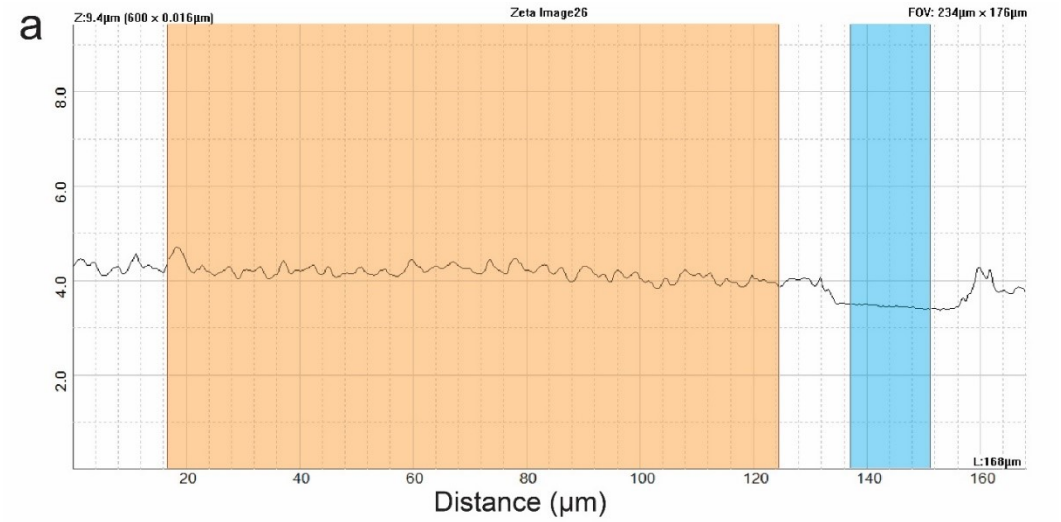

Measurement	1	2	3	4	5	6	7	8	**Average**
Thickness (µm)	0.27	0.41	0.22	0.47	0.25	0.71	0.17	0.75	**0.41**

Fig. S25. (a) Thickness measurement of compound **4** film; (b) Optical microscopic image of the measure area; (c) 3D topography of the measured area. The glass slide surface area is highlighted in blue, measured film area is in yellow, and the difference between the two areas is the thickness of film. Eight different areas were measured to get the average thickness of 0.41 µm.

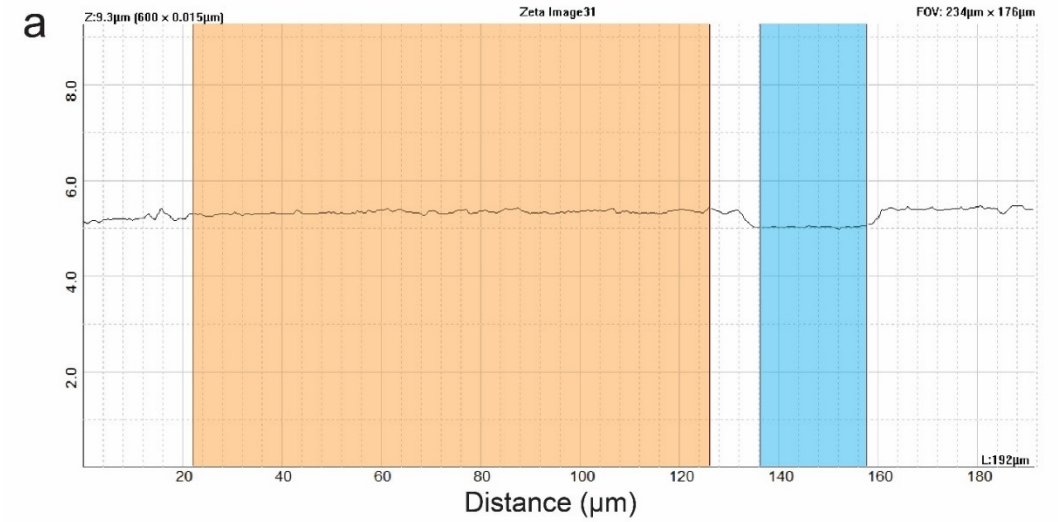

Measurement	1	2	3	4	5	6	7	8	**Average**
Thickness (µm)	0.75	0.49	0.31	0.36	0.19	0.37	0.29	0.23	**0.37**

Fig. S26. (a) Thickness measurement of compound **5** film; (b) Optical microscopic image of the measure area; (c) 3D topography of the measured area. The glass slide surface area is highlighted in blue, measured film area is in yellow, and the difference between the two areas is the thickness of film. Eight different areas were measured to get the average thickness of 0.37 µm.

11.2 Photo-isomerization in thin films

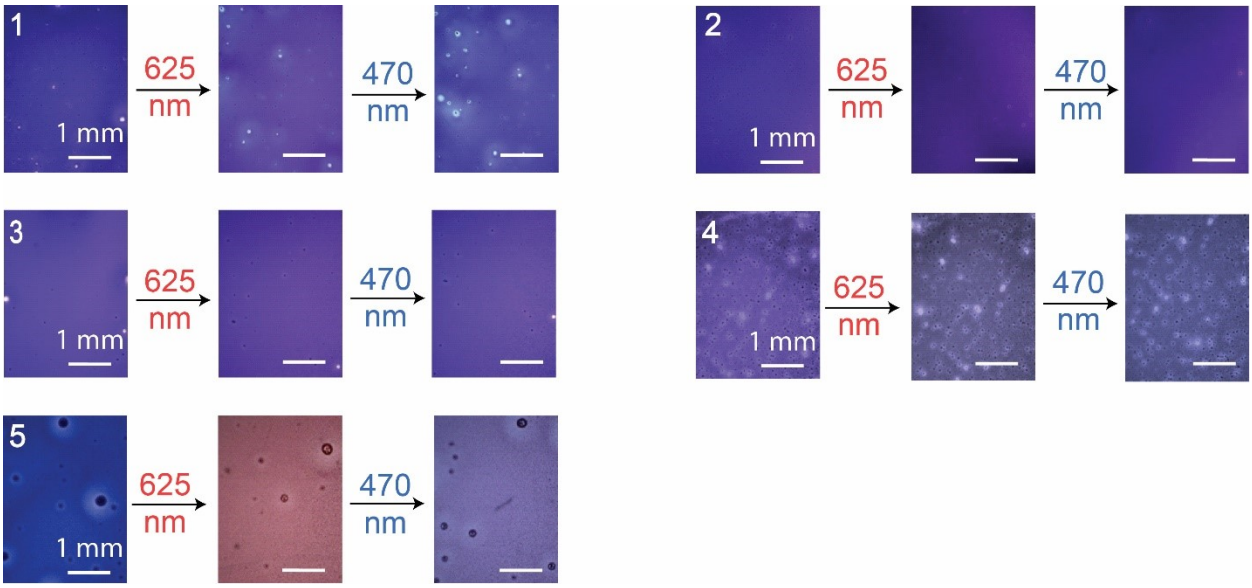

Fig. S27. The magnified optical microscopic images of compounds **1-5** after 625 nm and 470 nm irradiation. scale bars=1 mm.

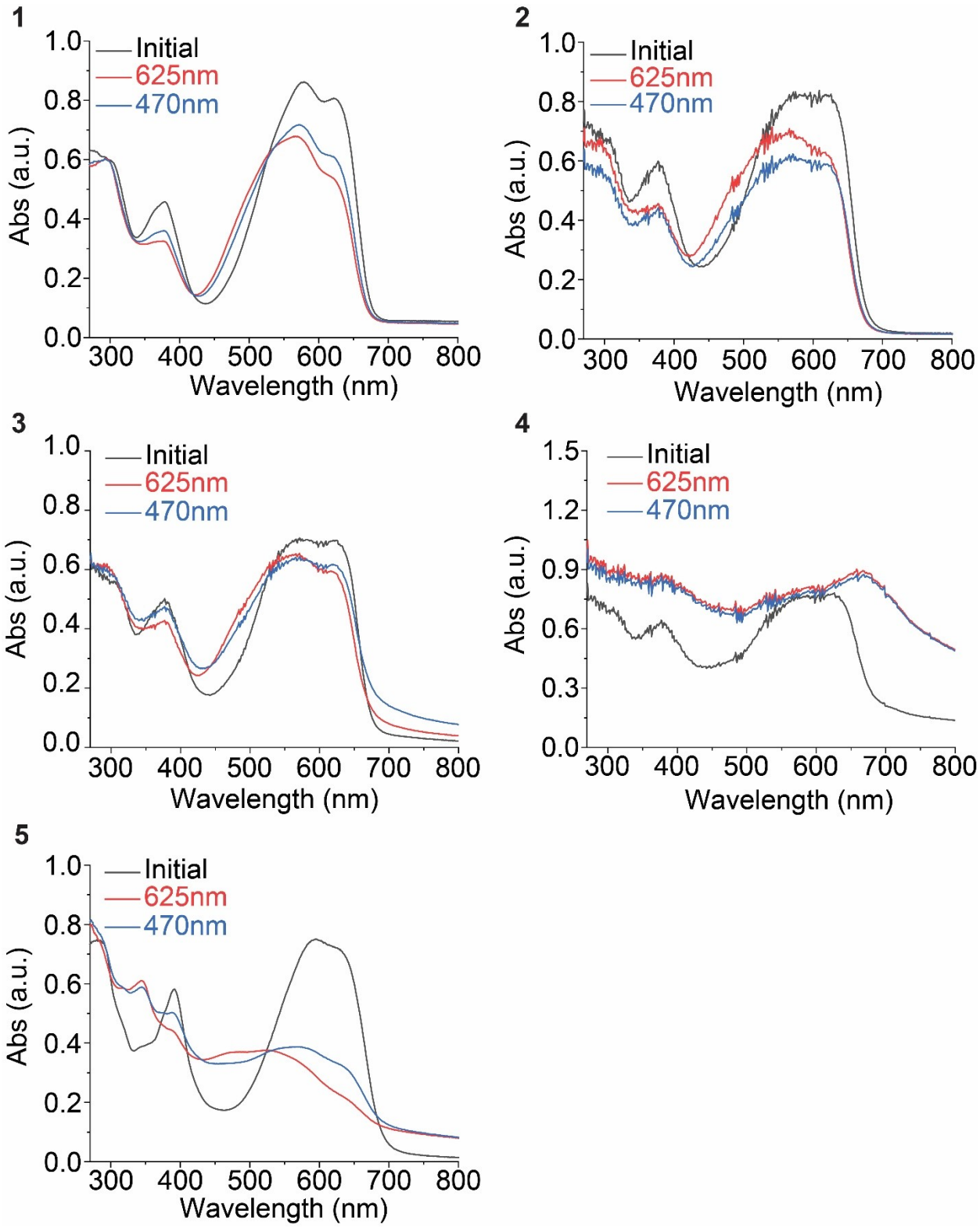

Fig. S28. UV-vis absorption spectra of condensed compounds **1-5** in thin films. All films were irradiated with 625nm for 10 minutes and 470nm for 2 minutes, respectively.

11.3 NMR of thin film

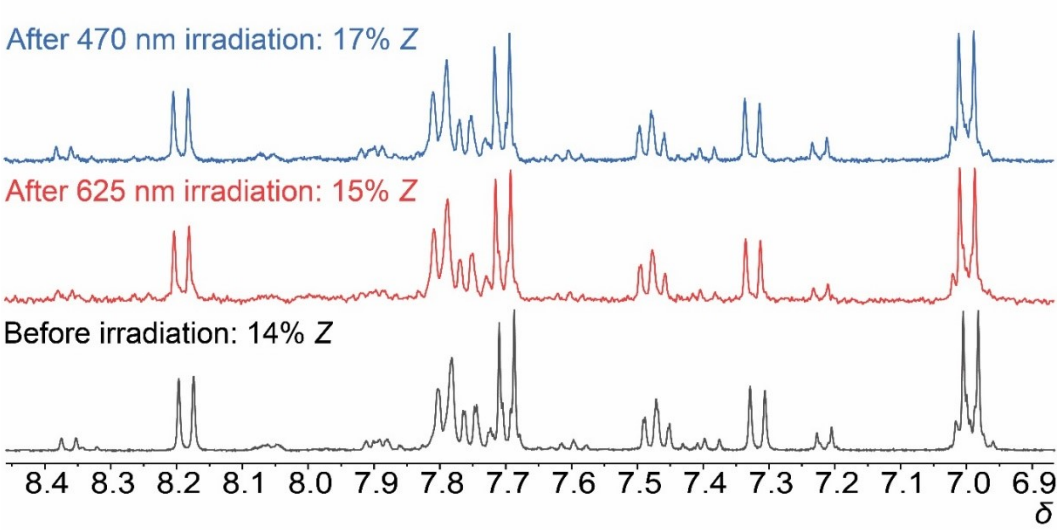

Fig. S29. The ratio of *Z* isomers in thin films of compound **1** before and after 625 nm, 470 nm irradiation by ^{1}H NMR.

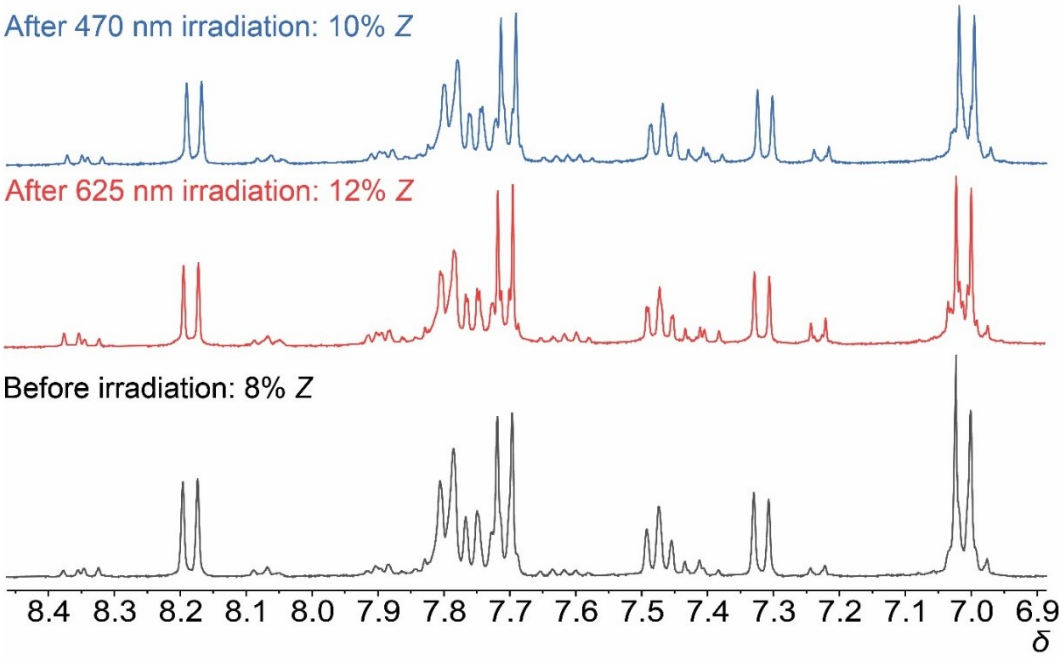

Fig. S30. The ratio of *Z* isomers in thin films of compound **2** before and after 625 nm, 470 nm irradiation by ^{1}H NMR

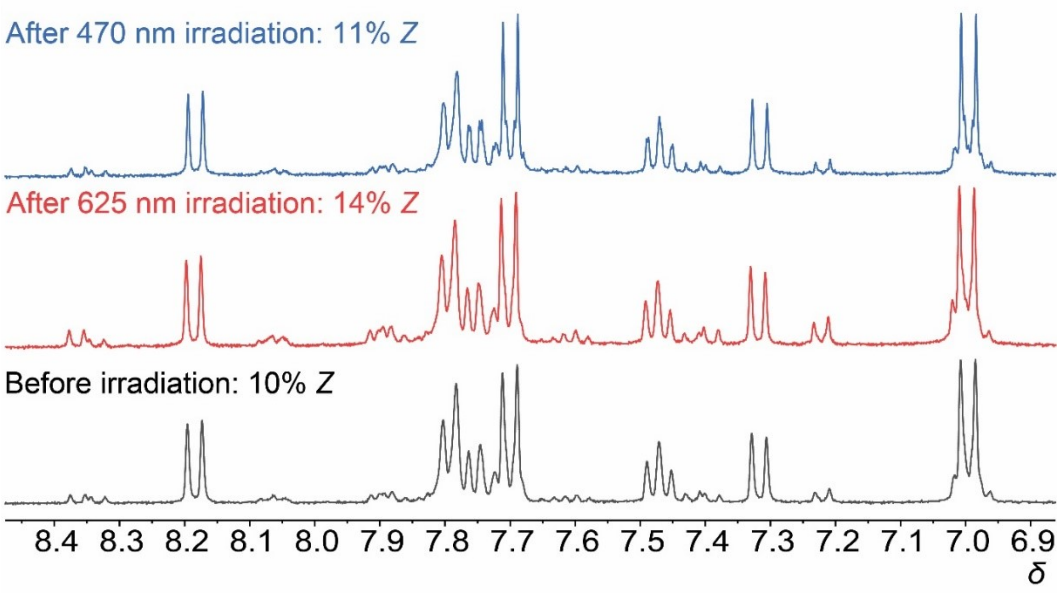

Fig. S31. The ratio of *Z* isomers in thin films of compound **3** before and after 625 nm, 470 nm irradiation by ^{1}H NMR

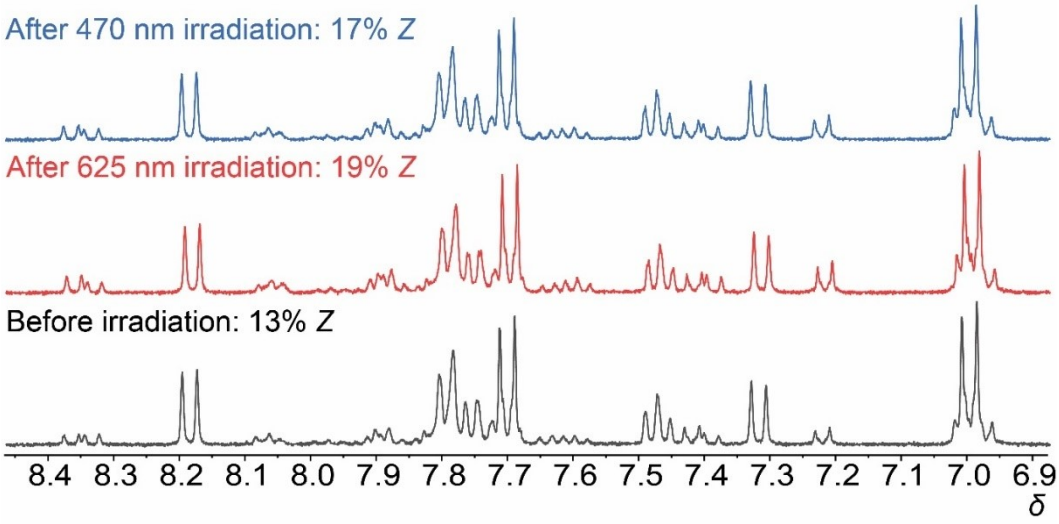

Fig. S32. The ratio of *Z* isomers in thin films of compound **4** before and after 625 nm, 470 nm irradiation by ^{1}H NMR

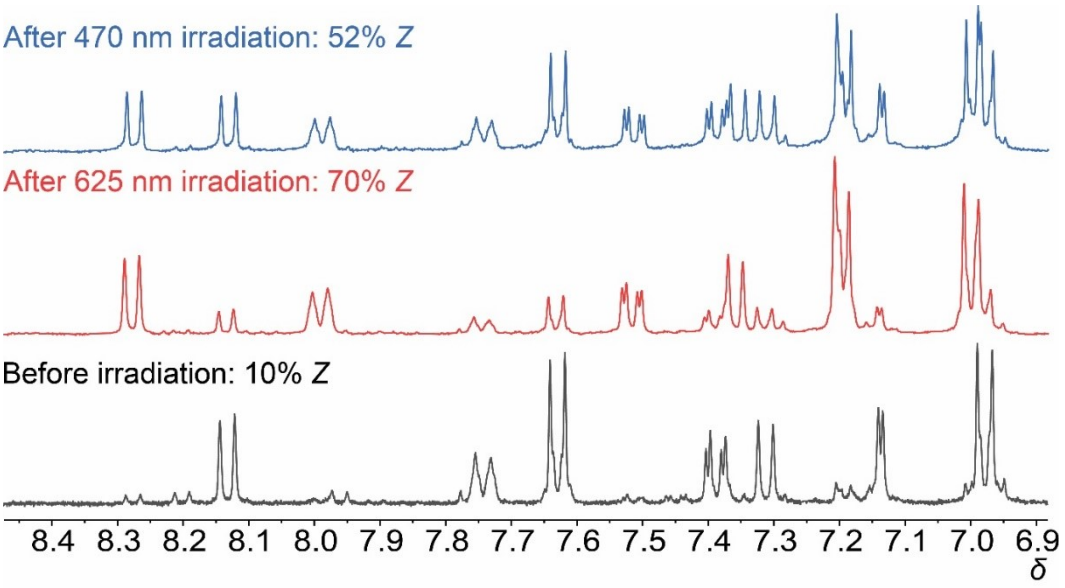

Fig. S33. The ratio of *Z* isomers in thin films of compounds **5** before and after 625 nm, 470 nm irradiation by ^{1}H NMR.

11.4 Static light penetration depth measurement

The calculation of penetration depth of compound **5** in the condensed phase was based on the reported method.[7]

Theoretically, the static penetration depths of E and Z isomers of **5** are estimated by

$$\delta_{p,E/Z} = \frac{d_{sol} \times n_{sol}}{A_{sol,E/Z} \times n_{film}}$$

where $A_{sol,\ E/Z}$ is the absorbance of **5**-*E*/*Z* in DCM solution obtained by decomposing the absorbance spectra of initial and final states, d_{sol} is the thickness of the solution, n_{sol} is the molar fraction of **5** in DCM, n_{film} is the molar fraction of **5** in film, which equals to 1. Within a static scenario, the penetration of the UV and visible light are limited by the attenuation within the *E* and *Z* isomers, respectively. The corresponding penetration depths are estimated to be 0.22 μm (for *E* at 470 nm) and 0.47 μm (for *Z* at 625 nm).

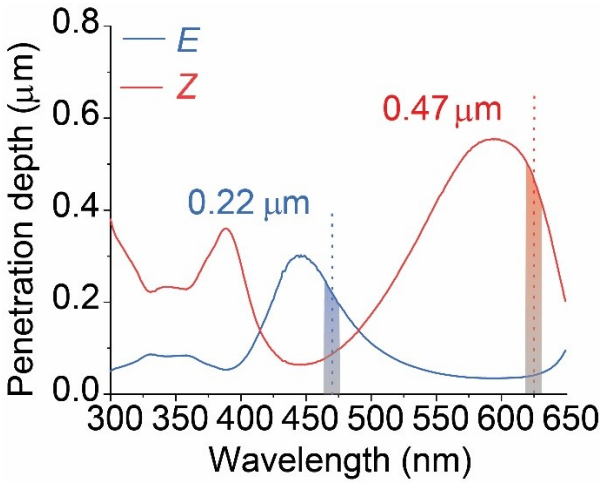

Fig. S34. The estimated penetration depth of 5-*E* and *Z* isomers in thin film. The gradient red/blue bars indicate the penetration depth of *Z* and *E* isomers upon 625 nm and 470 nm irradiation, respectively.

11.5 Thinner films thickness and isomerization

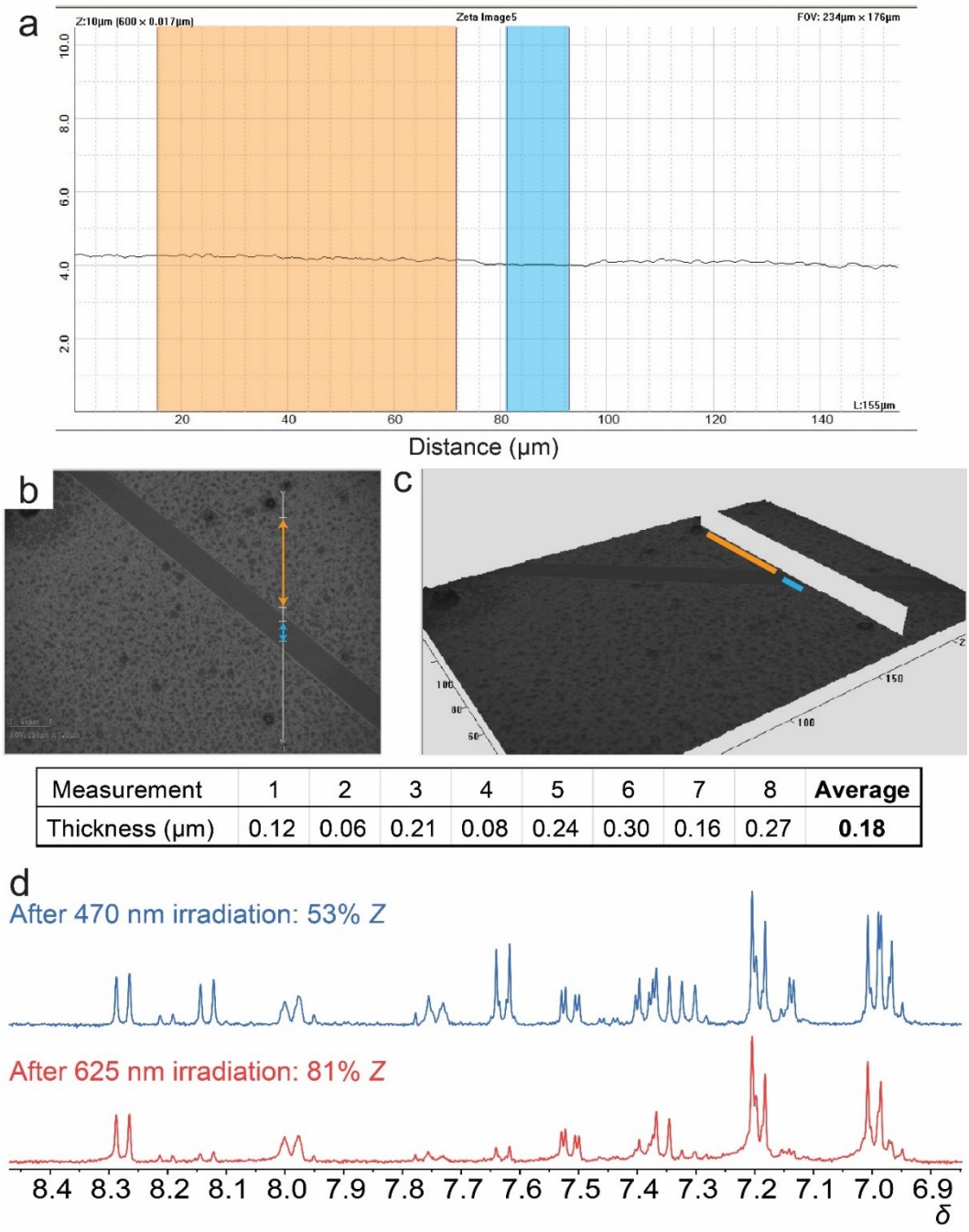

Measurement	1	2	3	4	5	6	7	8	**Average**
Thickness (µm)	0.12	0.06	0.21	0.08	0.24	0.30	0.16	0.27	**0.18**

Fig. S35. (a) Thickness measurement of ultra-thin compound **5** film; (b) Optical microscopic image of the measure area; (c) 3D topography of the measured area. The glass slide surface area is highlighted in blue, measured film area is in yellow, and the difference between the two areas is the thickness of film. Eight different areas were measured to get the average thickness of 0.18 µm. (d) The ratio of *Z* isomers in ultra-thin films of compounds **5** after 625 nm, 470 nm irradiation by ^{1}H NMR.

11.6 NMR of cycling-test thin film

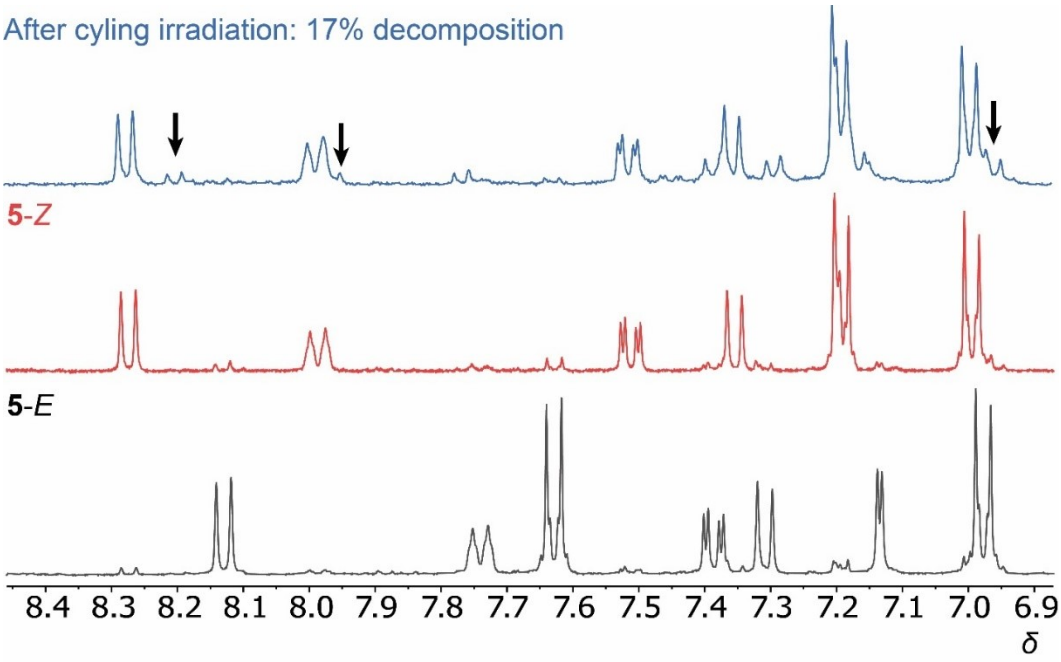

Fig. S36. ^{1}H NMR spectra of *E* (black) and *Z* (red) isomers of compound **5** for comparison, and the spectra of thin film after cycling irradiation (blue), the black arrows indicating the signals of decomposition.

11.7 Thermal reversion kinetics in the condensed phase

Compound **5** is the candidate that can isomerize in the condensed phase. *Z*-rich powder sample of **5** was heated at 60 °C in dark. The change of the ratios between the *Z* and *E* isomers was monitored by ^{1}H NMR.

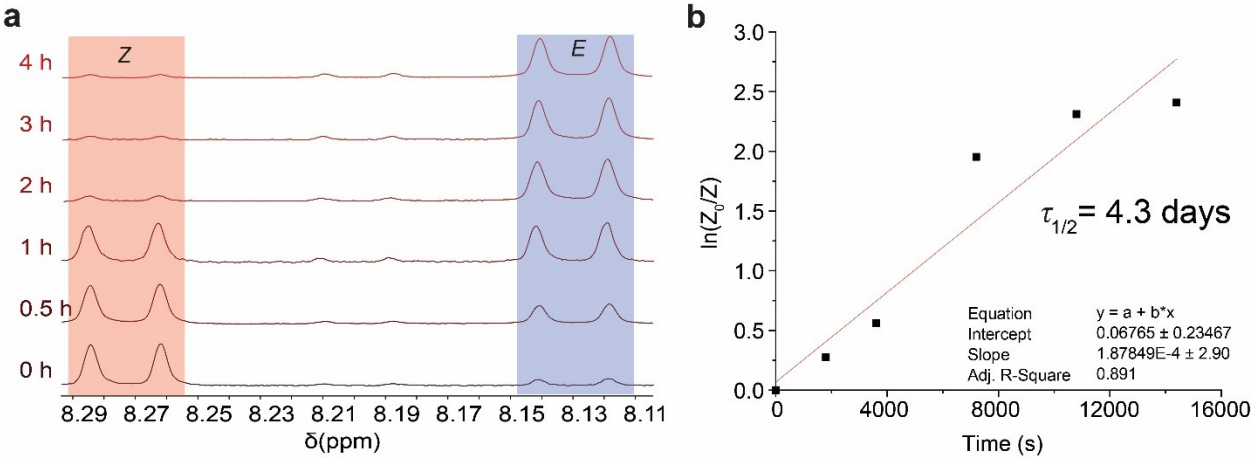

Fig. S37. (a) The ^{1}H NMR spectra of the change of ratios between **5**-*Z* and **5**-*E* over time. (b) A plot of ln(Z_0/*Z*) as a function of time showing the first-order decay of **5**-*Z* at 60 °C.[8] The Adj. R-Square = 0.891 indicates the unideal fitting of thermal relaxation, due to the noticeable thermal degradation of **5**.

Table S12. Summary of the rate of *Z* → *E* relaxation at elevated temperatures, energy barrier and half-life at 293 K in condensed phase of **5**-*Z*.

Compound	Experimental Temperature	k (s^{-1})	$\Delta G^{\neq}$ (kJ mol^{-1})	$\tau_{1/2}$ (days)
5	333 K	1.9 E−4	105.7	4.3

12. Single crystal data and collection parameters

Single crystals of compounds **1**, **3**, **4**, and **5** suitable for X-ray structural analysis were obtained by slow evaporation from their DCM/hexane solutions at room temperature (RT) under dark. Suitable crystals were selected and mounted on an XtaLAB Synergy, Dualflex, HyPix diffractometer. The crystal was kept at a steady T = 100.00(10) K during data collection. The structure was solved with the **ShelXT** (Sheldrick, 2015) solution program using dual methods[9] and by using **Olex2** 1.5 (Dolomanov et al., 2009) as the graphical interface.[10] The model was refined with **ShelXL** 2018/3 (Sheldrick, 2015) using full matrix least squares minimization on $\boldsymbol{F^2}$.[9] All non-hydrogen atoms were refined anisotropically. Hydrogen atom positions were calculated geometrically and refined using the riding model, except for the hydrogen atom on the non-carbon atom(s) which were found by difference Fourier methods and refined isotropically when data permits. CCDC: 2257907-2257910 contains the supplementary crystallographic data. These data can be obtained free of charge from the Cambridge Crystallographic Data Centre via www.ccdc.cam.ac.uk/structures/.

Table S13. Summary of the single crystal data and intensity collection parameters of three compounds.

Compound	**1**	**3**	**4**	**5**
Formula	$C_{19}H_{15}BF_2N_4O$	$C_{27}H_{31}BF_2N_4O$	$C_{29}H_{35}BF_2N_4O$	$C_{29}H_{34}BF_2N_4O_2$
$D_{calc.}$/ g.cm^{-3}	1.457	1.301	1.280	1.258
m /mm^{-1}	0.904	0.737	0.713	0.725
Formula Weight	364.16	476.37	504.42	519.41
Size/mm^3	0.20×0.04×0.02	0.44×0.07×0.03	0.33×0.04×0.01	0.46×0.16×0.03
T/K	100.09(10)	99.9(6)	100.0(4)	100.0(3)
Crystal System	orthorhombic	triclinic	triclinic	triclinic
Space Group	*Pbca*	*P-1*	*P*-1	*P*-1
a/Å	17.0351(2)	7.9997(3)	7.9249(2)	7.2509(3)
b/Å	7.02387(10)	11.4194(4)	11.3974(3)	41.2972(9)
c/Å	27.7571(4)	14.6997(6)	16.0639(4)	9.7380(2)
α, deg	90	72.158(3)	98.410(2)	90.122(2)
β, deg	90	82.260(3)	102.690(2)	109.885(3)
γ, deg	90	72.295(3)	108.100(2)	89.203(3)
V/Å^3	3321.20(8)	1216.43(8)	1308.96(6)	2741.83(15)
Z	8	2	2	4
Z'	1	1	1	2
Wavelength/Å	1.54184	1.54184	1.54184	1.5484
Radiation type	CuK$_\alpha$	Cu K$_\alpha$	Cu K$_\alpha$	Cu K$_\alpha$
θ range for data collection	3.184 to 80.464	3.162 to 80.234	2.898 to 80.287	3.211 to 80.555
Index ranges	-21<=h<=10, -8<=k<=8, -35<=l<=35	-10<=h<=8, -14<=k<=13, -18<=l<=18	-10<=h<=9, -14<=k<=14, -20<=l<=20	-9<=h<=9, -52<=k<=52, -12<=l<=9
Reflections measured	18821	25331	43444	51198
Independent reflections	3575	5193	5503	11633
Refl's I≥2 s(I)	3100	4543	4761	9165
R_{int}	0.0392	0.0377	0.0420	0.0870
Data/restraints/parameters	3575/0/245	5193/0/317	5503/0/335	11633/0/689
Largest peak and hole e. Å^{-3}	0.232-0.217	0.225-0.220	1.595-0.495	0.565-0.412
Goodness-of-fit on F^2	1.073	1.103	1.118	1.049
R_1, wR_2 (all data)	0.0451, 0.0930	0.0417, 0.1059	0.0999, 0.2478	0.0911, 0.2356
R_1, wR_2 [I> 2σ (I)]	0.0373, 0.0891	0.0369, 0.1023	0.0902, 0.2406	0.0783, 0.2231
CCDC	2257907	2257908	2257909	2257910

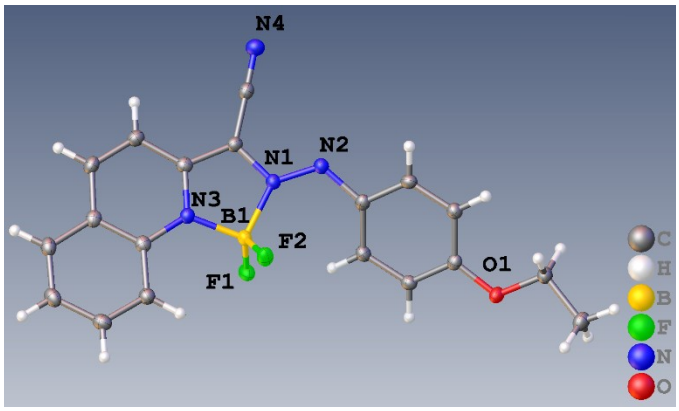

Fig. S38. ORTEP drawing of **1** at 50% ellipsoids with hetero atoms labelled.

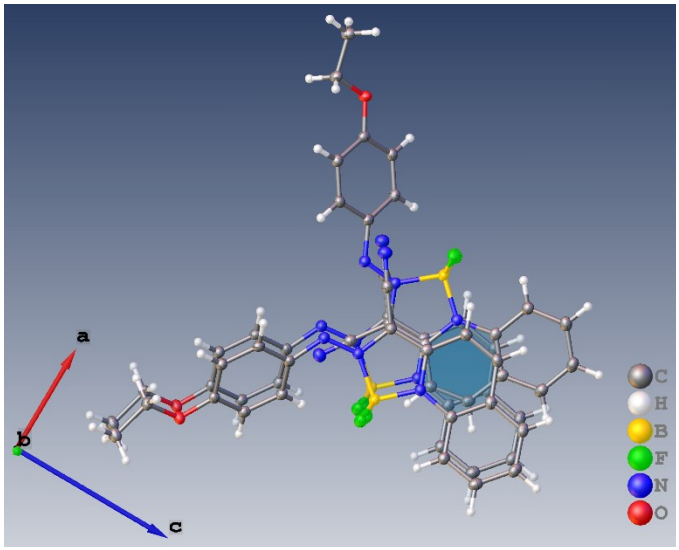

Fig. S39. The π-π interactions of **1**. **Plane 3 *to* #3@8_655 (1/2-X,-1/2+Y,+Z):** The angle between these two planes is 9.278 ˚, the Centroid-Centroid distance is 3.532 Å and the Shift Distance is 0.667 Å **Plane 3 *to* #3@8_665 (1/2-X,1/2+Y,+Z):** The angle between these two planes is 9.278 ˚, the Centroid-Centroid distance is 3.532 Å and the Shift Distance is 0.667 Å.

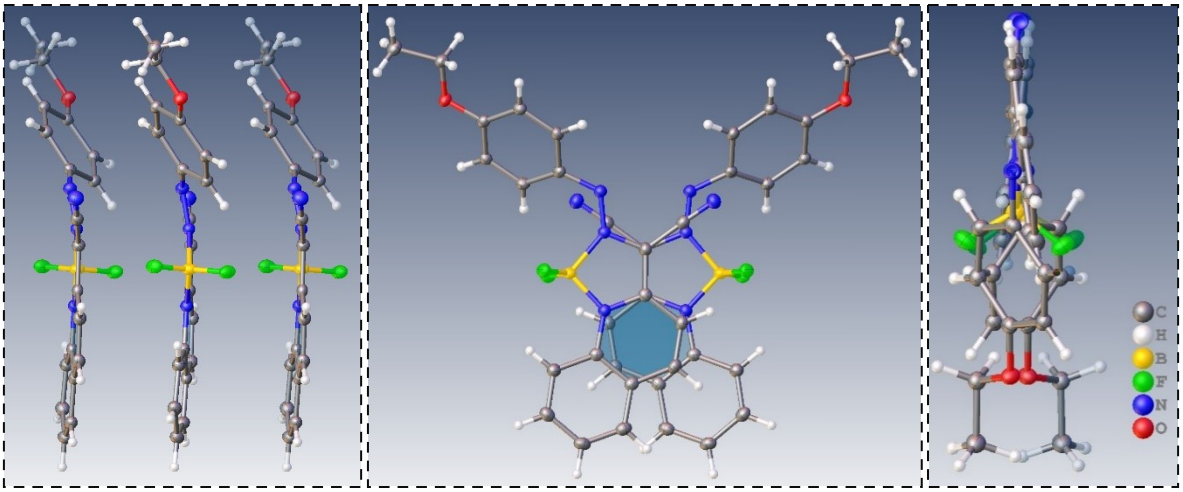

Fig. S40. Packing diagram of **1** viewed along the a, b, and c axis from left to right.

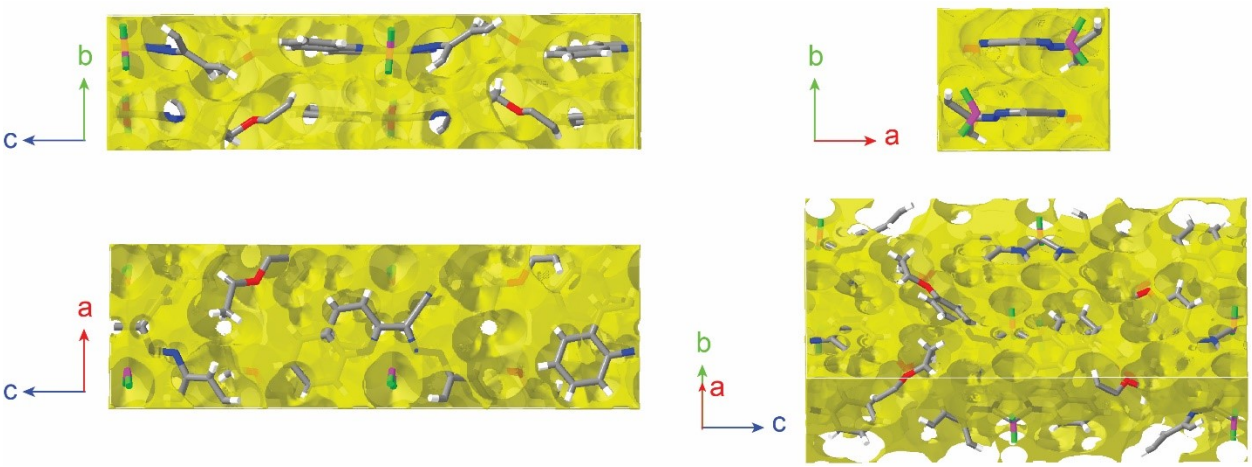

Fig. S41. Van deer Waals space fill mode for illustrating the occupancy of molecule and void space unit cell of compound **1** from four angles of view. Filled space: 2529.31 Å^3 (76.16%) per unit cell; Void space: 791.89 Å^3 (23.84%) per unit cell.

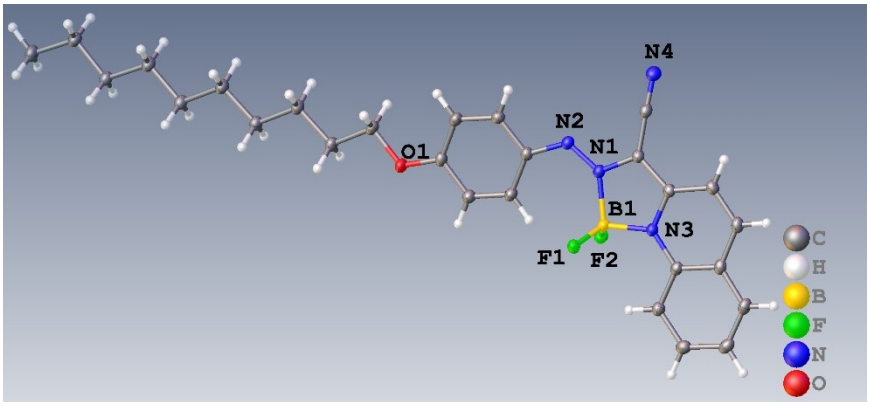

Fig. S42. ORTEP drawing of **3** at 50% ellipsoids with hetero atoms labelled.

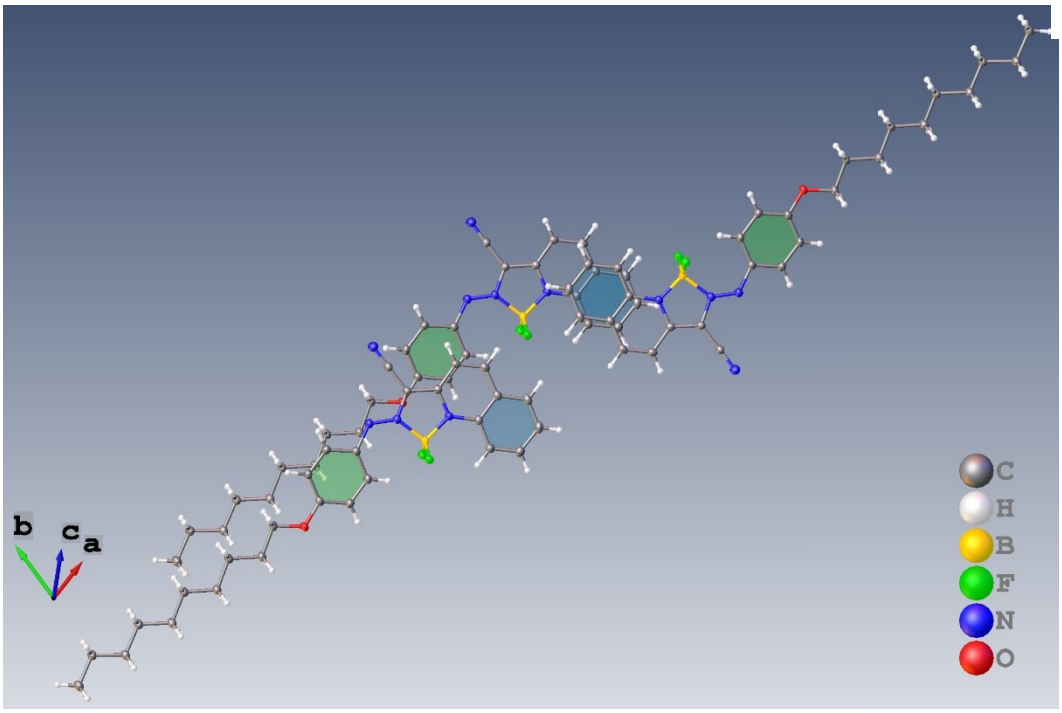

Fig. S43. The π-π interactions of **3**. **Plane 1 *to* #1@2_857 (3-X,-Y,2-Z):** The angle between these two planes is 0.000 °, the Centroid-Centroid distance is 3.604 Å and the Shift Distance is 1.111 Å **Plane 1 *to* #3@2_857 (3-X,-Y,2-Z):** The angle between these two planes is 0.000 °, the Centroid-Centroid distance is 3.604 Å and the Shift Distance is 1.111 Å **Plane 2 *to* #3@1_455 (-1+X,+Y,+Z):** The angle between these two planes is 6.190 °, the Centroid-Centroid distance is 3.760 Å and the Shift Distance is 1.383 Å.

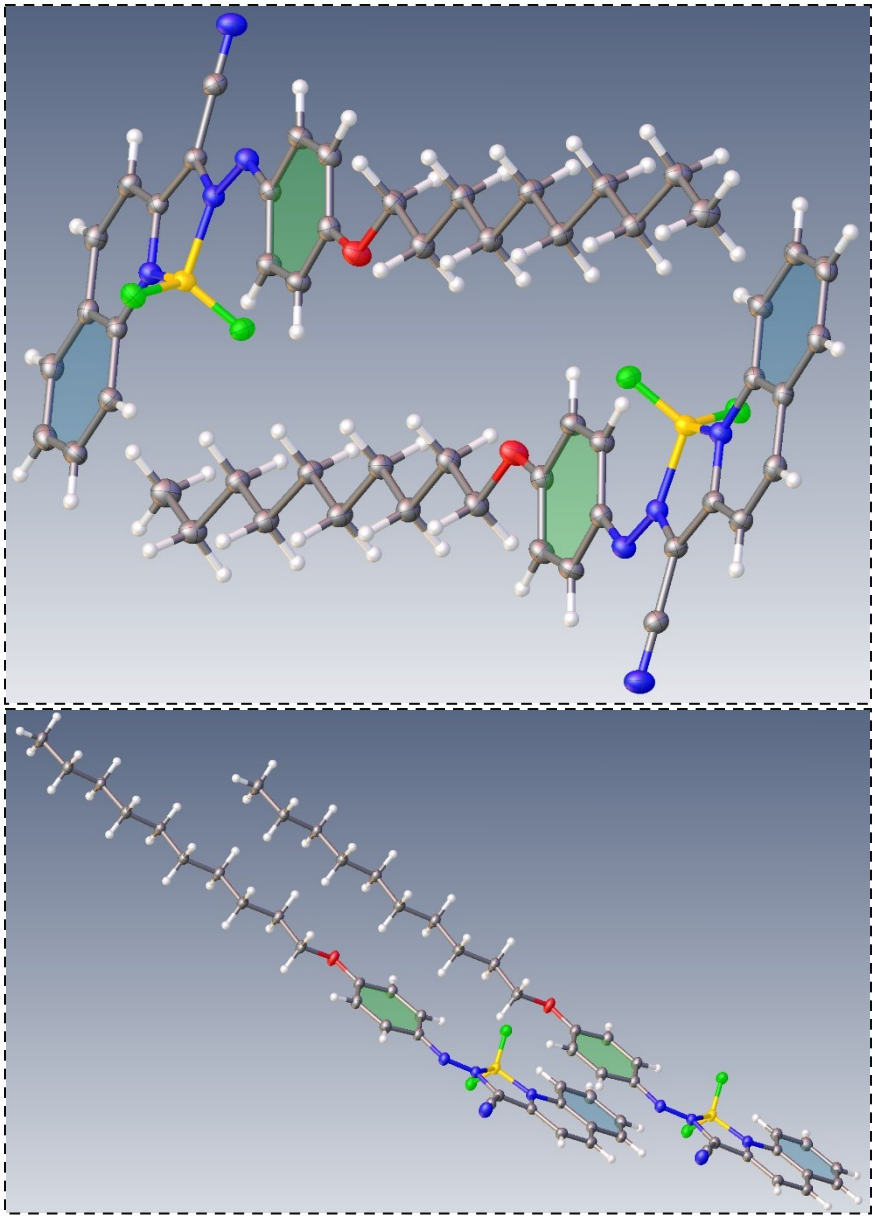

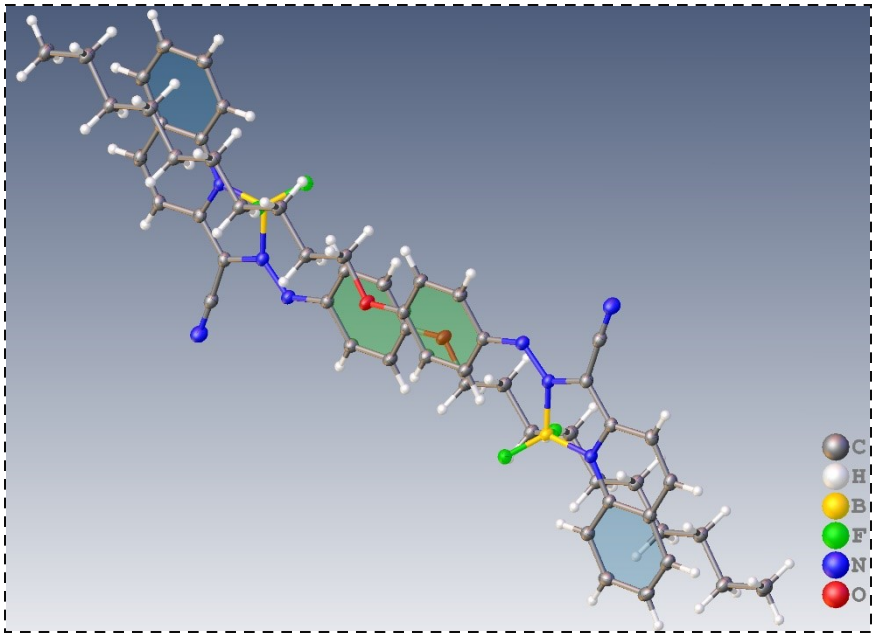

Fig. S44. Packing diagram of **3** viewed along the a, b, and c axis from top to bottom.

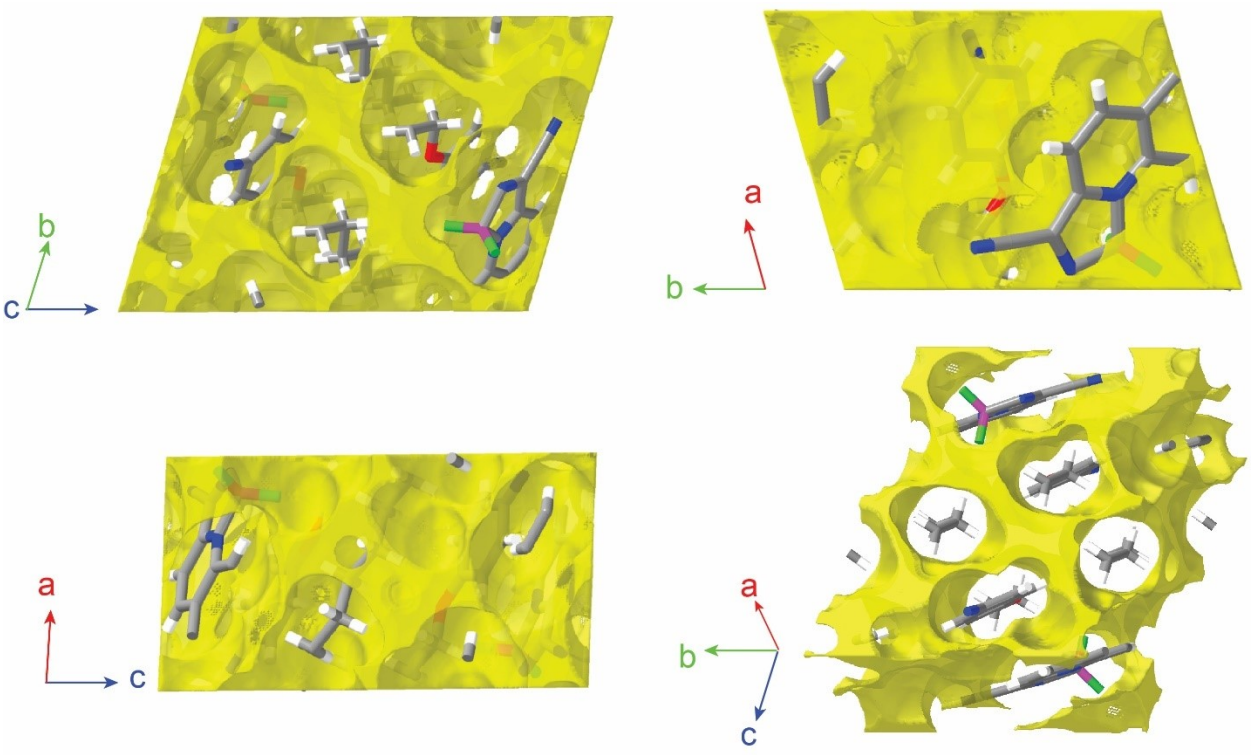

Fig. S45. Van deer Waals space fill mode for illustrating the occupancy of molecule and void space unit cell of compound **3** from four angles of view. Filled space: 887.08 Å^3 (72.92%) per unit cell; Void space: 329.36 Å^3 (27.08%) per unit cell.

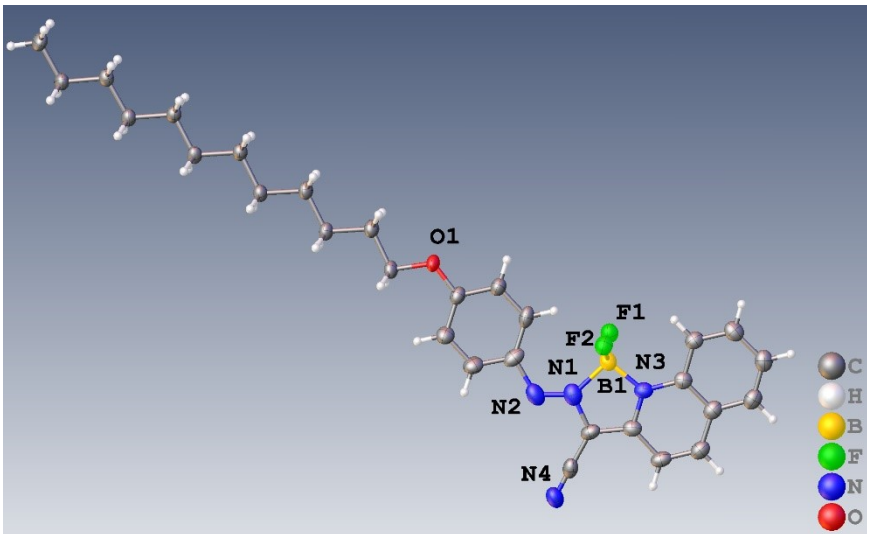

Fig. S46. ORTEP drawing of **4** at 50% ellipsoids with hetero atoms labelled.

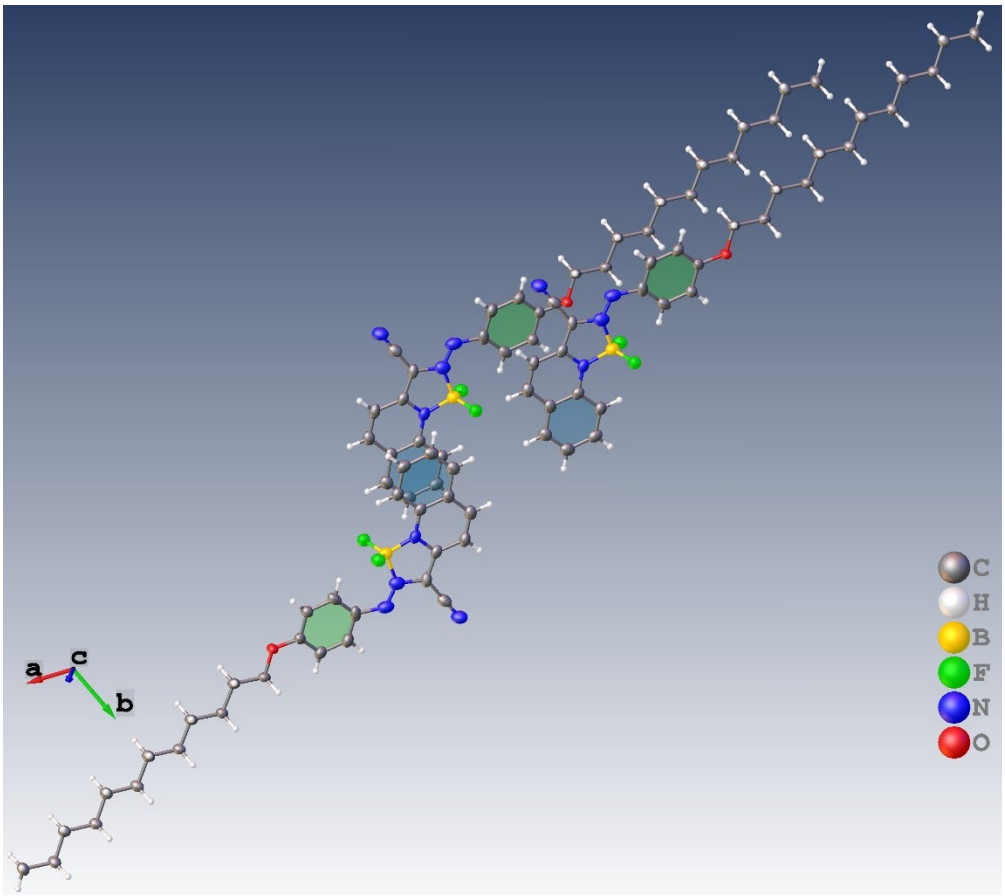

Fig. S47. The π-π interactions of **4**. **Plane 1** ***to*** **#1@2_977 (4-X,2-Y,2-Z):** The angle between these two planes is 0.000 ˚, the Centroid-Centroid distance is 3.583 Å and the Shift Distance is 1.106 Å **Plane 1** ***to*** **#3@2_977 (4-X,2-Y,2-Z):** The angle between these two planes is 0.000 ˚, the Centroid-Centroid distance is 3.583 Å and the Shift Distance is 1.106 Å **Plane 2** ***to*** **#3@1_455 (-1+X,+Y,+Z):** The angle between these two planes is 5.899 ˚, the Centroid-Centroid distance is 3.740 Å and the Shift Distance is 1.311 Å.

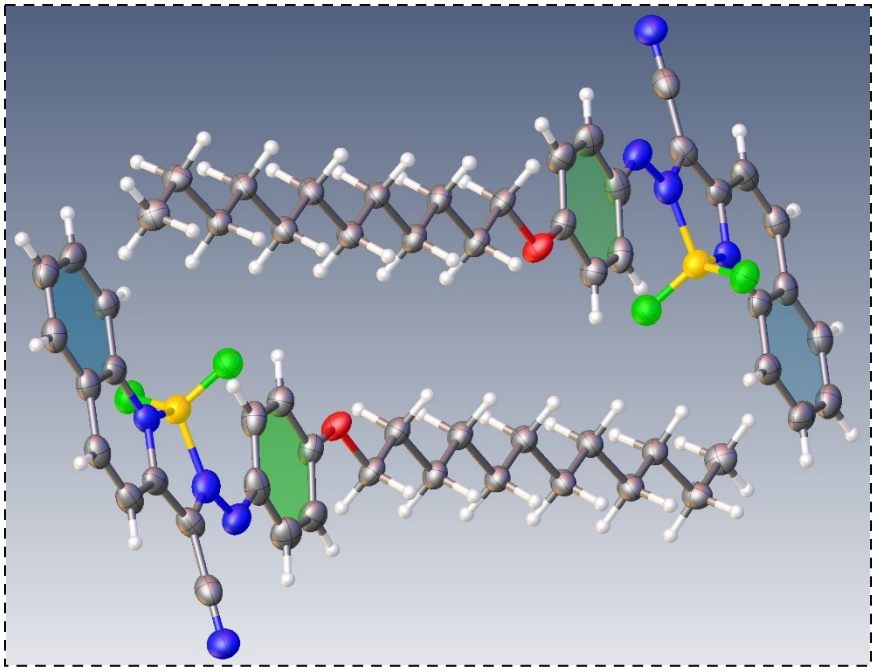

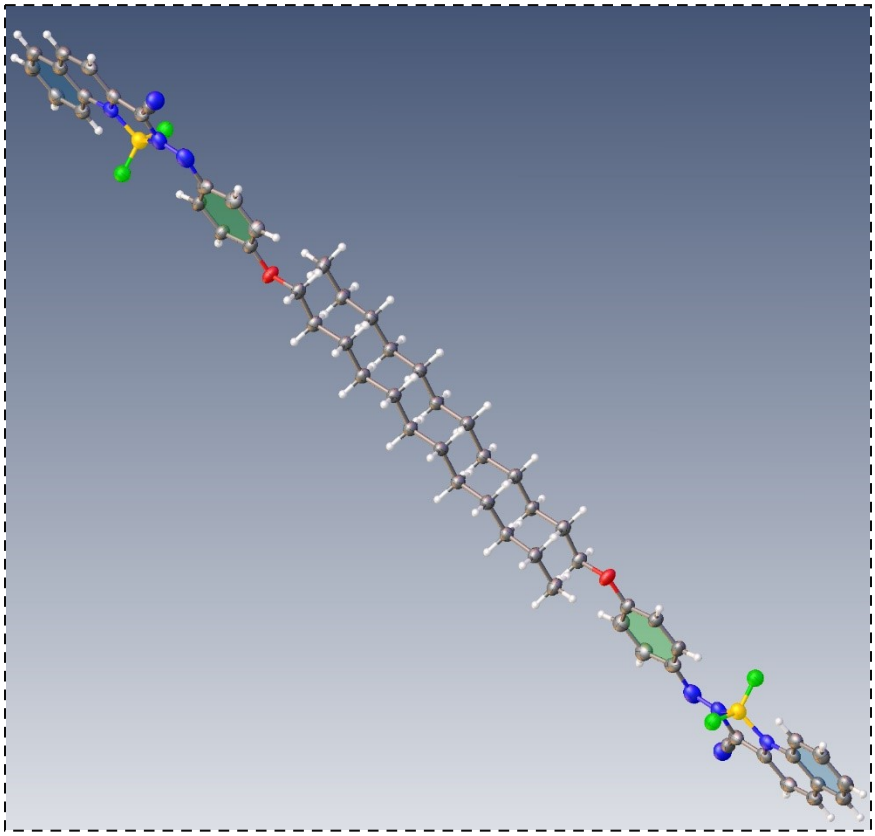

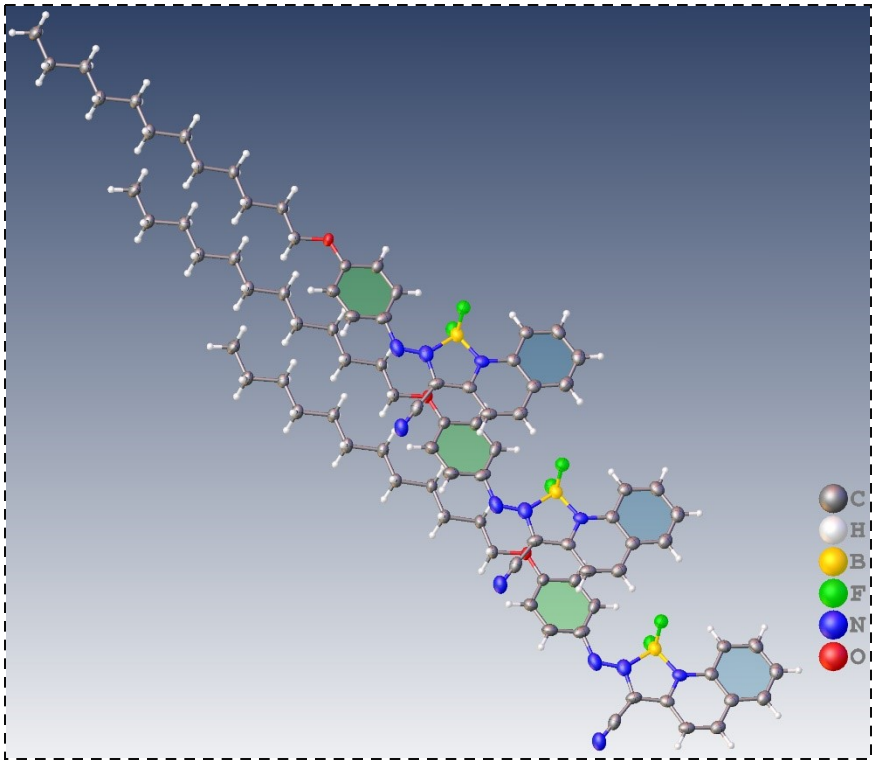

Fig. S48. Packing diagram of **4** viewed along the a, b, and c axis from top to bottom.

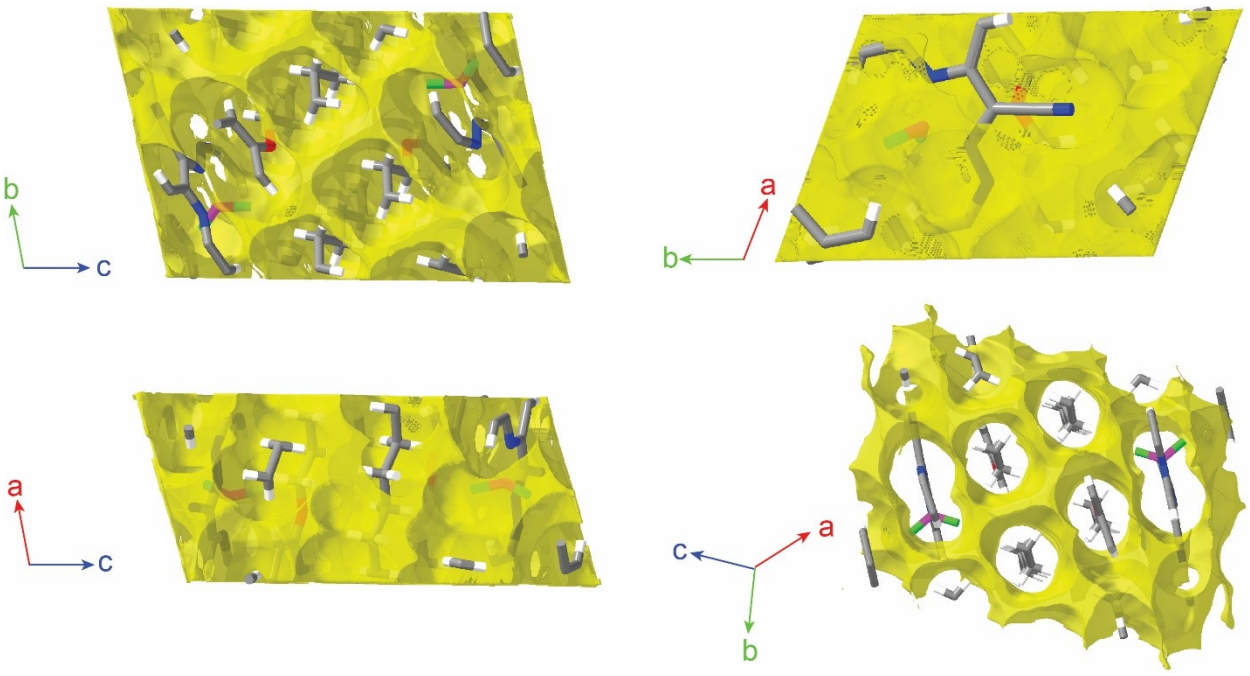

Fig. S49. Van deer Waals space fill mode for illustrating the occupancy of molecule and void space unit cell of compound **4** from four angles of view. Filled space: 949.23 Å^3 (72.52%) per unit cell; Void space: 359.74 Å^3 (27.48%) per unit cell.

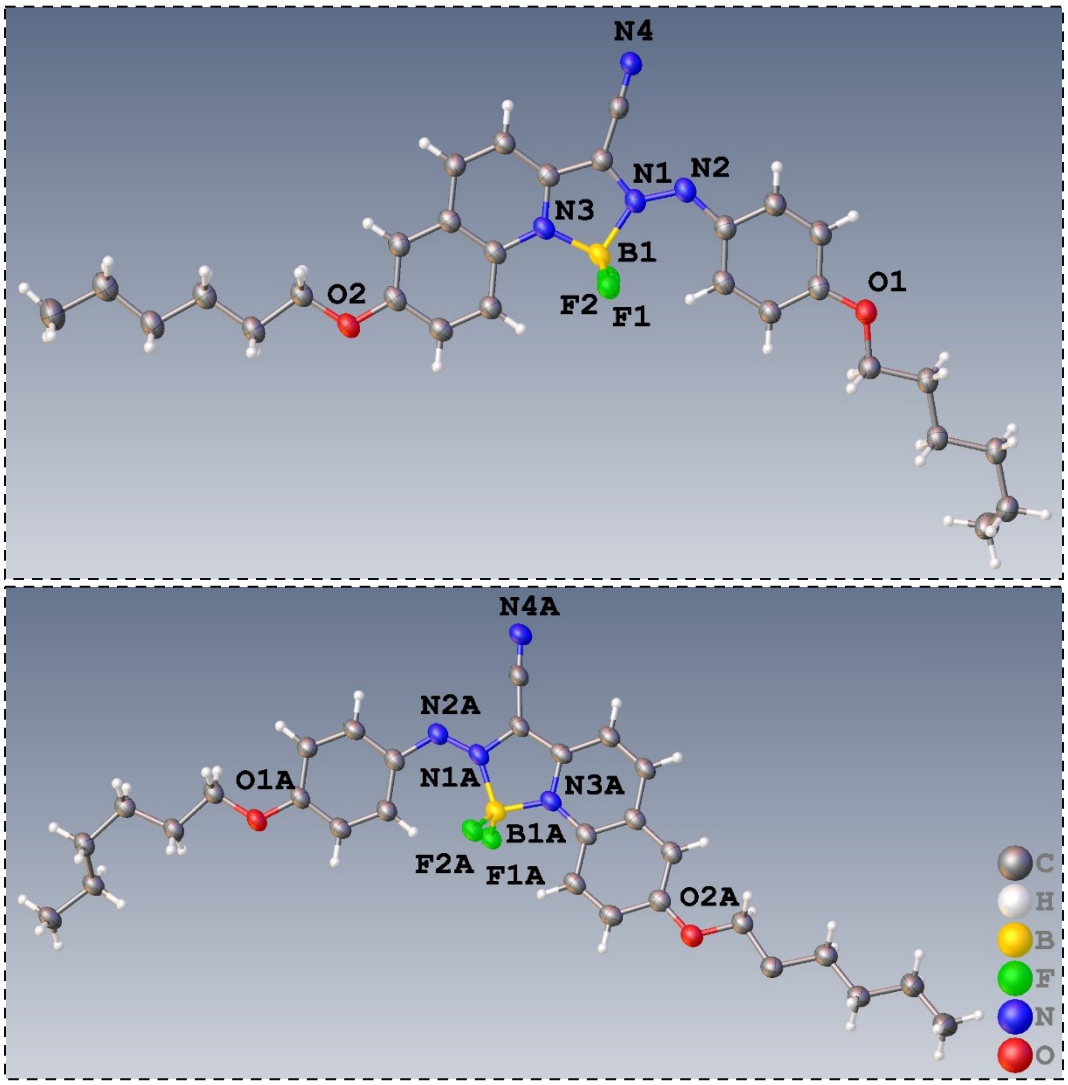

Fig. S50. ORTEP drawing of **5** (2 different configurations) at 50% ellipsoids in asymmetric unit cell with hetero atoms labelled.

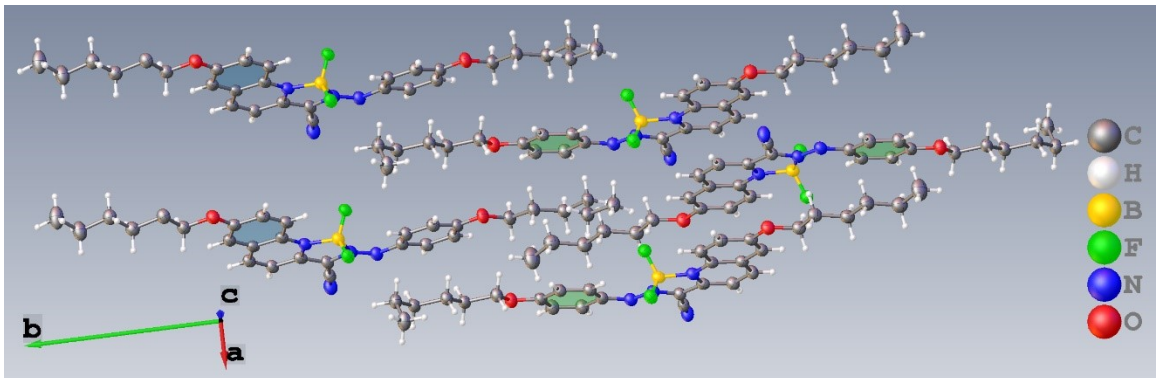

Fig. S51. The π-π interactions of **5**. **Plane 1** ***to*** **#3@2_475 (-1-X,2-Y,-Z):** The angle between these two planes is 0.406 ˚, the Centroid-Centroid distance is 3.699 Å and the Shift Distance is 1.425 Å **Plane 1** ***to*** **#3@2_575 (-X,2-Y,-Z):** The angle between these two planes is 0.406 ˚, the Centroid-

Centroid distance is 3.699 Å and the Shift Distance is 1.425 Å **Plane 3 *to* #3@2_475 (-1-X,2-Y,-Z):** The angle between these two planes is 0.000 °, the Centroid-Centroid distance is 3.637 Å and the Shift Distance is 1.252 Å **Plane 4 *to* #6@2_565 (-X,1-Y,-Z):** The angle between these two planes is 1.777 °, the Centroid-Centroid distance is 3.714 Å and the Shift Distance is 1.495 Å **Plane 4 *to* #6@2_665 (1-X,1-Y,-Z):** The angle between these two planes is 1.777 °, the Centroid-Centroid distance is 3.714 Å and the Shift Distance is 1.495 Å **Plane 6 *to* #6@2_565 (-X,1-Y,-Z):** The angle between these two planes is 0.000 °, the Centroid-Centroid distance is 3.566 Å and the Shift Distance is 1.044 Å

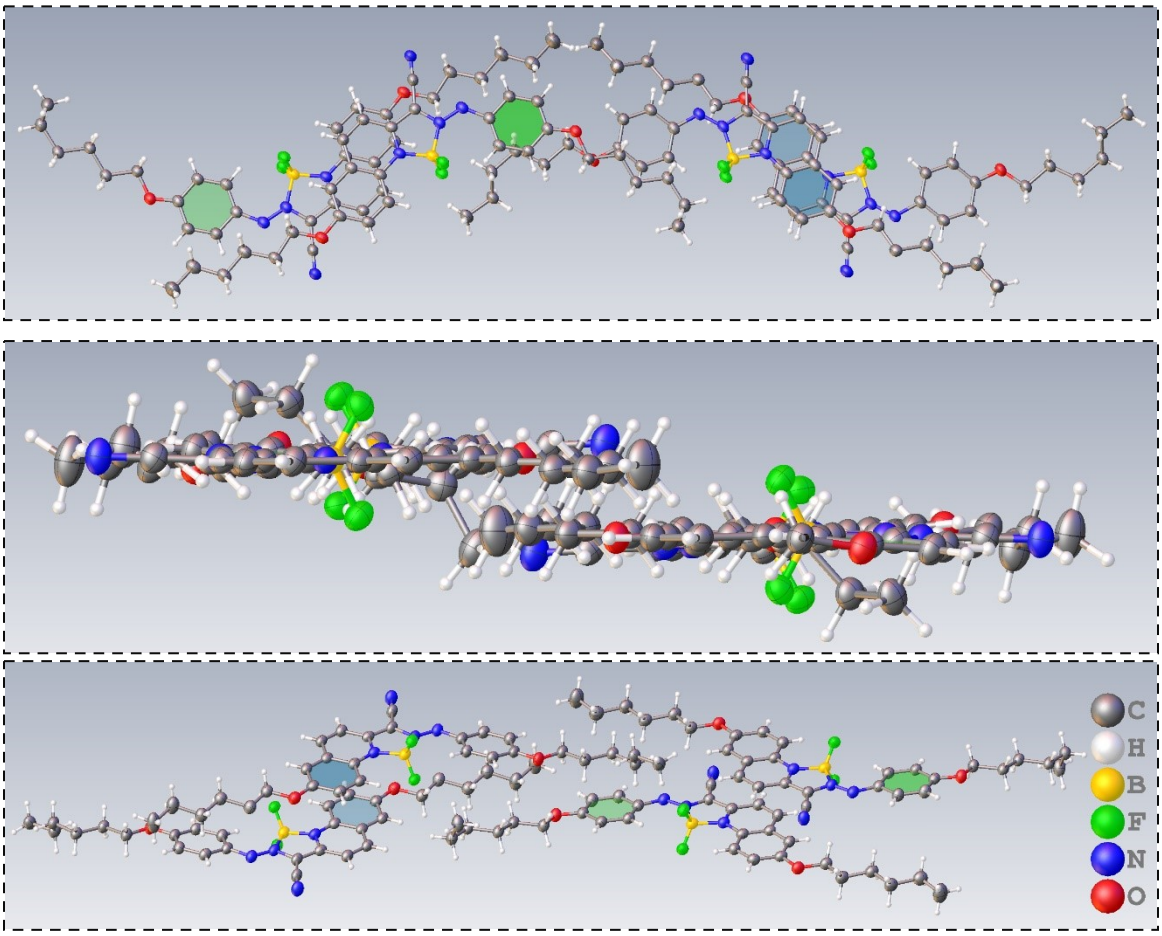

Fig. S52. Packing diagram of **5** viewed along the a, b, and c axis from top to bottom.

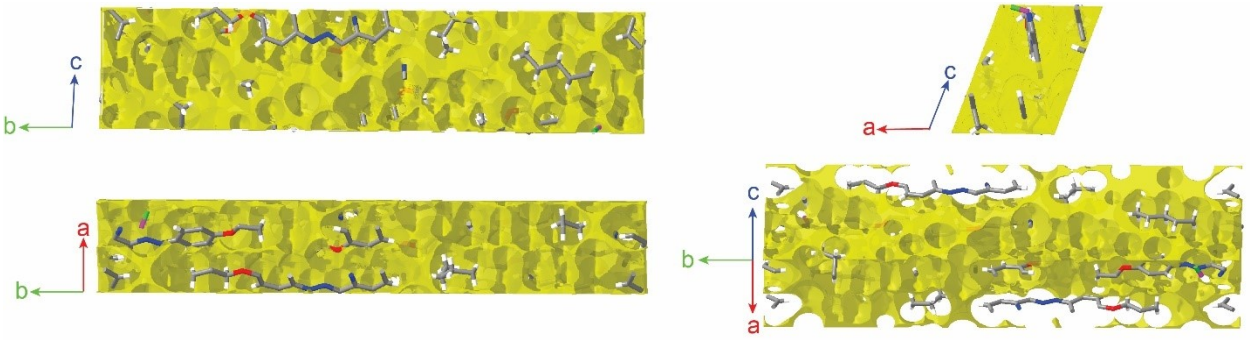

Fig. S53. Van deer Waals space fill mode for illustrating the occupancy of molecule and void space unit cell of compound **5** from four angles of view. Filled space: 1933.06 Å^3 (70.50%) per unit cell; Void space: 808.78 Å^3 (29.50%) per unit cell.

13. References

1 Y. Yang, R. P. Hughes and I. Aprahamian, *J. Am. Chem. Soc.*, 2012, **134**, 15221–15224.

2 G. D. Han, S. S. Park, Y. Liu, D. Zhitomirsky, E. Cho, M. DincĂ and J. C. Grossman, *J. Mater. Chem. A*, 2016, **4**, 16157–16165.

3 H. Qian, S. Pramanik and I. Aprahamian, *J. Am. Chem. Soc.*, 2017, **139**, 9140–9143.

4 A. D. Becke, *J. Chem. Phys.*, 1993, **98**, 5648–5652.

5 M. J. Frisch, G. W. Trucks, H. B. Schlegel, G. E. Scuseria, M. a. Robb, J. R. Cheeseman, G. Scalmani, V. Barone, G. a. Petersson, H. Nakatsuji, X. Li, M. Caricato, a. V. Marenich, J. Bloino, B. G. Janesko, R. Gomperts, B. Mennucci, H. P. Hratchian, J. V. Ortiz, a. F. Izmaylov, J. L. Sonnenberg, Williams, F. Ding, F. Lipparini, F. Egidi, J. Goings, B. Peng, A. Petrone, T. Henderson, D. Ranasinghe, V. G. Zakrzewski, J. Gao, N. Rega, G. Zheng, W. Liang, M. Hada, M. Ehara, K. Toyota, R. Fukuda, J. Hasegawa, M. Ishida, T. Nakajima, Y. Honda, O. Kitao, H. Nakai, T. Vreven, K. Throssell, J. a. Montgomery Jr., J. E. Peralta, F. Ogliaro, M. J. Bearpark, J. J. Heyd, E. N. Brothers, K. N. Kudin, V. N. Staroverov, T. a. Keith, R. Kobayashi, J. Normand, K. Raghavachari, a. P. Rendell, J. C. Burant, S. S. Iyengar, J. Tomasi, M. Cossi, J. M. Millam, M. Klene, C. Adamo, R. Cammi, J. W. Ochterski, R. L. Martin, K. Morokuma, O. Farkas, J. B. Foresman and D. J. Fox, 2016, Gaussian 16, Revision C.01, Gaussian, Inc., Wallin.

6 J. Olmsted, J. Lawrence and G. G. Yee, *Sol. Energy*, 1983, **30**, 271–274.

7 G. G. D. Han, H. Li and J. C. Grossman, *Nat. Commun.*, 2017, **8**, No. 1446.

8 M. J. Moran, M. Magrini, D. M. Walba and I. Aprahamian, *J. Am. Chem. Soc.*, 2018, **140**, 13623–13627.

9 G. M. Sheldrick, *Acta Crystallogr. Sect. A Found. Crystallogr.*, 2015, **71**, 3–8.

10 O. V. Dolomanov, L. J. Bourhis, R. J. Gildea, J. A. K. Howard and H. Puschmann, *J. Appl. Crystallogr.*, 2009, **42**, 339–341.